DISSERTATION

MORPHOLOGIC CHARACTERIZATION OF URBAN WATERSHEDS AND ITS USE IN QUANTIFYING HYDROLOGIC RESPONSE

Submitted by

Jorge Gironás

Department of Civil and Environmental Engineering

In partial fulfillment of the requirements

For the Degree of Doctor of Philosophy

Colorado State University

Fort Collins, Colorado

Summer 2009

COLORADO STATE UNIVERSITY

May 05, 2009

WE HEREBY RECOMMEND THAT THE DISSERTATION PREPARED UNDER OUR SUPERVISION BY JORGE GIRONÁS ENTITLED MORPHOLOGIC CHARACTERIZATION OF URBAN WATERSHEDS AND ITS USE IN QUANTIFYING HYDROLOGIC RESPONSE BE ACCEPTED AS FULFILLING IN PART REQUIREMENTS FOR THE DEGREE OF DOCTOR OF PHILOSOPHY.

Committee on Graduate work

Jorge A. Ramírez

John D. Stednick

Larry A. Roesner, Advisor

Jeffrey D. Niemann, Coadvisor

Luis A. García, Department Head

ABSTRACT OF DISSERTATION

MORPHOLOGIC CHARACTERIZATION OF URBAN WATERSHEDS AND ITS USE IN QUANTIFYING HYDROLOGIC RESPONSE

Current methods for hydrologic characterization of urban watersheds and analysis of the impacts of urbanization are primarily based on the description of imperviousness and how changes in this characteristic affect storage, infiltration, and runoff generation. The morphology of urban watersheds and the effects of urbanization on the structure of the drainage system have been much less studied. The overarching objectives of this study are to develop methodologies to characterize the morphology of urban drainage systems including the hillslopes, streets, pipes, and channels and to use this characterization to model the hydrologic response of the watershed. These objectives are accomplished through: (a) an exploration of potential applications of morphologic theories in the characterization of urban watersheds and the impacts of urbanization; (b) the development and testing of a methodology to generate urban terrains (i.e. a raster representation of the topography) in which the effects of conduits typically observed in urban areas are represented; and (c) the development and testing of a new rainfall-runoff model called the U-McIUH (Urban Morpho-climatic Instantaneous Unit Hydrograph). The model is based on the morpho-climatic instantaneous unit hydrograph theory, in which the hydrologic response is identified from the spatial structure of the watershed and the properties of the storm event.

The morphologic approach adopted reveals significant impacts of urbanization on the internal structure of natural watersheds at a wide range of scales. This finding is relevant

when building stormwater models intended to simulate and compare the pre- and post-development catchment response. These morphologic impacts should be incorporated into stormwater models through the redefinition of model parameters that characterize both the channelized and unchannelized portions of the catchment when the urbanized scenario is simulated. This research also shows the importance of incorporating artificial conduits into urban terrain for hydrologic modeling. A new method to incorporate the artificial conduits into the DEM based on the real elevation of these conduits proved to be superior to other previously available methods because it better represents the flow directions and flow paths. Finally, the new rainfall-runoff model developed in this study fills an existing gap in the field of distributed stormwater modeling. It provides a more thorough treatment of the flows in minor conduits and unchannelized portions of the watershed, which enhances the simulations of runoff accumulation that are traditionally used in conceptual models. The model is parsimonious and uses a simplification of kinematic wave routing that considers the dependence of the unit hydrograph on rainfall intensity and the effect of upstream contributions on the travel times without explicitly solving the flow equation at each cell for each time step. This simplification reduces the complexity of the model computations while still producing reasonable model performance.

Jorge Gironás
Department of Civil and Environmental Engineering
Colorado State University
Fort Collins, CO 80523
Summer 2009

ACKNOWLEDGEMENTS

I gratefully acknowledge my advisor Dr. Larry Roesner for his constant support, encouragement and friendship. My experience as a PhD student was much richer because of his total commitment to my education. His willingness to help me with each of my ideas and projects was fundamental to the accomplishment of this work. Thank you very much Larry.

I am also very grateful for the support and guidance provided by Dr. Jeffrey Niemann, my coadvisor. This research would not have been possible without his ideas, intellectual contributions and numerous suggestions. Dr Niemann's guidance was essential for defining the specific goals of each part of this project. Finally, I gratefully acknowledge all of his hard work in preparing the journal articles originated from my dissertation.

Thanks to Dr. Jorge Ramírez and Dr. John Stednick, members of my committee, for their time in reviewing and commenting this work. I gratefully acknowledge Dr. Hervé Andrieu and Dr. Fabrice Rodriguez from the Laboratoire Central des Ponts et Chausseés (LCPC) in Nantes, France. The data, suggestions, and knowledge they provided allowed me to develop many of the tools created in this work. My research stay at the LCPC was fundamental to formulate many of the ideas that originated this dissertation.

A special thanks to all of my fellow graduate students in the HHS Lab, with whom I had great moments over the years: Christine Pomeroy, Rajesh Rajan, Melanie Criswell,

Matthew Garcia, Ramadan Alkhatib, Jennifer Davis, Ivan Rivas, Liz Kidner, Yongdeok Cho, Daeryong Park, Adam Jokerst, Chris Olson and Xiaoju Zhang. Thanks also to those friends I met through my days in Fort Collins: Fernando Ramirez, Paulo Hemsi, Jose Manuel Molina, Eric Aoki, Fernando Valerio, Javier González, John R. Wade, Lisa Auer, Alfonso Rivera and many others. Lastly, I want to thank Panagiotis Oikonomou, Barmak Azizimoghaddam and Dr. Evan Vlachos for their friendship and optimism during this last and intense year.

A special thanks to Ernesto Trujillo, Ricardo Fernández and John Edgerly. With them I experienced most of the best moments in Fort Collins. I miss all of you guys.

I want to thank my family for the unwavering love and support throughout my life. Mamá, Papá and Jano, you have supported every step I have taken. Without you I could not have achieved anything in life.

As I write these final lines my wonderful wife, Tara Lee, is taking care of the last details before moving to Chile. I could not ask for a better partner for the rest of my life. Her love, encouragement and support gave me the strength to accomplish this dream. This work is dedicated to you mi patita.

To Tara Lee, mi amada

TABLE OF CONTENTS

LIST OF TABLES

LIST OF FIGURES

1. General Introduction

Urbanization impacts the rainfall-runoff process in a variety of ways by modifying the natural conditions of a watershed. The natural surface interception and detention, the infiltration characteristics and the drainage pattern are drastically changed by urban development (Akan and Houghtalen, 2003). The impacts of urbanization are typically assessed in terms of the increase of impervious area, which affects the infiltration and storage capacity of the catchment. Imperviousness is commonly used as the explanatory variable to depict hydrologic, geomorphic and ecologic effects of urbanizing natural areas (e.g. Brabec et al., 2002; Kim et al., 2002; Cheng and Wang, 2002; Beighley and Moglen, 2003; Melesse and Graham, 2004; Claessens et al., 2006; Huang et al., 2008; Sheng and Wilson, 2009). The special focus on the imperviousness and its effects on runoff generation has resulted in the requirement to use stormwater control practices on new development that attempt to replicate the storage and infiltration characteristics existent previous to urbanization. Simply stated, the study of the hydrology of urban settings has focused mainly on understanding and modeling the runoff generation and the impacts of land-use change on the storage and infiltration capacity once natural ground becomes impervious.

On the other hand, the morphology of urban watersheds and the effects of urbanization on the structure of the drainage system has been much less studied (as suggested by Rodriguez et al. (2005), the term "morphology" is used here instead of

"geomorphology" because artificial conduits are a major portion of the urban drainage network). Research in these topics has been mainly limited to two aspects: (1) the study of changes in runoff discharges due to the replacement of the natural drainage with a drainage system of artificial conduit and channels (Bedient and Huber, 2002; Akan and Houghtalen, 2003), and (2) the study of channel instability and incision following drainage basin urbanization (e.g. Allen and Narramore, 1985; Booth, 1990; Bledsoe and Watson, 2001; Allen et al., 2008.). As a result, the study of geomorphic effects of urbanization has mainly focused on single streams located at the outlet of catchments or subcatchments. But, our understanding of the impact of urbanization in the catchment organization and the natural drainage system as a whole is still very incomplete.

Morphology of river basins has been studied in great detail in natural watersheds. Currently we have a good set of tools to characterize qualitatively and quantitatively natural drainage networks, and a consistent framework to link the morphology of natural watersheds and their hydrological responses (see Rodríguez-Iturbe and Rinaldo (1997) for a detailed discussion in these topics). But the applicability of such tools in urban watersheds has been barely explored, despite the increasing availability of data describing both the surface and subsurface drainage systems. Our current knowledge in the field of river basin morphology provides us with new research opportunities to better understand the hydrology of urban settings and their impacts. Some of the topics in which morphologic theories developed for natural watersheds might be used in urban settings include: (1) the detection of urbanization impacts on the geomorphology of the basin and its internal organization, (2) the morphologic characterization of urban watersheds and different imperviousness patterns identified from urban terrains truly representing the

drainage structure, (3) the definition of a framework to link the urban morphology and the hydrologic response, and (4) the design of stormwater control practices especially oriented to replicate not only processes such as infiltration or storage, but also the spatial morphologic properties of undeveloped catchments. The study of some of these topics is what inspires the research documented in this work.

The overarching objectives of this study are to develop methodologies to characterize the morphology of urban drainage systems including the hillslopes, streets, pipes, and channels, and to use this characterization to model the hydrologic response of the watershed. These objectives are accomplished through (a) an exploration of potential applications of morphologic theories, originally developed in the field of river basin morphology, to urban watersheds, (b) the development and testing of a methodology to generate urban terrains, so that artificial conduits and other characteristics typically observed in urban areas can be incorporated in a raster representation of the morphology of urban drainage networks, and (c) the development and testing of a rainfall-runoff model identified from the spatial structure of urban watersheds. This document is organized into three main chapters, each corresponding to a self-contained presentation in which specific components of the objectives presented above are addressed. The organization is as follows:

Chapter 2 introduces the study and characterization of urban watersheds from a morphologic point of view. Different areas of interest in the study of urban hydrology are studied using this morphologic approach. Morphologic properties developed in the field of basin morphology are used in a real catchment to illustrate how these topics can be addressed. Major alterations to the channelized and unchannelized portions of the

watershed as well as its internal organization are discussed throughout the result sections. Additionally, the morphologic characterization of the watershed by means of the imperviousness function, an extension of the width function, is presented. The quality of the urban terrain directly extracted from the digital elevation model (DEM) and the potential link between the morphology (particularly the imperviousness function) and the hydrological response, are identified as issues that deserve more research. These issues are studied in Chapters 3 and 4 respectively.

A new method to generate urban terrains in a raster file is introduced in Chapter 3. The method attempts to incorporate artificial elements (particularly the pipes) more properly by making use of known conduit elevations, so that more realistic flow paths are reproduced. The method is successfully evaluated against other existing alternatives through a morphologic and hydrologic approach.

Chapter 4 explores the relationship between the morphologic description of urban watersheds and the hydrologic response. In this chapter a new stormwater model called the U-McIUH (Urban Morpho-climatic Instantaneous Unit Hydrograph) is introduced. The model is based on the geomorphoclimatic instantaneous unit hydrograph theory, which links the instantaneous unit hydrograph (IUH) to the structure of the drainage network and the characteristics of the rainfall events. According to the theory, the IUH corresponds to the probability density function of the travel times of flows along the flow paths to the outlet of the watershed. The flow paths are extracted from the urban terrain generated using the methodology presented in Chapter 3 and travel times are computed using the kinematic wave theory. Rainfall pulses and the corresponding IUHs are convoluted and superimposed to generate the response to the entire storm event. The

model is tested in a real catchment in which rainfall and runoff records for a period of 3 years are available. Finally, the main characteristics of the U-McIUH that differentiate it from other existing models are evaluated in order to detect the most relevant improvements with respect to other available tools.

The last chapter of this document comprises a summary of the research, the most relevant conclusions of this work and recommendations for future research.

1.1 References

Akan, A.O., Houghtalen, R.J., 2003. Urban Hydrology, Hydraulics, and Stormwater Quality. John Wiley and sons Inc., Hoboken, NJ, p.373.

Allen, P.M., Narramore, R.L., 1985. Bedrock controls on stream channel enlargement with urbanization, North Central Texas. Water Resources Bulletin 21(6), 1037-1048.

Allen, P.M., Arnold, J.G., Skipwith, W., 2008. Prediction of channel degradation rates in urbanizing watersheds. Hydrological Sciences Journal 53(5), 1013-1029.

Bedient, P.B., Huber, W.C., 2002. Hydrology and Floodplain Analysis, 3rd Ed. Prentice-Hall, Upper Saddle River, NJ, p. 763.

Beighley, R.E., Moglen G.E., 2003. Adjusting measured peak discharges from an urbanizing watershed to reflect a stationary land use signal. Water Resources Research 39(4). doi:10.1029/2002WR001846.

Bledsoe, B.P., Watson, C.C., 2001. Effects of urbanization on channel instability. Journal of the American Water Resources Association 37(2), 255-270.

Booth, D.B., 1990. Stream channel incision following drainage basin urbanization. Water Resources Bulletin 26(3), 407-417.

Brabec, E., Schulte, S., and Richards, P.L., 2002. Impervious surfaces and water quality: a review of current literature and its implications for watershed planning. Journal of Planning Literature 16(4), 499-514.

Cheng, S.J., Wang, R.Y., 2002. An approach for evaluating the hydrological effects of urbanization and its application. Hydrological Processes 16(7), 1403-1418.

Claessens, L., Hopkinson, C., Rastetter, E., Vallino, J., 2006. Effect of historical changes in land use and climate on the water budget of an urbanizing watershed. Water Resources Research 42 (3). doi:10.1029/2005WR004131.

Huang H.J., Cheng, S.J., Wen, J.C., Lee, J.H., 2008. Effect of growing watershed imperviousness on hydrograph parameters and peak discharge. Hydrological Processes 22(13), 2075-2085.

Kim, Y., Engel, B.A., Lim, K.J., Larson, V., Duncan, B., 2002. Runoff impacts of land-use change in Indian River lagoon watershed. Journal of Hydrologic Engineering 7(3), 245-251.

Melesse, A.M., Graham, W.D., 2004. Storm runoff prediction based on a spatially distributed travel time method utilizing remote sensing and GIS. Journal of the American Water Resources Association 40(4), 863-879.

Rodriguez, F., Cudennec, C., Andrieu H., 2005. Application of morphological approaches to determine unit hydrographs of urban catchments. Hydrological Processes 19(5), 1021-1035.

Rodríguez-Iturbe I., Rinaldo A., 1997. Fractal River Basins: Chance and Self-Organization. Cambridge University Press, New York, pp. 547.

Sheng, J., Wilson, J.P., 2009. Watershed urbanization and changing flood behavior across the Los Angeles metropolitan region. Natural Hazards 48(1), 41-57.

2. Morphologic Approach in Studying Urban Watersheds

Abstract: Current characterization of urban watersheds and the modifications produced in natural areas by development focus primarily on the description of changes in the land-use and the effect of these changes on the hydrologic processes of storage, infiltration and runoff generation. In this work we take this approach one step further by evaluating the impact of urbanization on the morphology of watersheds. We identify three hypotheses to be tested in evaluating these impacts: (1) morphologic features can be used to quantify the impact of urbanization; (2) morphologic features can be used to determine the spatial scales at which urbanization impacts occur and are more significant; and (3) morphologic features can be used to classify and characterize urban settings or patterns. Different morphologic properties from the field of basin morphology are used in a real urban watershed to test these hypotheses. Results show major alterations to morphologic properties of streams and unchannelized portions of the watershed as well as its internal organization. It is concluded that these changes should be incorporated through the redefinition of model parameters when predicting the effect of urbanization. Additionally, the application of morphologic functions provides with alternative ways to characterize urban watersheds and urbanization patterns. The study proposes future research courses for which this characterization can be used. Finally, a series of improvements to current approaches in the study and modeling of urban watersheds are discussed.

2.1 Introduction

In a natural watershed, the drainage network is formed as a result of the combined effects of climate and geology on watershed topography (Eagleson, 1970). Some of the early fundamental works describing the drainage structure include the classification scheme of channel networks (Horton, 1945; Strahler, 1957), the empirical laws characterizing the geometry of drainage networks (Horton, 1945; Schumm, 1956), the functional relationship between the main stream length and the watershed's area (Hack, 1957), and the introduction of models describing the evolution of drainage networks (Shreve, 1966; Shreve, 1967; Scheidegger, 1967; Howard, 1971a; Howard, 1971b). With the increasing availability of digital elevation models (DEMs), research in the field of basin morphology has expanded enormously. Several topics have been studied, including (Bras, 1990; Rodríguez-Iturbe and Rinaldo, 1997): network growth and landscape evolution, landscape morphology, channel network organization, channel geometry, and the relationship between hydrologic response and fluvial geomorphology. Currently, a number of morphologic descriptors and scaling and multi-scaling laws are used to characterize and quantify morphologic and topologic features of natural basins. Extensive research has proven that comparable characteristics and scaling properties can be observed at different locations with diverse geological conditions, climate, vegetation and soil. The scaling parameters and the morphologic descriptors for this variety of conditions are typically restricted to well-defined ranges of values (Dodds and Rothmann, 1999). These similarities respond to general operating criteria that control the manner in which river basins organize and perform. Nonetheless, Mejía and Niemann (2008) recently showed that deviations from these consistent observations occur and can be

formally characterized through the scaling parameters and the morphologic descriptors. In summary, a natural watershed is a self-organizing system whose form, drainage network, ground and channel slopes, channel hydraulic geometries, soils and vegetation, are all a result of adaptive, ecological, geomorphic or land forming processes (Sivapalan, 2005).

Significant changes to the morphology of basins occur once they are urbanized. Simply stated, new impervious surfaces require additional water to be conducted out of the watershed so that new transport elements become part of the drainage system and old ones are modified. The addition of new artificial elements hydraulically more "efficient" (Bedient and Huber, 2002) is usually considered to be the only modification to the drainage system of a watershed. This addition leads to an increase of the overall drainage densities (Graf, 1977; Bannister, 1979; Hayden, 1981; Phillips, 1985, Smith et al., 2002). One of the first studies to assess changes to the morphology of basins caused by urbanization was carried out by Graf (1977). He pointed out that typical suburban channel networks can have spatial characteristics that are substantially different from natural networks. Stream networks in suburbanizing areas change, greatly affecting the characteristics of stream discharges. Based on his results, he concluded that changes in the characteristics of channel networks should be considered in addition to changes in imperviousness when the hydrologic impact of suburbanization is assessed. Erosion, instability and incision following drainage basin urbanization are typically studied only at the channel scales (e.g. Allen and Narramore, 1985; Booth, 1990; Bledsoe and Watson, 2001; Allen et al., 2008). Few studies have attempted to describe changes to the drainage structure at different scales within the catchment. Bannister (1979) observed that road

networks truncate natural drainage channels and force the coalescence of smaller order basins. This phenomenon tends to increase downcutting and runoff discharges in channels in which the natural erosional development would have been much less. Hayden (1981) evaluated the effects of road drainage on the geomorphic equilibrium of small stream basins using the Horton's law of stream lengths (Horton, 1945). He analyzed the effects of eight different types of road networks on a hypothetical stream basin and suggested a method to predict the location and extent of the disequilibrium. Smith et al. (2002) computed the width function of an urban watershed, that is the number of channel links at a specified distance from the basin outlet (Rodríguez-Iturbe and Rinaldo, 1997). For this purpose, the drainage network was represented as the sewer network combined with the natural drainage network. They also computed the width function of the equivalent natural drainage system, i.e. the drainage network directly extracted from the DEM. A comparison of both functions showed an amplification of the width function near the outlet that the authors attributed to the increase in the drainage density caused by urban development. Moreover, part of the change in the hydrologic response of the watershed was linked to this phenomenon. Finally, Pomeroy et al. (2008) demonstrated the importance of considering changes in the cross sections of the entire system of streams when simulating the effects of future urbanization using a stormwater model. This conclusion is relevant because it suggests that land-use parameters are not sufficient to represent changes caused by urbanization, and other modifications affecting the natural drainage pattern should also be considered in hydrologic modeling. This literature review demonstrates that the study of urban watersheds using a morphologic approach has been limited, and that many aspects of the morphology of urban watersheds

and its impact on the natural drainage network remain to be addressed. What happens to the entire watershed organization and the natural drainage structure? How does it change and at which scales are these changes relevant? Should these changes be incorporated in the construction of stormwater models that simulate the hydrologic response of future urbanization?

The aim of this study is to gain insight into how morphological properties developed in the field of basin morphology can be used to characterize urban watersheds and the impacts of urbanization on the morphology of watersheds. Three hypotheses regarding the applicability of morphologic theories to urban watersheds are identified: (1) morphologic features can be used to quantify the impact of urbanization; (2) morphologic features can be used to determine the spatial scales at which these impacts occur and are more significant; (3) morphologic features can be used to classify and characterize different urban settings or patterns. Hypotheses 1 and 2 are tested by assessing the differences, at different spatial scales, between the values of scaling parameters and morphologic descriptors well-defined for natural watersheds with those obtained for an urban watershed. Hypothesis 3 will be tested by assessing the differences in morphologic functions for different spatial patterns of urbanization. The schematic representation in Figure 2.1 illustrates how these hypotheses, which are tied together, cannot be addressed separately. The integrated analysis of them will eventually have a significant impact on the way we characterize and model the hydrology of urban watersheds, and the way we develop urban planning policies and drainage criteria. The paper is organized as follows. The study area and the methods used in this work are presented in the following section. Then, in the results section, we use different morphological measurements to test the

three hypotheses previously identified. The paper closes with a brief analysis of other possible applications of morphologic metrics in urban settings and the final conclusions.

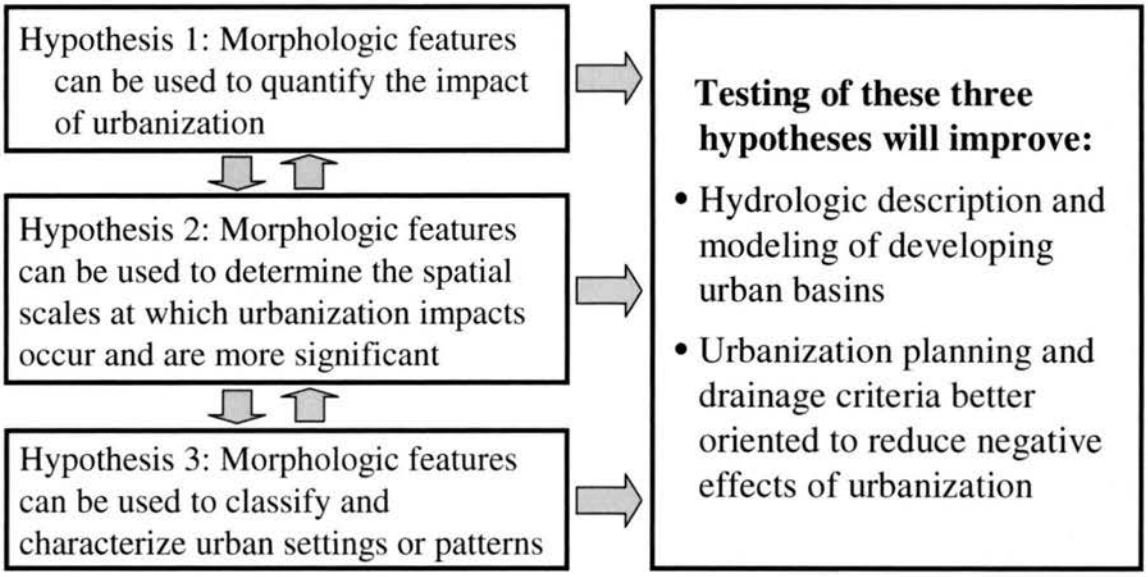

Figure 2.1. A schematic representation of the main hypotheses and possible benefits identified in the study of urban watersheds using a morphologic approach.

2.2 Methods and Study Area

The Pigeon House Creek watershed (Figure 2.2) is located in the city of Raleigh and is used in this study to test the three hypotheses previously identified. The city of Raleigh is located in the northeast central region of North Carolina at an average elevation of 96 m. It has a humid subtropical climate and the total annual precipitation is around 1150 mm (National Climatic Data Center station #317079, period of record between 1/1/1921 and 12/31/2007). A 10 m raster file of total imperviousness for the area was obtained from the 2001 National Land Cover Database Zone 60 Imperviousness Layer (USGS, 2003). The watershed is highly and heterogeneously developed, with an

approximate total imperviousness of 30%. It has a surface area of 11.33 km^2 and it is drained by the Pigeon House Creek. The USGS site number for this catchment is USGS 0208732610. A 10 m DEM obtained from the USGS Seamless Web site (USGS, 2006) was used to extract the morphologic information required for this analysis data. Pre-processing of the DEM was done with tools available in Arc GIS and Arc Hydro (Olivera et al., 2002). These tools include pit filling, determination of flow directions (using the direction of steepest descent), accumulation of flow, computation of flow lengths and slopes. Ideally, DEM for this location previous to urbanization should be use in the computation of morphologic properties and testing of hypotheses 1 and 2. Unfortunately this information is not available. Thus, the morphologic properties used to test these hypotheses are computed only for the urban case, and the values of scaling parameters and descriptors are compared to values typically observed in natural areas. An alternative approach would have been to use a natural watershed located nearby as a control and to compute the morphologic properties for this watershed. This approach would have allowed the detection of local conditions (e.g. geology) that may affect the results and remains as a task for future research.

The urban DEM was not modified to represent conduits or artificial paths because it is expected to reflect the main features of the urbanized landscape. Nonetheless, other authors have modified the DEM to improve the representation of flows in artificial conduits in stormwater modeling (e.g. Rodriguez, et al., 2000; Lhomme et al., 2004). The use of the non-modified DEM also allows us to verify the concept of "equivalent natural network" developed by Smith et al. (2002). According to this concept, the topography given by a raw DEM of an urban area corresponds to the natural topography

before urbanization. Thus, the drainage network extracted from the DEM using an area-threshold algorithm would correspond to the natural drainage network existing before development took place. If this assumption were valid, the morphologic features extracted from the DEM should be similar to the ones observed in natural undisturbed watersheds, and our hypotheses 1 and 2 would be rejected.

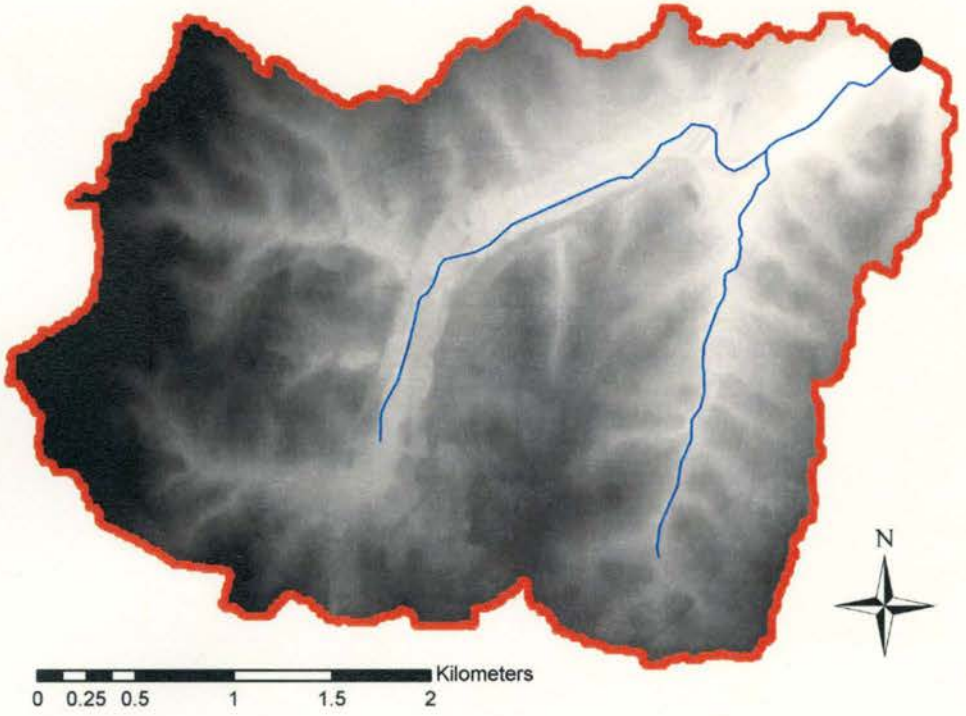

Figure 2.2. Study area, Pigeon House Creek watershed. The two main streams are shown as well as the outlet located in the northeast part of the watershed.

Four geometric variables are defined for each cell i to compute the morphologic properties used in this study (Figure 2.3): (1) the local slope of the cell, S_i, (2) the area contributing to the cell A_i, (3) the flow distance from the cell to the outlet along the flow path x_i, (4) and the maximum flow distance from the cell to the watershed divide along

the main stream, L_i. Figure 2.3 also shows the Euclidean length l_i, which corresponds to the straight-line or geometric length from the cell i to the divide. This variable is not computed directly, but will be indirectly used later in this study. What follows in the next section is the testing of the three hypotheses previously defined.

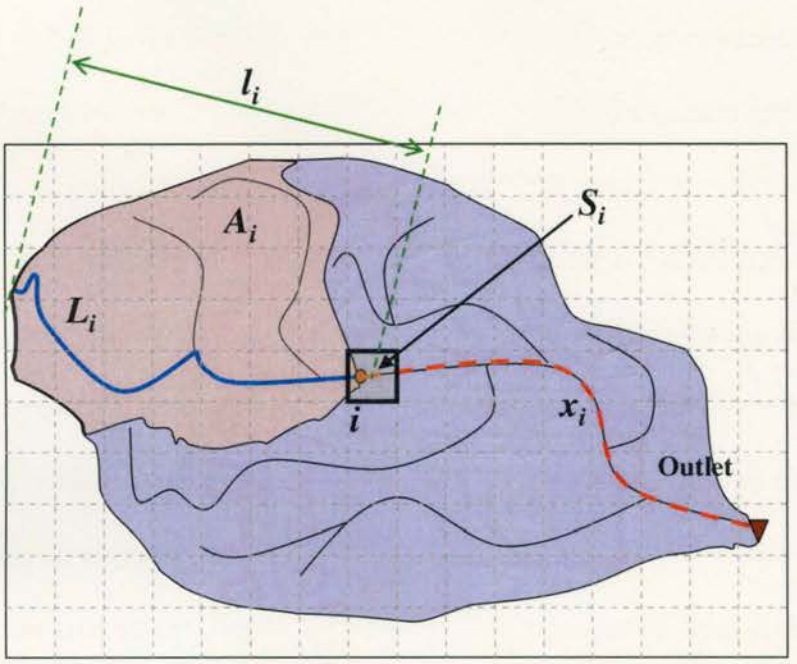

Figure 2.3. Morphologic properties extracted from the DEM at each cell *i*.

2.3 Results

2.3.1 Hypothesis 1: Morphologic features can be used to quantify the impact of urbanization

Two properties extensively studied in the field of river basin morphology are Hack's Law and the cumulative distribution of contributing areas (Rodríguez-Iturbe and Rinaldo, 1997). We will use these two properties to test our hypothesis 1.

Hack's Law

The Hack's Law (Hack, 1957) states that the main stream length, measured along the flow path to the divide from a given point on a stream, is functionally related to the area of watershed draining to that point. This relationship has the form of a power law:

$$L_i = bA_i^h \tag{2.1}$$

where b is a coefficient and h is the scaling exponent, which is typically referred as Hack's exponent. It has been observed that h is in the range of 0.57-0.6 for natural basins (Maritan et al., 1996).

Figure 2.4 plots this relation for the Pigeon House Creek watershed. The points in this plot are obtained by aggregating the pairs A_i,L_i using constant bins in the log-area domain (200 bins were used). As a comparison, a power relationship typical of natural watersheds (Gray, 1961), with a coefficient b = 1.4 and exponent h = 0.568, is also plotted. A power law with an exponent h = 0.456 fits the results very well (R^2 = 0.991), even though some variation around the function is observed for areas larger than 10 ha. Points with areas below 1000 m^2 do not follow this power function; this occurs because the small scales are in the realm of unchannelized, diffusive hillslopes that run in parallel. Thus, subcatchments are very narrow and are equivalent to lines of flow, so that the length and area have a relationship 1 to 1 (Dodds and Rothman, 2000). The value of the exponent h is out of the range of values typically observed in nature. In fact, $h < 0.5$ is in disagreement with what is expected for natural watersheds of this size. Only at extremely large watersheds, where streams belong to a random regime, the exponent h approximates to 0.5 (Mesa and Gupta, 1987; Dodds and Rothman, 2000). The fact that $h > 0.5$ in natural watersheds has been explained both by the fractal sinuosity of streams and the

observation that basins become more elongated with increasing size (Rodríguez-Iturbe and Rinaldo, 1997). Using a simple example, Hergarten (2002) showed that both explanations can contribute significantly to the Hack's law. It is not clear which of these two factors is more relevant in explaining the low value of h in the Pigeon House Creek watershed. The behavior of the area-length relationship can be explained either by a straightening of the main channels or a modification of the drainage structure to bring in more lateral area. A visual inspection of the satellite image shows that the areas at which streams start to be noticeable are in the range of 40 ha to 70 ha. Figure 2.4 shows that the points below this area threshold are well fitted by the power function. Hence, one could assume that, at these small scales, urbanization causes changes to the internal organization of the drainage structure, so that subcatchments tend to be short and wide. On the other hand, the area threshold also indicates the area at which the variation around the fitted line becomes higher and the power relationship becomes less evident. This variation might be caused by alterations to the main streams, (i.e. straightening of portions of them). Unfortunately, the fact that only three or less streams are represented in this area of the plot implies that very few points are available to truly characterize the length-area relationship at these large areas. Consequently a more detailed study of these areas is necessary for this relationship to be well understood. Overall, variations around Hack's law could potentially indicate the scale at which urban streams begin as well as reflect the disturbance experienced by them. Although no definitive explanation to describe the area-length relationship is available, it is clear that an unexpected behavior of this function is observed at all the spatial scales in this particular watershed. Further discussion related to this topic is presented later in this study.

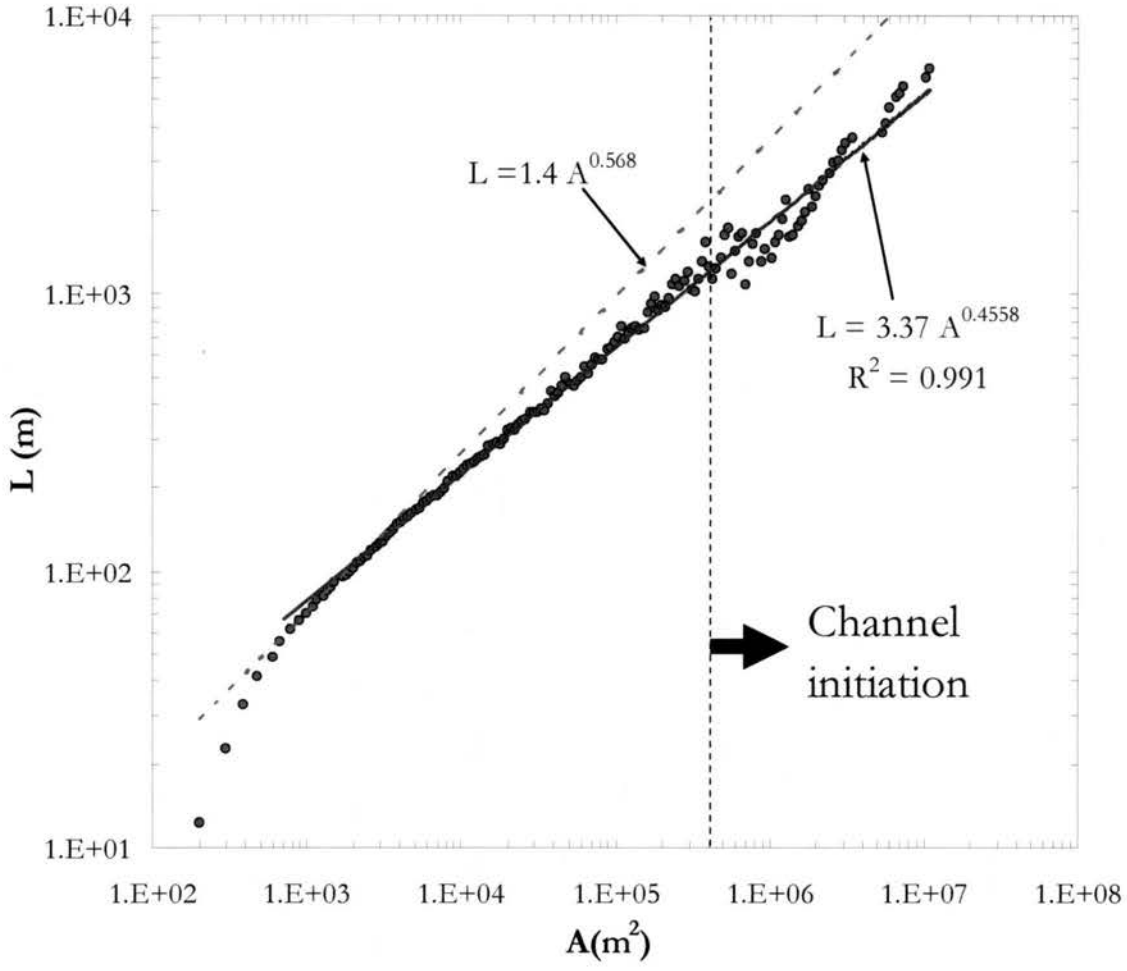

Figure 2.4. Hack's relationship *L* vs. *A* for the Pigeon House Creek watershed. The power law proposed by Gray et al. (1961) for natural watershed is shown as a reference.

Cumulative distribution of contributing areas

Rodríguez-Iturbe et al. (1992) found that the aggregating structure of the channel network is organized such that the cumulative distribution of contributing areas A_i responds as a power law of the form:

$$P[A_i \geq a] \sim a^{-\beta} \tag{2-2}$$

In this expression β is the scaling exponent, which usually ranges between 0.41 and 0.45 in natural watersheds (Maritan et al., 1996). At very large scales, this relationship

does not hold because of the effects of the tributaries joining the main channel which causes large step increases in the contributing area (McNamara et al., 2006). On the other hand, a break in this power law distribution is sometimes observed at small scales, and it is explained by predominant divergent flows at those scales (Ijjász-Vásquez and Bras, 1995). Maritan et al. (1996) studied the relationship between the Hack's exponent and the scaling exponent β. For this purpose, they used the following well-known power law relationships.

$$\ell_i \sim l_i^{\varphi} \tag{2-3}$$

$$L_i \sim l_i^{d} \tag{2-4}$$

In Eq. (2-3) ℓ_i correspond to the mean of the flow distances from all the cells within the subcatchment contributing to cell i, and is given by:

$$\ell_i = \frac{1}{N_i} \sum_{j=1}^{N_i} x_j \tag{2-5}$$

where j is an index of cells, x_j is the flow distance along the flow path from cell j to cell i, and N_i is the number of cells within the subcatchment contributing to cell i. Hence, Eq. (2-3) corresponds to a scaling law relating ℓ_i to l_i, the longitudinal length from the cell i to the divider of the corresponding contributing area A_i. On the other hand, Eq. (2-4) corresponds to a scaling law relating the length of the main stream L_i to l_i. Maritan et al. (1996) demonstrated that h and β are simply related by the following expression when exponents φ and d are the same:

$$h + \beta = 1 \tag{2-6}$$

The equality between these exponents has been indeed observed and typically holds in a wide range of drainage basins (Maritan et al., 1996), however, the authors stated that

this equality cannot be justified theoretically given the different origin of both scaling laws.

Figure 2.5 shows this distribution for the Pigeon House Creek Basin. $P[A \geq a]$ is computed empirically for the contributing areas to all the grid cells in the watershed. A power law describing the aggregation of areas is well-defined for a large range of scales (almost five orders of magnitude). However, the value of the scaling exponent ($\beta = 0.53$) is larger than typical values observed in natural watersheds. Assuming that the scaling exponent β before urbanization was in the typical range defined for natural basins, we can conclude that the urbanization has changed the pre-existing internal organization of the basin. Particularly, the probability of having contributing areas larger than a certain value decreases faster in the developed case, which implies a high degree of aggregation at small scales. This may confirm the findings by Bannister (1979) who observed that road networks truncate natural drainage channels and force the coalescence of smaller order basins. This aggregation is also in agreement with the observation derived from the analysis of the Hack's law. A great degree of aggregation at small scales implies large increases of contributing area that are not necessarily related to the corresponding increases in the length of the main flow path. Thus, the elongation of watersheds typically observed in natural areas is not observed at these scales in this particular urban watershed. Interestingly, the values of h and β for the Pigeon House Creek watershed satisfy Eq. (2-6) very well ($h + \beta = 0.456 + 0.531 = 0.987 \approx 1$). This provides a degree of certitude to the values of the exponents found in our study.

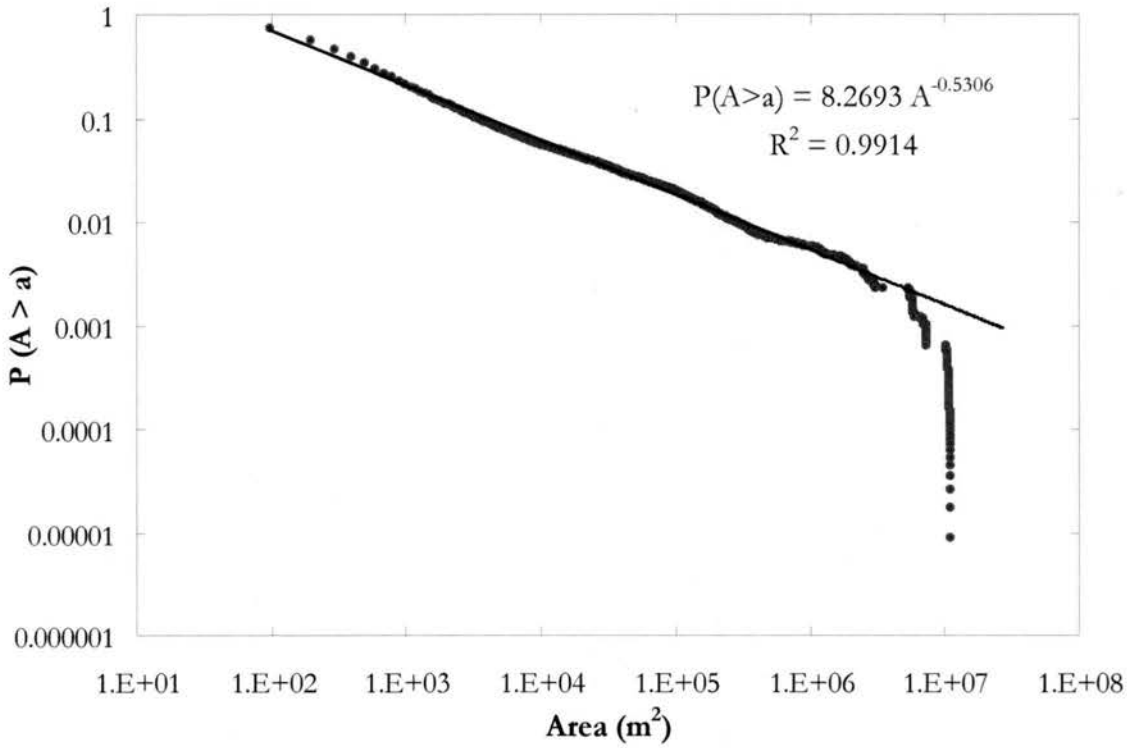

Figure 2.5. Cumulative distribution of contributing areas for the Pigeon House Creek watershed.

The application of Hack's law and the cumulative distribution of contributing areas to this particular watershed shows that hypothesis 1 can be valid. Both relationships display features not commonly observed when computed for natural watersheds. However, local geological conditions explaining these differences cannot be discarded, and more research in areas nearby as well as other geographic locations is necessary to finally validate the hypothesis. Two limitations are identified in applying the Hack's law and the cumulative distribution of contributing areas to raw urban DEMs: (1) small surface conduits (e.g. street gutters and swales) and pipes are likely not resolved in the DEM, so the real flow paths along these conduits are probably not represented (2) flow paths are

identified based only on the topography given by the DEM, and no other restrictions to the flows typically observed in urban setting are considered (e.g., curbs, inlets, culverts). Because of these 2 limitations, it is likely that Hack's law and the cumulative distribution of contributing areas provide only an approximate characterization of the drainage structure of the Pigeon watershed. Nonetheless, the application of these morphological functions to this particular urban watershed shows that some of the attributes of urban areas might be resolved from high-resolution DEMs. The difference between the observed scaling exponents and the values typically observed in nature suggests that the topography and internal structure extracted from the DEM of this particular watershed might not be the same as those of the previously existent natural area. Therefore this study shows that the "equivalent natural network" assumption proposed by Smith et al. (2002) may not be adequate. The application of the previously discussed methodology to other urban watersheds located in different geological and climatic areas is necessary to validate this conclusion.

2.3.2 Hypothesis 2: Morphologic features can be used to determine the spatial scales at which urbanization impacts occur and are more significant

Unexpected features of Hack's law and the cumulative distribution of contributing areas were previously identified for all the spatial scales. Our hypothesis 2 indicates that morphologic features can be used to detect the spatial scales at which urban impacts are more relevant. A better understanding of this issue can provide an insight into the determination of spatial distribution and integration of drainage control facilities. In this section we tested hypothesis 2 by means of the slope-area relationship, a well-known

morphologic feature.

The power relationship $S \sim A^{-\theta}$ (also called the slope-area relationship) has been long studied in fluvial geomorphology (e.g., Flint, 1974; Willgoose et al., 1991; Montgomery and Foufoula-Georgiou, 1993; Ijjász-Vásquez and Bras, 1995; Tucker and Bras, 1998; McNamara et al., 2006). Geomorphologic thresholds in watersheds have been derived by evaluating distributions of surface slope, S, and contributing area, A (McNamara et al., 2006). These variables, coupled with site-specific field information, are commonly used to calculate the potential for specific erosion processes to occur in a watershed (Dietrich et al., 1993). More recent studies have defined different scaling regimes and the boundaries between them that represent transitions in the erosive processes and in the curvature of the topography. Ijjász-Vásquez and Bras (1995) identified four regions in the slope-area diagram of a typical river basin as illustrated in Figure 2.6. Region I characterizes the convex topography of hillslopes in which, for small spatial scales, an increasing slope in the downhill direction is observed. The transition between Regions I and II is related to the change from diffusive to fluvial sediment transport processes (or from the convex shape of hillslopes to the concave topography of larger hillslopes and unchannelized valleys). In this concave topography the slope decreases in the downhill direction. Region III is interpreted as the transition at relatively constant slopes between unchannelized valleys and the channel regime that is completed at the beginning of Region IV. Tucker and Bras (1998) studied in detail the relationship between these regions and the different erosion processes at hillslopes by means of a model of drainage basin evolution. Slope-area scaling relationships of the form $S \sim A^{-\theta}$ can be typically fitted to the data points in regions II and IV (Ijjász-Vásquez and Bras, 1995). Ranges for the

scaling exponent θ in natural watersheds are not as well defined as for the case of scaling exponents h and β. Flint (1974) reported values of θ between 0.2 and 0.6 while Tarboton et al. (1989) reported a range of 0.4-0.7, with a typical value around 0.5. Figure 2.7 shows this relationship for the Pigeon House Creek watershed after aggregating the points A_i,S_i in 300 constant bins in the log-area domain. Regions I and II are clearly observed in the plot, with the slope reversal occurring at a watershed area of 400 m^2. Points in region II are well characterized by a power relationship with a scaling exponent $\theta = 0.14$. The value of θ is smaller than those typically observed in natural watersheds. Region III is also identified although the degree of scattering of the slope-area points is a little bit higher than what is observed in natural watersheds. Range III is located in areas between 2 and 20 ha, although the transition between regions III and IV is not clear. For areas of 20 ha or higher, a large scatter in data is observed. Some slopes in this region are quite high, with many of them being larger than the slope at the transition between region I and II. This behavior of the slope-area relationship is in disagreement with what is observed in natural watersheds where the higher slopes are located in the upstream sections of the watershed. Figure 2.7 also shows the area at which the surface channels are observed from a satellite image (A = 40 ha), already identified in Figure 2.4. This threshold coincides with the area at which scattering in the plot becomes more significant. In fact, the threshold also indicates the drainage areas in region IV at which slopes larger than the maximum defined by the transition between Region I and II are observed. The considerable instability and high slopes identified after this threshold area may indicate a status of high anthropogenic modification of the streams. This can be explained by large upstream discharges associated with urbanization, which cause either

stream bed erosion or straightness of the streams. Interestingly, the area threshold at which the slopes become excessively large (A = 40 ha) also represents the scale at which the Hack's law becomes less evident and many flow lengths are shorter than what is expected (Figure 2.4). This would indicate an overall shortening of the flow paths at these spatial scales that implies changes of elevation in shorter distances, and therefore larger slopes as the ones detected in Figure 2.7. Though a final explanation cannot be provided for this phenomenon yet, the slope-area relationship applied to this particular watershed is showing that streams can be altered by urbanization at certain spatial scales. This issue has relevant implications in using stormwater models to simulate and compare the hydrologic response of areas before and after urbanization. When building a model to represent future urbanization, artificial elements of the drainage system are defined in addition to the existing natural streams that will remain part of the drainage system. Typically the cross-sections, slopes and planar locations of these streams are assumed to remain constant. Hence, these geometric properties are measured from the natural area and entered into the model representing post-development conditions. In this particular example, the slope-area relationship shows that some of these parameters will change for scales larger than approximately 20 ha. In fact, given the location of the streams' headwater in the Pigeon House Creek watershed, this area threshold implies geomorphic impacts not only to the totality of the streams, but also to unchannelized portions of the watershed. Thus, new parameters characterizing both subcatchment and streams would have to be identified in order to develop a stormwater model representing future urban conditions. The application of the slope-area relationship to this particular watershed shows that hypothesis 2 can be valid. As with the case of hypothesis 1, more research in

areas nearby as well as other geographic locations is necessary to finally validate the hypothesis. A more reliable validation of this hypothesis might represent a departure from the current practices in which the effects are typically studied at single scales rather than at all the spatial scales within the watershed.

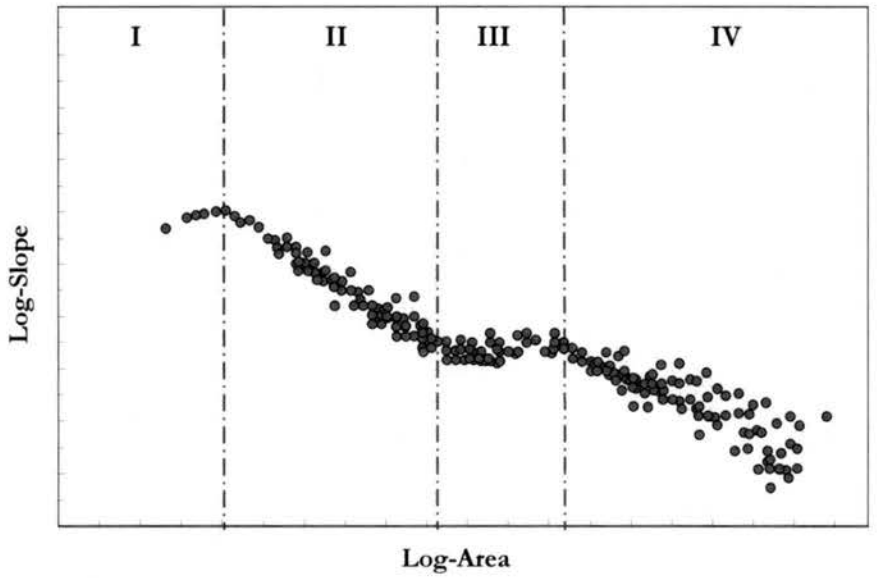

Figure 2.6. Slope-area diagram for a typical river basin

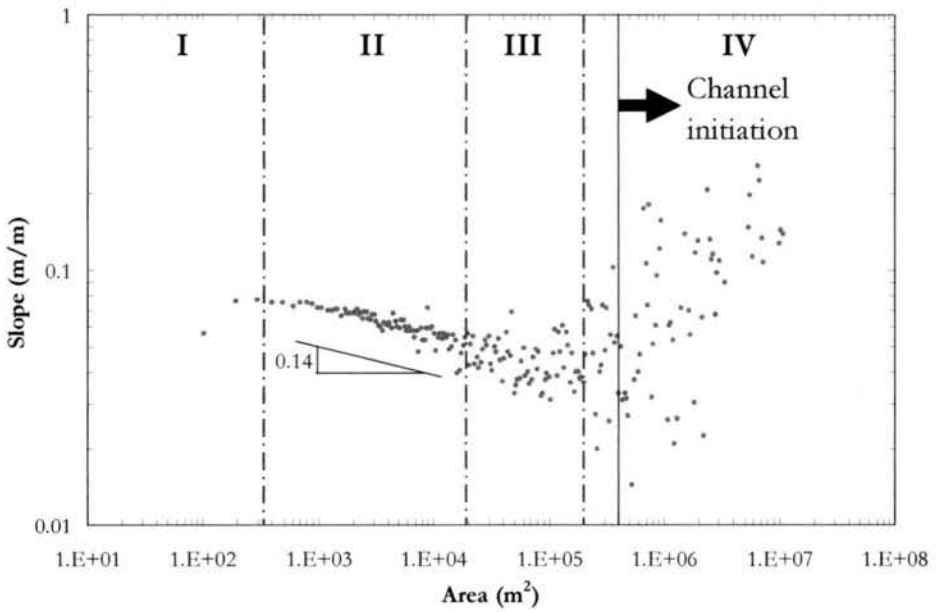

Figure 2.7. Slope-area diagram for Pigeon House Creek watershed

2.3.3 Hypothesis 3: Morphologic features can be used to classify and characterize urban settings or patterns

Imperviousness has typically been the parameter used to characterize urbanization from a hydrologic and environmental point of view. Concepts such as the total impervious area or the effective impervious area, that is the portion of the total impervious area connected to the stormwater drainage system by an entirely impervious path (Han and Burian, 2009), are utilized to depict the degree of impact caused by development of natural areas (e.g. Kim et al., 2002; Melesse and Graham, 2004; Claessens et al., 2006; Huang et al., 2008;). The effects of different spatial patterns of imperviousness in the hydrologic response of a watershed have not been extensively studied yet, and the few available studies typically compare peak discharges which are linked to the imperviousness patterns using a hydrologic model (e.g. Yeo et al., 2004; Tang et al., 2005; Yeo et al., 2007; Mejía and Moglen, 2009). Thus, the approach in these studies is to characterize different urbanization patterns and classify them based on the magnitude of the corresponding impact to the peak discharges. According to our hypothesis 3, morphologic -rather than hydrologic- features can be used to perform a similar task. A benefit of this morphologic approach would be that no uncertainty associated with the definition of the inputs and parameters for the hydrologic model is incorporated in the assessment. In this section we tested the hypothesis 3 by means of the width function, a widely used morphologic function in natural catchments, and the imperviousness function, an extension defined for this study.

The width function, $W(x)$, is defined as the portion of area in the drainage network at a flow distance x from the outlet (Rodríguez-Iturbe and Rinaldo, 1997). $W(x)$

incorporates some essential characteristics of the hydrologic response because the travel time from each point in the basin is related in part to the flow distance that must be traversed. For this study we also define the imperviousness function, $H(x)$, which corresponds to the portion of the area in the drainage network at a flow distance x from the outlet. This function approximately depicts the runoff production under the assumption that only impervious areas produce runoff. $H(x)$ also allows for the description of the two-dimensional spatial variability of the imperviousness in a simpler one-dimensional function.

Figure 2.8a shows both functions for the Pigeon House Creek watershed. $W(x)$ was computed by summing the area located at different flow distances x from the outlet. $H(x)$ was computed by summing only the impervious areas located at different flow distances x from the outlet. Figure 2.8a also shows the imperviousness function that is obtained if all the cells have an imperviousness of $H = 30\%$, which is the average imperviousness for the entire watershed. This final function is simply a rescaled version of $W(x)$ using a factor of 0.3. Thus, to test our hypothesis we will use $H(x)$ to differentiate these two imperviousness distributions: the real distribution and a hypothetical one in which imperviousness is homogeneously distributed. Figure 2.8a shows that the largest contribution of the watersheds (i.e. Maximum value of $W(x)$) comes from areas located at a flow distance of 5000 m from the outlet. This area is also more impervious than the average ($H(x) > H = 30\%$). $H(x)$ and $H = 30\%$ are indeed quite different. This is explained by the heterogeneous real distribution of imperviousness within the watershed. Figure 2.8a shows three important locations from the outlet that are more impervious than the average: (1) areas located in the range 0 - 1000 m, (2) areas located in the range 4500

- 5300 m, and (3) areas located in the range 5900 - 6800 m. An alternative way to visualize the location of this highly impervious areas is by means of the plot showing the value of the ratio $H(x)/W(x)$ at different flow distances from the outlet (Figure 2.8b). In this case, the homogeneous distribution of imperviousness with $H = 30\%$ corresponds to a horizontal line at 30%. Values above and below this line indicate areas with higher and lower imperviousness than the average. Figure 2.8b shows large portions of the curve below and above the line. This is an indication that the watershed has relatively large sectors that are either highly impervious or highly pervious. A more homogeneous distribution of the imperviousness would imply both less deviation from the horizontal line and smaller portions consistently above or below the line. The three regions with high imperviousness identified in Figure 2.8 are shown in a map of the watershed (Figure 2.9). The region located in the range 0 - 1000 m from the outlet has several buildings and parking lots (section a). A big portion of the regions located in the range 4500 - 5300 m from the outlet corresponds to the downtown area, in which vegetation is limited and where entire blocks are used for parking lots (section b). The other portion located at this range (section c) does not show areas as impervious as those observed in section "b". Finally, Figure 2.9 shows five big buildings, with their respective parking lots, in the area located in the range 5900 - 6800 m from the outlet (section d).

The application of $H(x)$ to this specific watershed validates hypothesis 3. In particular, we showed that this function can be used to differentiate various patterns of imperviousness. This or other similar tools can be used in planning and optimizing new urban development and serve as a complementary approach to others previously developed. In fact, $H(x)$ and $W(x)$ can be used to define an initial scenario for

optimization routines that aim to achieve the optimum distribution of imperviousness (Yeo et al., 2004; Tang et al., 2005; Mejía and Moglen, 2009). Another potential application of $H(x)$ is in the estimation of the hydrologic response of the watershed. The spatial representation of the runoff generation provided by $H(x)$ can be rescaled to the temporal scale by defining constant or variable flow velocities along the flow paths. The result of this rescaling process would correspond to the instantaneous unit hydrograph (IUH), that is the response of the watershed to a unit excess pulse of excess rainfall. The IUH can then be used to build responses to longer, more complex storms (Chow et al., 1988). The major drawback in using this approach as shown in this study is that artificial surface and subsurface conduits are not considered in the identification of the flow paths. Thus, flow distances extracted from the DEM may be different to the actual distances and the use of $W(x)$ and $H(x)$ in existent watersheds can be limited. However, this disadvantage would be less restrictive at early stages in urban planning in which the natural drainage network can be used as an initial approximation of the future stormwater drainage network. In such scenario, $W(x)$ and $H(x)$ can be used to define optimum spatial patterns of impervious area.

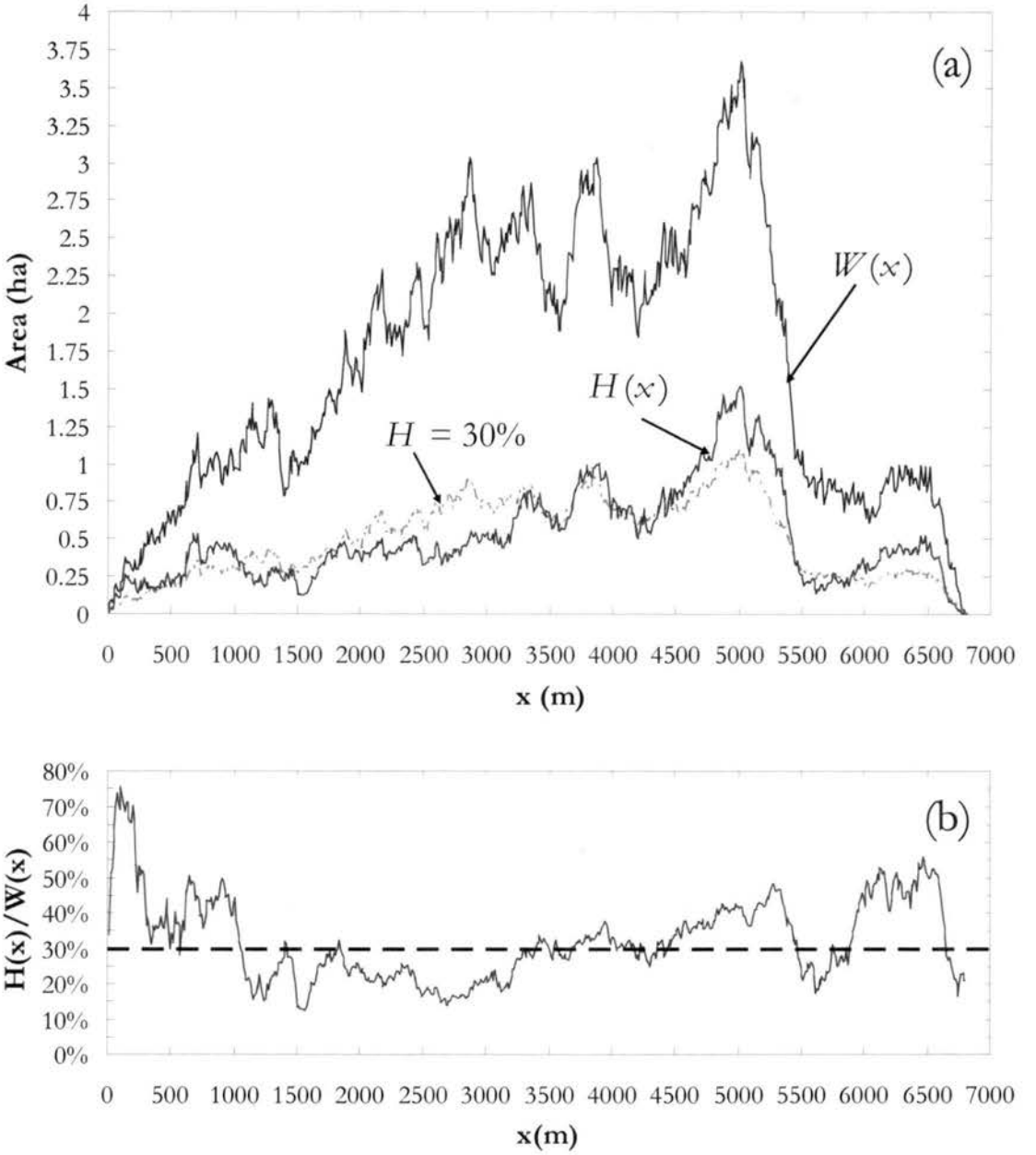

Figure 2.8. Distribution of imperviousness within the Pigeon House Creek watershed. (a) The width function, $W(x)$, the imperviousness function, $H(x)$, and the imperviousness function assuming a constant imperviousness distribution of 30%, (b) ratio $H(x)/W(x)$ indicating the distances at which the percentage of imperviousness is larger than the average (above the 30% line) and smaller than the average (below the 30% line).

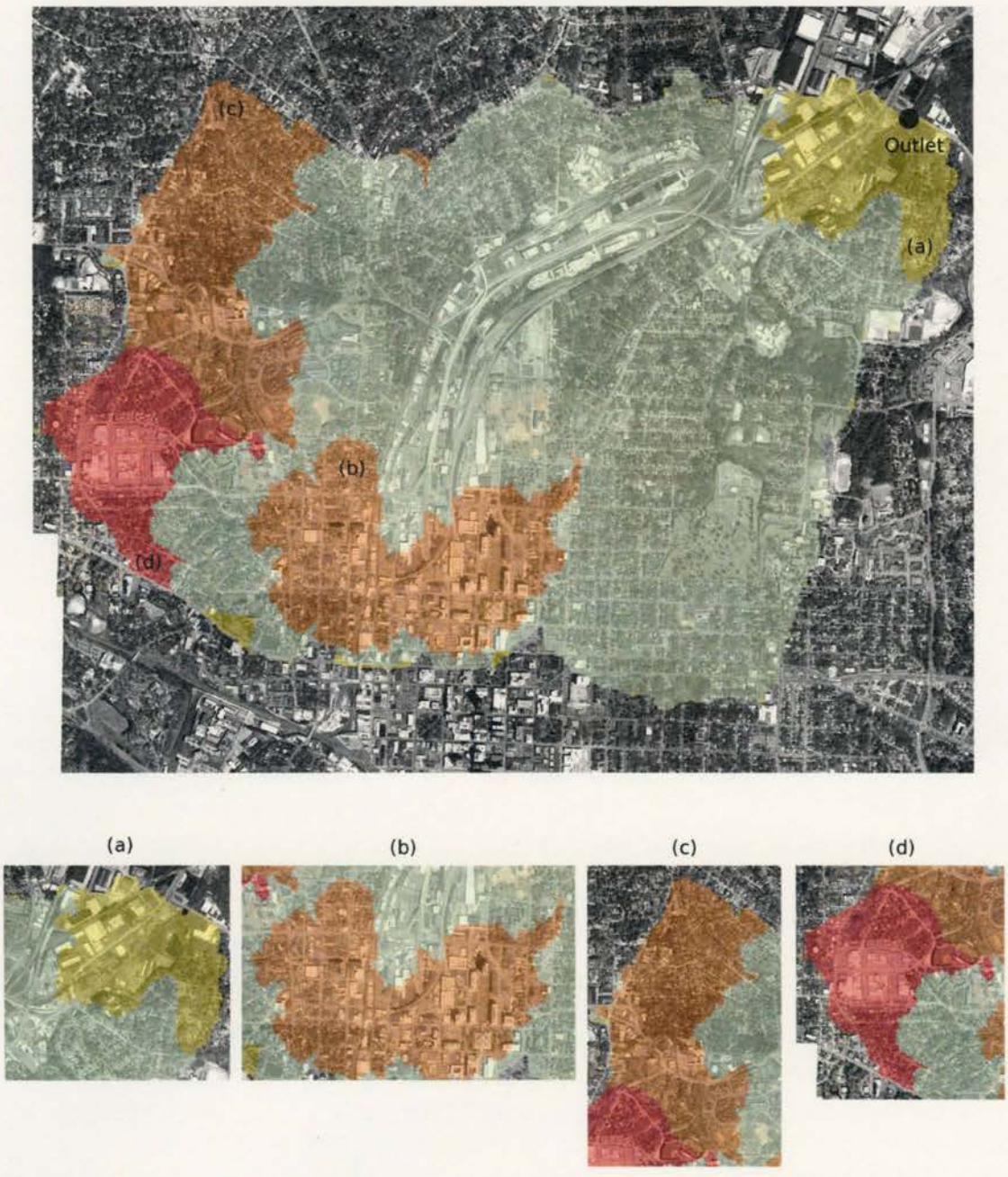

Figure 2.9. Location of areas highly developed within the Pigeon House Creek watershed according the imperviousness function. (a) area located in the range 0 - 1000 m from the outlet, (b and c) area located in the range 4500 - 5300 m from the outlet, (d) area located in the range 5900 - 6800 m from the outlet.

2.4 Conclusions

Morphology of river basins has been studied in detail in natural watersheds. Nevertheless, only a portion of this research has occurred in urban settings, and many aspects of the morphology of urban watersheds and the impacts of urbanization on the natural drainage network remain to be addressed. Three hypotheses regarding the applicability of morphologic theories to urban watersheds were identified in this study. These hypotheses were tested using different morphological measurements widely applied in the field of basin morphology. The main conclusions from this analysis are as follow:

1. Morphologic features can be used to quantify the impact of urbanization. Scaling exponent of the Hack's law (h = 0.46) and the cumulative distribution of contributing areas ($\beta = 0.53$) are quite different to those observed in natural catchments. The low value of h and high value of β might be related to changes in the internal organization of the watershed associated with a high degree of aggregation at smaller scales.

2. Morphologic features can be used to determine the spatial scales at which these impacts occur and are more significant. The slope-area relationship shows alteration to morphologic properties of streams and unchannelized portions of the watershed. Unusually high slopes are observed in the main streams which can be associated with an overall shortening of these streams that implies changes of elevation in shorter distances

3. Morphologic features can be used to classify and characterize different urban settings or patterns. This was demonstrated by applying the width function and the imperviousness function to two differentiate imperviousness distributions. As a representation of the runoff production in urban settings, the imperviousness function

may have a remarkable potential for the quantification of the hydrologic response. Such a quantification would be of the highest relevance given that hydrologic data for more traditional modeling approaches are not typically available in urban watersheds.

4. Given that only one watershed was used in this study, our findings may not necessarily be valid for other urban watersheds. In addition, the explanations provided for some of the results here are not definitive and more research is needed to validate them. However, the results show that the study of morphologic features in urban setting can reveal possible modifications in the watershed structure.

5. Although the results show that some of the urban features are probably resolved in raw DEMs, it is clear that many artificial conduits (e.g. streets, pipes, swales) cannot be extracted from such data. Thus, flow paths identified from raw DEMs do not necessarily represent the real flow paths. This issue can affect in some degree the computation of some of the morphologic properties studied or other not included in this work. Existing alternatives to preprocess DEMs (e.g. Zech et al., 1994; Rodriguez et al., 2000) can be used to "burn" the artificial conduits into the raw DEM before computing flow directions and flow distances. These methods are based on the constant reduction of the elevation of cells where these conduits are located. The validity of these methods remains to be studied, and a better methodology may be developed in case they do not allow for a good representation of the drainage structure.

6. From this work we identify possible improvements to current approaches in the study and modeling of urban watersheds, which are summarized in Figure 2.10. First, the study of morphologic characteristics can provide with alternative methodologies to evaluate impacts of urbanization. Current methodologies are largely focused on the

imperviousness as the main explanatory variable of ecologic, biologic and hydrologic effects of urbanization. This work shows that other properties characterizing the watershed's drainage structure change as well with urban development. The correct assessment of these changes can be of relevancy to explain urbanization impacts. Second, the study of basin morphologic characteristics can provide us with tools to evaluate the impact of urbanization at a wide range of scales. Currently the study of geomorphic effects of urbanization has mainly focused on single streams located at the outlet of the watershed. However, urbanization impacts take place not only downstream from the watershed, but also within it, affecting the entire drainage structure of the basin as a whole. The correct assessment of the scales and magnitudes of these changes can be achieved through the use of tools such as the ones presented in this study. Finally, morphologic properties defined at different spatial scales may provide new insight in the adequate spatial distribution and integration of drainage solutions. Current drainage practices are mostly conceived for operating at relatively small scales within the urban context (i.e. from the lot to the sub-division scale). Thus, the real effect of these practices over the entire watershed as a whole remains unclear. Morphologic considerations might be also incorporated in more recent studies that attempt to identify optimum distributions of BMPs within the watershed (e.g. Zhen et al., 2004 and Perez-Pedini et al., 2005).

2.5 Acknowledgments

The authors thank the generous financial support from the Harold H. Short endowed fund for the Civil Infrastructure System Laboratory at Colorado State University.

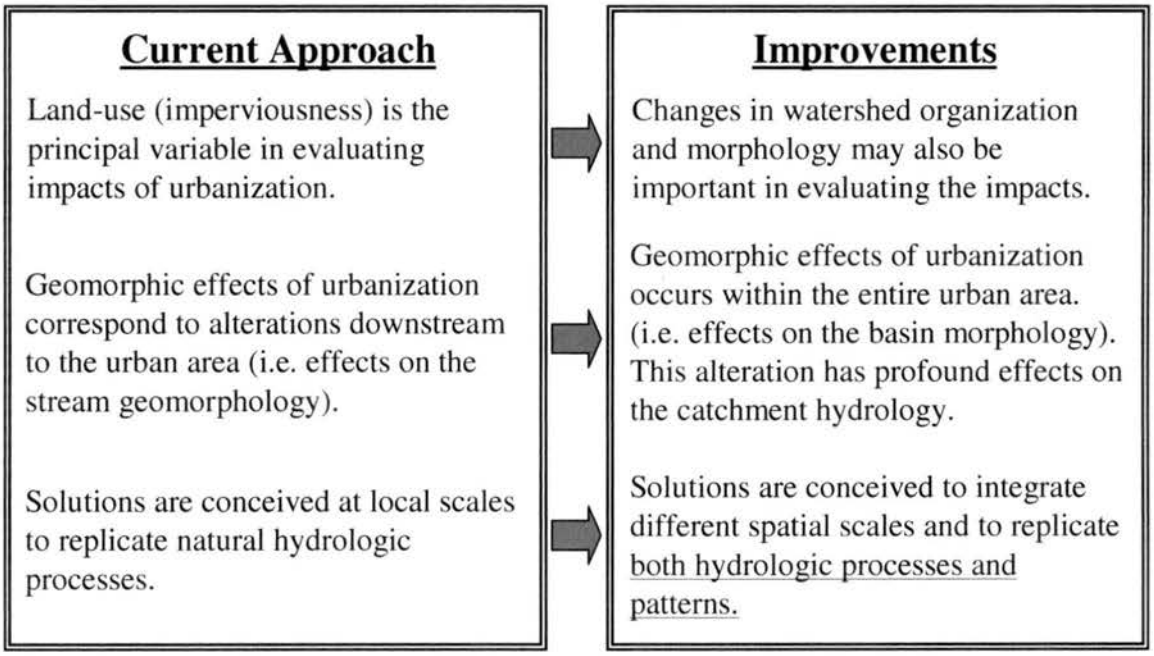

Figure 2.10. Possible improvements in the study of urban watersheds based on a morphologic approach.

2.6 References

Allen, P.M., Narramore, R.L., 1985. Bedrock controls on stream channel enlargement with urbanization, North Central Texas. Water Resources Bulletin 21(6), 1037-1048.

Allen, P.M., Arnold, J.G., Skipwith, W., 2008. Prediction of channel degradation rates in urbanizing watersheds. Hydrological Sciences Journal 53(5), 1013-1029.

Bannister, E.N., 1979. Impact of road networks on southeastern Michigan Lakeshore drainage. Water Resources Research 15(6), 1515-1520.

Bedient, P.B., Huber, W.C., 2002. Hydrology and Floodplain Analysis, 3rd Ed. Prentice-Hall, Upper Saddle River, NJ, p. 763.

Bledsoe, B.P., Watson, C.C., 2001. Effects of urbanization on channel instability. Journal of the American Water Resources Association 37(2), 255-270.

Booth, D.B., 1990. Stream channel incision following drainage basin urbanization. Water Resources Bulletin 26(3), 407-417.

Bras, R., 1990. Hydrology, an Introduction to Hydrologic Science. Addison-Wesley, Reading, MA, p. 643.

Chow, V.T, Maidment, D.R., Mays, L.W., 1988. Applied Hydrology. McGraw-Hill, Inc, NY, p. 572.

Claessens, L., Hopkinson, C., Rastetter, E., Vallino, J., 2006. Effect of historical changes in land use and climate on the water budget of an urbanizing watershed. Water Resources Research 42 (3). doi:10.1029/2005WR004131.

Dietrich, W.E., Wilson, C.J., Montgomery, D.R., McKean, J., 1993. Analysis of erosion thresholds channel networks and landscape morphology using a digital terrain model. Journal of Geology 101(2), 259-278.

Dodds, P.S., Rothman, D.H., 1999. Unified view of scaling laws for river networks. Physical Review E 59(5), 4865-4877.

Dodds, P.S., Rothman, D.H., 2000. Scaling, universality, and geomorphology. Annual Review of Earth and Planetary Sciences 28, 571-610.

Eagleson, P.S., 1970. Dynamic Hydrology. McGraw-Hill, Inc, NY, p. 462.

Flint, J.J., 1974. Stream gradient as a function of order, magnitude and discharge. Water Resources Research 10(5), 969-973.

Graf, W.L., 1977. Network characteristics in suburbanizing streams. Water Resources Research 13(2), 459-463.

Gray, D.M., 1961. Interrelationships of watersheds characteristics. Journal of Geophysical Research 66(4), 1215-1223.

Hack, J.T., 1957. Studies of longitudinal stream profiles in Virginia and Maryland. US Geological Survey Professional Paper 294-B, 45-97.

Han, W.S, Burian, S.J., 2009. Determining effective impervious area for urban hydrologic modeling. Journal of Hydrologic Engineering 14(2), 111-120.

Hergarten, S., 2002. Self-organized Criticality in Earth Systems. Springer-Verlag, Berlin, Germany.

Hayden, R.S., 1981. Road drainage and equilibrium in small stream basins. The Professional Geographer 33(4), 429-435.

Horton, R.E., 1945. Erosional development of streams and their drainage basins: hydrophysical approach to quantitative morphology. Bulletin of the Geological Society of America 56(3), 275-370.

Howard, A.D., 1971a. Optimal angles of stream junctions: geometric, stability to capture, and minimum power criteria. Water Resources Research 7(4), 863-873.

Howard, A.D., 1971b. Simulation of stream networks by headward growth and branching. Geographical Analysis 3(1), 29-50.

Huang H.J., Cheng, S.J., Wen, J.C., Lee, J.H., 2008. Effect of growing watershed imperviousness on hydrograph parameters and peak discharge. Hydrological Processes 22(13), 2075–2085.

Ijjász-Vásquez E.J., Bras R.L., 1995. Scaling regimes of local slope versus contributing area in digital elevation models. Geomorphology 12(4), 299-311.

Kim, Y., Engel, B.A., Lim, K.J., Larson, V., Duncan, B., 2002. Runoff impacts of land-use change in Indian River lagoon watershed. Journal of Hydrologic Engineering 7(3), 245-251.

Lhomme, J., Bouvier, C., Perrin, J. L., 2004. Applying a GIS-based geomorphological routing model in urban catchments. Journal of Hydrology 299(3-4), 203-216.

Maritan, A., Rinaldo, A., Rigon, R., Giacometti, A., Rodríguez-Iturbe, I., 1996. Scaling laws for river networks. Physical Review E 53(2), 1510-1515.

McNamara, J.P., Ziegler, A.D., Wood, S.H, Vogler, J.B., 2006. Channel head locations with respect to geomorphologic thresholds derived from a digital elevation model: a case study in northern Thailand. Forest Ecology and Management 224(1-2), 147-156.

Mejía, A.I., Niemann, J.D., 2008. Identification and characterization of dendritic, parallel, pinnate, rectangular, and trellis networks based on deviations from planform

self-similarity. Journal of Geophysical Research 113. F02015 doi:10.1029/2007 JF000781.

Mejía, A.I., Moglen, G.E., 2009. Spatial patterns of urban development from optimization of flood peaks and imperviousness-based measures. Journal of Hydrologic Engineering 14(4), 416-424.

Melesse, A.M., Graham, W.D., 2004. Storm runoff prediction based on a spatially distributed travel time method utilizing remote sensing and GIS. Journal of the American Water Resources Association 40(4), 863-879.

Mesa, O.J., Gupta, V.K., 1987. Main channel length-area relationship for channel networks. Water Resources Research 23(11), 2119-2122.

Montgomery, D.R., Foufoula-Georgiou, E., 1993. Channel network source representation using digital elevation models. Water Resources Research 29(12), 3925-3934.

Olivera, F., Furnans, J., Maidment, D.R., Djokic, D., Ye, Z., 2002. Drainage systems. In: Maidment, D.R. (Ed), Arc Hydro, GIS for Water Resources. ESRI, Redlands, CA, pp. 55-86.

Perez-Pedini,C., Limbrunner, J.F., Vogel, R.M., 2005. Optimal number and location of BMPs for stormwater management. Journal of Water Resources Planing and Management 131(6), 441-448.

Phillips, J.D., 1985. Stability of artificially-drained lowlands - a theoretical assessment. Ecological Modelling 27(1-2), 69-79.

Pomeroy, C.A., Roesner, L.A., Coleman II, J.C., Rankin, E., 2008. Protocols for studying wet weather impacts and urbanization patterns, Report 03WSM3. Water Environment Research Foundation, Alexandria, VA.

Rodriguez, F., Andrieu, H., Zech, Y., 2000. Evaluation of a distributed model for urban catchments using a 7-year continuous data series. Hydrological Processes 14(5), 899-914.

Rodríguez-Iturbe, I., Ijjász-Vásquez, E.J., Bras, R.L., Tarboton, D.G., 1992. Power law distributions of discharge mass and energy in river basins. Water Resources Research 28(4), 1089-1093.

Rodríguez-Iturbe I., Rinaldo A., 1997. Fractal River Basins: Chance and Self-Organization. Cambridge University Press, New York, pp. 547.

Scheidegger, A.E., 1967. A stochastic model for drainage patterns into an intramontane trench. Bulletin of the International Association of Hydrologists 12(1), 15-20.

Schumm, S.A., 1956. Evolution of drainage systems and slopes in Badlands and Perth Amboy, New Jersey. Bulletin of the Geological Society of America 67(5), 597-646.

Shreve, R.L., 1966. Statistical law of stream numbers. Journal of Geology 74(1), 17-37.

Shreve, R.L., 1967. Infinite topologically random channel networks. Journal of Geology 75(2), 178-186.

Sivapalan, M., 2005. Pattern, process and function: elements of a unified theory of hydrology at the catchment scale. In: Anderson, M.G. (Ed), Encyclopedia of Hydrological Sciences, Chapter 13. John Wiley & Sons, Ltd., UK, pp. 193-219.

Smith, J.A., Baeck, M.L., Morrison, J.E., Sturdevant-Rees, P., Turner-Gillespie, D.F., Bates, P.D., 2002. The regional hydrology of extreme floods in an urbanizing drainage basin. Journal of Hydrometeorology 3(3), 267-282.

Strahler, A.N., 1957. Quantitative analysis of watershed geomorphology. Transactions of the American Geophysical Union 38(6), 913-920.

U.S. Geological Survey (USGS), 2003. National Land Cover Database Zone 60 Imperviousness Layer. Edition 1.0. U.S. Geological Survey. Sioux Falls, SD.

U.S. Geological Survey (USGS), 2006. National Elevation Dataset (NED) 1/3 Arc Second (~10m) Digital Elevation Map. U.S. Geological Survey. Sioux Falls, SD.

Tang, Z., Engel, B.A., Lim, K.J. Pijanowski, B.C., Harbor, J., 2005. Minimizing the impact of urbanization on long term runoff. Journal of the American Water Resources Association 41(6), 1347-1359.

Tarboton, D.G., Bras, R.L., Rodríguez-Iturbe, I., 1989. Scaling and elevation in river networks. Water Resources Research 25(9), 2037-2051.

Tucker, G.E., Bras, R.L., 1998. Hillslope processes, drainage density, and landscape morphology. Water Resources Research 34(10), 2751-2764.

Willgoose, G.R., Bras, R.L., Rodríguez-Iturbe, I., 1991. A physical explanation of an observed link area-slope relationship. Water Resources Research 27(7), 1697-1702.

Yeo, I.-Y., Gordon, S.I, Guldmann, J.-M., 2004. Optimizing patterns of land use to reduce peak runoff flow and nonpoint source pollution with an integrated hydrological and land-use model. Earth Interactions 8(6), 1-20.

Yeo, I.-Y., Guldmann, J.-M., Gordon, S.I., 2007. A hierarchical optimization approach to watershed land use planning. Water Resources Research 43, W11416, doi:10.1029/2006WR005315.

Zech, Y., Sillen, X., Debources, C., Van Hauwaert, A., 1994. Rainfall-runoff modelling of partly urbanized watersheds: comparison between a distributed model using GIS and other models sensitivity analysis. Water Science and Technology 29(1-2), 163-170.

Zhen, X.Y., Yu, S.L., Lin, J.Y., 2004. Optimal location and sizing of stormwater basins at watershed scale. Journal of Water Resources Planing and Management 130(4), 339-347.

3. Evaluation of Methods for Representing Urban Terrain in Stormwater Modeling

Abstract: Many stormwater modeling problems consider watersheds comprised of complex flow networks including surfaces, streets, pipes, and channels. Ideally, hydrologic methods would be used to model the accumulation of runoff on surfaces while hydraulic methods would be used to explicitly model the flow in each street, pipe, and channel. In many practical circumstances, only the largest pipes and channels are explicitly modeled with hydraulic methods. Thus, most subcatchments include numerous streets and small pipes that can affect the accumulation and movement of flow. Digital Elevation Models (DEMs) are widely used to determine geometric characteristics of these subcatchments, but street gutters and pipes are not resolved in such data. To overcome this problem, known streets and pipes are often "burned" into the surface by reducing the local elevations by a specified amount before calculating flow paths and the associated subcatchment characteristics. In this paper, existing and proposed methods for including these conduits into DEM surfaces are evaluated. The results suggest that the derived characteristics are sensitive to the selected method. We also find that a new method, which makes use of known pipe elevations, is most successful at reproducing realistic flow paths. Finally, we find that errors in the implied watershed characteristics are difficult to overcome by calibration of other model parameters.

3.1 Introduction

Distributed and semi-distributed models are widely used to study and solve stormwater problems. These models typically have a hydrologic component that calculates the production and accumulation of runoff at inlets on the drainage system and a hydraulic component that routes flow through the drainage system. When modeling mid to large areas, all inlets on the drainage system and their associated subcatchments are typically not modeled explicitly due to the cost associated in collecting and using this data in the model (Huber and Dickinson, 1988). Instead, the watershed is divided into a selected number of subcatchments that direct flow into the major elements of the drainage system. The number of subcatchments is usually selected to capture the most important variations in site characteristics and processes and to generate results at points of interest (Huber and Dickinson, 1988; Bedient and Huber, 2002). Each subcatchment therefore contains numerous streets, pipes, swales and even small natural channels that can play significant roles in directing flow within the subcatchment. Most stormwater models represent the hydrologic response of these subcatchments using a lumped approach, so the catchment structure is described using a small number of geometric or kinematic properties. Table 3.1 shows the hydrologic methods used to describe subcatchment flow accumulation in five widely-used stormwater models as well as the required geometric or kinematic properties. All the models in Table 3.1 require either a flow-path length or a travel time to represent the response time of the subcatchment as well as other parameters to simulate the storage effect. These characteristics likely depend on the configuration of streets, pipes, and channels within each subcatchment.

Table 3.1. Geometric and kinematic properties required in widely-used stormwater models.

Model	Reference	Subcatchment hydrologic method	Geometric or kinematic properties
SWMM[1]	Rossman (2008) Huber and Dickinson (1988)	Non-linear reservoir model	Area, width, slope, and roughness coefficients
CANOE	Lhomme et al. (2004)	Linear reservoir model	Parameter K depending on area, slope, length and impervious coefficient
RORB[2]	Laurenson et al. (2007) Laurenson and Mein (1995) Selvalingam et al. (1987)	Non-linear reservoir model	Empirical exponent m, a coefficient characterizing the watershed, Kc and the relative delay time, Kr
HEC-HMS[3]	USACE-HEC (2006)	Seven methods: Clark Unit Hydrograph (CUH), Kinematic Wave (KW), ModClark Transform (MCT), SCS Unit Hydrograph (SCSUH), Snyder Unit (SUH) Hydrograph, User-Specified S-Graph (USS) and User-Specified Unit Hydrograph (USUH)	Time of concentration and storage coefficient (CUH, MCT); area, and length, slope and roughness coefficients of subcatchment and downstream channel (KW); lag-time (SCSUH, USS); standard lag, peaking coefficient (SUH)
MUSIC[4]	MUSIC Development Team (2005)	No explicit routing. Muskingum Cunge with a time step of 6 min can be adapted to simulate a drainage link (Elliott and Trowsdale, 2007)	Muskingkingum-Cunge parameters K (translation time) and θ (dimensionless weighting factor)

[1] *SWMM : Storm Water Management Model*
[2] *RORB : Originally stands for Runoff Routing on a Burroughs B6700 computer (Laurenson et al. 2007)*
[3] *HEC-HMS : Hydrologic Engineering Center-Hydrologic Modeling System*
[4] *MUSIC : Model for Urban Stormwater Improvements Conceptualization*

Geographical information system (GIS) tools are often used to calculate the required geometric or kinematic properties from Digital Elevation Models (DEMs). Just like DEMs for rural areas, urban DEMs are used to define subcatchment boundaries and drainage patterns and to perform simplified flow calculations (Djokic and Maidment, 1991). Numerous successful applications of GIS have also been reported not only in the scientific literature but also in current stormwater management practice (e.g., Doan,

2000; Jordan and Grimison, 2001; Barco et al., 2008). Nonetheless, the uncertainty associated with the extraction of geometric properties from urban DEMs can be significant. Subsurface conduits are obviously not represented in DEMs, and features such as streets (particularly gutters), small channels, and buildings may not be visible even in relatively high-resolution DEMs. Failure to account for these features may introduce significant errors in the hydrologic characteristics derived from the DEM. Therefore, algorithms developed to characterize rural watersheds based on DEMs should not be applied directly to urban terrain (e.g., Djokic and Maidment, 1991; Smith, 1993; Doan, 2000; Maksimovic and Prodanovic, 2001).

The most common method used to improve the representation of anthropogenic features in urban DEMs is the "burning" technique. In this method, a constant depth is subtracted at all cells that include a known conduit that is not resolved by the DEM (e.g., Elgy et al., 1993; Zech et al., 1994; Zech and Escarmelle, 1999; Rodriguez et al., 2000; Mark et al., 2004; Lhomme et al., 2004; Hunter et al., 2008, Hankin et al., 2008). After the DEM is modified by this method, it is used to extract the required properties for modeling (Table 3.1). In addition to this method, other authors have explored manual processing of DEMs and restrictions on the flow direction algorithm (Smith and Vidmar, 1994) as well as the use of high-resolution DEMs (less than 5 m) (e.g., Blackwell and Wells, 1999; Schmitt et al., 2004). Rodriguez et al. (2003, 2005 and 2008) represented flow paths explicitly along all known streets and pipes as a vector map that was independent of the DEM representation. Unchannelized surface flow was also defined independent of the DEM by assuming a straight flow path from each hydrologic element to the closest street. Others authors have artificially increased the elevations of DEM

cells where buildings or houses are known to occur (Elgy et al., 1993; Zech et al., 1994; Beffa, 1998; Zech and Escarmelle, 1999; Rodriguez et al., 2000; Nie et al., 2002; Mark et al., 2004; Ryan, 2005; Hunter et al., 2008). Several successful applications of modified DEMs have been reported in the literature (see next section), but the effect of the modification method on the computed geometric and kinematic properties as well as the hydrologic response remains unclear. Bedient and Huber (2002) identified factors affecting the shape and timing of the response hydrograph for a given watershed. Several of these factors are related to properties extracted from the modified DEM such as the subcatchment area, slope, shape and drainage network organization. Therefore, it is possible that the choice of the modification method has significant implications and that one particular method is better suited to reproduce the subcatchment characteristics.

The objective of this paper is to evaluate different methods for representing urban terrain in stormwater modeling. We consider using the raw DEM as well as "burning" the anthropogenic conduits in the DEM by subtracting a constant elevation for cells with known streets and a larger constant elevation for cells with known pipes. Two pairs of burning depths are evaluated. We also propose a method where different elevations are subtracted to capture the known slopes of streets and pipes. These alternatives are compared against a new method in which the entire pipe system within each subcatchment is represented as a distinct GIS layer that receives inflow at assumed inlet locations. In this method, the surface flow is derived from a modified DEM in which streets have been "burned" using the variable burning depth. These methods are applied and compared for multiple catchments in the city of Nantes, France, where comprehensive information allows identification of the entire drainage network and an

accurate representation of the flow paths and geometric and kinematic properties. The methods are evaluated in terms of the geometric and kinematic properties that they produce and in terms of the resulting hydrologic behavior. The hydrologic implications are evaluated using the Storm Water Management Model (SWMM) (Rossman, 2008) with both synthetic and real storms. The outline of the paper is as follows. The next section provides detailed explanations of the methods used to represent urban terrain. Then, the study area and associated dataset are described. Next, the geomorphic and hydrologic implications of the terrain-processing methods are analyzed, and finally, the key conclusions are summarized.

3.2 Methods for Urban Terrain Representation

We consider four methods to represent anthropogenic elements in urban DEMs. Three of them are defined in one layer of information, corresponding to a raw or modified DEM. The fourth method includes a surface layer (a modified DEM) and a vector subsurface layer. All these methods are applied to square-grid DEMs because they are most widely available and used (Garbrecht et al., 2001), and facilitate mathematical processing (Olivera et al., 2002). Post-processing of the resulting DEMs is done with tools available in Arc GIS and Arc Hydro (Olivera et al., 2002). These tools include sink filling, determination of flow directions (using the direction of steepest descent), accumulation of flow, and computation of flow lengths. Once these procedures are applied, all of the geometric properties that are required by the hydrologic models in Table 3.1 can be calculated. The following subsections describe the four methods including previous applications and reasons justifying their use in this work.

3.2.1 Method 1, use of raw DEM

The first method we consider (method 1) is the direct use of the DEM. This practice is very common in urban stormwater modeling. For example, Doan (2000) represented an urban terrain using a raw DEM, which was then used to construct a HEC-HMS model. Although the observed and simulated peak flows were similar, he concluded that the DEM resolution (30 m) was too coarse to support detailed representation of subcatchments and streams and that flow patterns affected by man-made structures were not properly derived from the DEM. Jordan and Grimison (2001) used a raw DEM to generate flow patterns and delineate subcatchments in an urban area, and they built a model in SWMM to simulate the performance of a storage pond. Once the model was calibrated, the simulated behavior matched the measured values almost exactly. Barco et al. (2008) used a raw 7.5 min DEM to compute urban subcatchment properties for a SWMM model and developed an automatic calibration process. After calibration, only two of ten simulations had errors in either volume or peak flow greater than 16%. Finally, Pomeroy et al. (2008) used raw 10 m DEMs to develop and calibrate SWMM models for several urban and semi-urban watersheds in North Carolina in order to study the effects of urbanization on ecology and geomorphic stability of streams.

3.2.2 Method 2, street and pipe burning

Several studies have developed methods to force the runoff to flow along streets and pipes by defining an artificial reduction in the elevation of grid cells with these features. Some authors use the actual average depth of these conduits when burning them, while

others exaggerate the vertical dimension to guarantee that no flow in them returns to the surface. Lhomme et al. (2004) used a 25 m DEM to successfully apply both a semi-distributed model and a GIS-based geomorphological routing model to study an urban catchment. They modified the DEM by subtracting a constant, exaggerated depth of 50 m from each cell that is crossed by a pipe or a channel before processing the flow paths. Hankin et al. (2008) compared different approaches in modeling urban flooding in which road networks were "stamped" by lowering the DEM elevations by 0.1 - 0.15 m. They used this DEM to test different flooding models. Numerous authors have proposed reductions of cell elevations representing conduits in addition to increasing the elevation of cells occupied by buildings. Elgy et al. (1993) lowered by 0.5 m all the cells occupied by streets in a gridded terrain model with a resolution of 1 m. Flow simulations with parameters derived from the modified DEM agreed well with simulations based on manually derived parameters. Zech et al. (1994) used a 5 m DEM and represented the collectors by fictitious trenches whose depths were not specified in the reference. The resulting urban terrain was used to build a distributed hydrologic model whose results agreed well with observations and results from other models. Zech and Escarmelle (1999) used a similar approach with a 30 m DEM in which trenches were produced by decreasing elevations by 1 m. Rodriguez et al. (2000) modified a 5 m DEM to represent the sewer network. This modified DEM was used to evaluate the model SURF (Zech et al., 1994). Mark et al. (2004) used a 1D model to simulate urban flooding in which streets were "burned" on the DEM. They concluded that a 5 m resolution DEM (or finer) allows sufficiently accurate representation of the different man-made elements of the urban terrain in urban flood analysis. Finally, Hunter et al. (2008) developed a so-called

benchmark DEM (2 m resolution), in which roads and curbs were "burned" by decreasing the cells elevations by 0.1 m.

In this paper, the burning technique is implemented by lowering the elevation of all grid cells that are occupied by streets or pipes. Streets are burned because flow in them is typically conveyed by gutters and curbs disallow this flow to leave the street. In our implementation, the elevation adjustment is smaller for grid cells occupied by streets than pipes. If a grid cell contains both pipes and streets, then the elevation adjustment for pipes is used. This approach attempts to prioritize the flow through pipes and avoid flows from pipes back to streets or the surface. Pipes sometimes flow into natural streams, so we also burned streams as though they were pipes to avoid flow spilling onto the surface. For this paper, we implemented two burning methods (methods 2a and 2b). Method 2a uses elevation reductions of 1 m and 2 m for street cells and pipe cells, respectively, and method 2b uses reductions of 2 m and 5 m, respectively.

3.2.3 Method 3, variable burning of pipes and streets

A major drawback of method 2 is that the flow directions in the trenches are determined by the slope of the ground surface as represented in the original DEM. Because pipes often do not flow in the same direction as the ground surface, we developed a new method (method 3). In this method, the elevation adjustments for streets and pipes vary by location according to the real depths in each cell to be modified. Thus, the flow directions in the anthropogenic conduits do not necessarily coincide with the flow directions implied by the original DEM.

The main points of our algorithm are as follows. The algorithm requires a shapefile

for the streets and another shapefile for the pipes. Each shapefile contains the planar coordinates x and y, and the elevation coordinates z for both ends of every street or pipe segment. The algorithm is applied in two phases. The first burns the streets, and the second burns the pipes. The algorithm begins by transforming the street shapefile feature into a raster map, which has the same resolution and spatial extent as the DEM to be modified. The elevations of all the cells belonging to this new raster are first obtained from the raw DEM and then modified using the following steps. First, the cells where segment endpoints are located are assigned the elevations corresponding to those endpoints. Then, the elevations of the cells crossed by conduits connecting two endpoints are defined by interpolating between the endpoint elevations. Once the DEM has been modified to include the streets, the methodology is repeated for the pipes, using the street-modified DEM as the DEM into which the pipes will be burned. Figure 3.1 illustrates these steps.

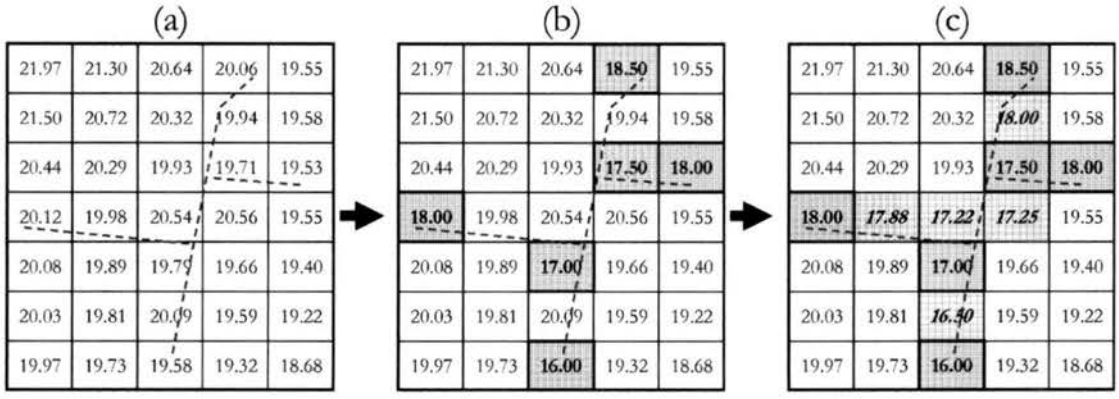

Figure 3.1. Modification of the DEM using method 3. (a) original DEM (in meters) and conduits (dash lines) (b) elevations of cells corresponding to conduit endpoints are redefined (grey cells in bold), and (c) elevations of cells between endpoints are interpolated.

3.2.4 Method 4, surface and subsurface layers

We also developed a more complete method in which the surface drainage (including the land surface and streets) and the pipe system are defined using separate GIS layers. The surface drainage is represented by a modified DEM and the pipe system and known natural channels are represented by a vector layer. Natural channels are included in the vector layer because some pipes drain into natural channels. Flow can move between the surface layer and the pipe system through designated inlet locations. Whenever surface flow encounters a cell with an inlet, it is assumed to move into the pipe system. The pipes in the vector layer are not modeled using hydraulic methods. Instead, they are used in combination with the surface layer to calculate the basic geometric and kinematic characteristics of the subcatchments. For example, the total area contributing to a particular point is defined as the sum of the areas draining into the pipe system that conveys flows to that point. Once flow enters the pipe system, it is assumed to remain in the pipe system (i.e. overflow of stormwater pipes is not considered). This is a common assumption for frequent storm events (Greene and Cruise 1995; Rodriguez et al. 2003, 2005, 2008) because pipe systems are usually designed to convey the discharges produced by these storms.

This method (method 4) requires information regarding the pipe network in order to be implemented. Like the method 3, it needs pipe locations and elevations in order to define the directions of flow in the pipe network. It also uses the real lengths of the pipes to compute the flow path lengths. Ideally, known inlet locations would be used to transfer flow between the surface and subsurface layers. However, these locations are rarely known, so their locations are assumed. The steps required to implement method 4

are given below.

1. The DEM is modified to represent the streets according to the methodology defined in method 3 that uses the x, y and z coordinates of the ends.
2. The resulting DEM from step 1 is processed using the terrain processing tools available in Arc Hydro to remove any pits and define the flow directions.
3. The locations of the first of three types of inlets are identified. These so-called type *I* inlets are located in cells at the beginning of the pipe system (upstream ends of the most upstream pipes).
4. The locations of the second type of inlets (type *II*) are identified. These inlets are located in pipes near street intersections as proposed by Rodriguez et al. (2003, 2005). If a pipe lies within10 m of an intersection, an inlet is specified on the pipe at the point closest to the intersection. If more than one pipe is located in the 10 m buffer, the inlet is defined in the closest pipe to the intersection.
5. Next, type *III* inlets are identified. These inlets are defined anywhere a flow path on the DEM intersects a natural channel in the vector layer. These inlets are specified because flow can enter natural channels anywhere along their path.
6. The flow distances L_n from each inlet n to the outlet of the subcatchment are calculated next. This distance is calculated as follows:

$$\begin{aligned} L_n &= \sum_{k=1}^{k=j} L_{n,k} && \text{if n = inlet type I and III} \\ L_n &= d_n + \sum_{k=1}^{k=j} L_{n,k} && \text{if n = inlet type II} \end{aligned} \tag{3-1}$$

where j=the number of pipes connecting inlet n to the subcatchment outlet, $L_{n,k}$=flow distance of the k^{th} pipe belonging to the j pipes connecting inlet n and the watershed

outlet; d_n=horizontal distance between the street intersection and the inlet n, defined only for type *II* inlets and measured orthogonal to the orientation of $L_{n,1}$, the pipe where the inlet is located. As an example, Figure 3.2 illustrates the computation of L_n for a type *II* inlet. Note that if n is a type *I* inlet, $L_{n,1}$ equals the entire length of the pipe into which the flow enters. Otherwise, $L_{n,1}$ is only a fraction of the total length of the first pipe segment depending on the location of the inlet. Thus, the length of pipe between the inlet and the downstream endpoint is estimated by multiplying the supplied length of the pipe segment by the ratio between the length of the straight line from the inlet to the downstream end of the pipe segment and the length of straight line connecting the upstream and downstream endpoints of the pipe segment. The total flow length from any point in a subcatchment to the subcatchment outlet can be calculated by summing the overland flow distance (on the DEM) calculated via Arc Hydro with the flow distance in the pipe network as described above.

7. Finally, the subcatchment contributing area is calculated. The contributing area is the sum of the contributing areas associated with the inlets defined in steps 3-5, which can be found using the ArcHydro tools.

Because method 4 is the most detailed in describing the flowpaths in any subcatchment with anthropogenic conduits, we will use this description as the reference to which the ones generated by the other methods are compared. Although there is no proof that the flow paths and distances obtained using method 4 are the real ones, it is reasonable to assume that they are the most accurate because they explicitly consider every pipe segment including its known endpoints, elevations and length. The only major assumption in this method is the identification of inlets,

which are not known. The use of method 4 as a reference point is also supported by Lhomme et al. (2004), who concluded that an explicit description of the flow paths in an urban watershed is sufficient to reproduce the hydrologic response in spite of the uncertainty associated with the subcatchments flowing into the drainage system.

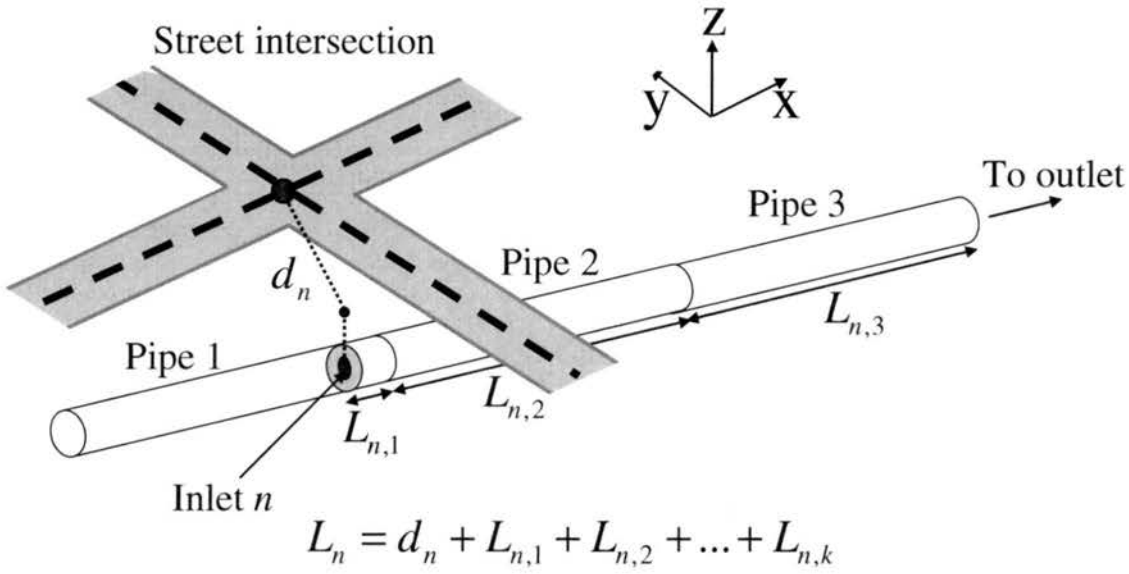

Figure 3.2. Definition of inlet and flow distance to the subcatchment outlet using method 4.

3.3 Application to Study Site

The Aubinière is a watershed located in the metropolitan area of Nantes, France, and is used to compare the four methods for representing urban terrain. The city is located at an average elevation of 27 m, close to the Atlantic coast. It has an oceanic climate, and the total annual precipitation is around 800 mm. The Aubinière has a separated stormwater system and drains into the right bank of the Loire River. It has an approximate area of 10.5 km^2 and an estimated total imperviousness of 30% (estimated

from a GIS imperviousness layer). Pervious and impervious areas are heterogeneously distributed throughout the watershed. Large vegetated plots, highly impervious areas (corresponding to single- and multi-family housing), commercial areas, and industrial zones are all common within the watershed. The Gohards, a catchment located within the study area, has been used previously to develop hydrologic models (Rodriguez et al. 2003, 2005 and 2008). The available information for this watershed includes a DEM with a resolution of 20 m and drainage layers delineating streets, storm pipes, and natural channels. These drainage layers include all the information required to use and evaluate the four methods described in the previous section. Figure 3.3 shows the watershed and the pipe system.

The methods for representing urban terrain were applied to the Aubinière in both a lumped and a semi-distributed manner. In the lumped approach, a single watershed outlet is specified, and all four methods are used to characterize the terrain of the watershed as a whole. In the semi-distributed approach, the main elements of the drainage system are retained for explicit hydraulic modeling, and the watershed is divided into subcatchments that provide flow to the main drainage system. The main drainage system shown in Figure 3.3 was defined by including all natural streams and pipes whose diameter is 1 m or larger. Two pipes with diameters of 80 cm were also included because they connect a section of 1 m pipes that is separated from the rest of the main system. Subcatchment outlets are located at the upstream ends of the main drainage system elements and at regularly-spaced points along the system. The locations of these nodes were selected so that the subcatchments defined by method 4 at these nodes have relatively similar areas of 30-40 ha. This size was selected based on a study by Pomeroy

et al. (2008), who defined an average target size of 75 acres (around 30 ha) for subcatchments in developed watersheds with sizes similar to our study area. In the end, 28 subcatchments were identified. Notice that method 4 explicitly represents the entire drainage system no matter whether the watershed is treated as lumped or semi-distributed. Using this algorithm, the entire watershed contains 465 type *I* inlets, 440 type *II* inlets, and 91 type *III* inlets, which makes a total of 996 subcatchments contributing to the entire pipe network shown in Figure 3.3.

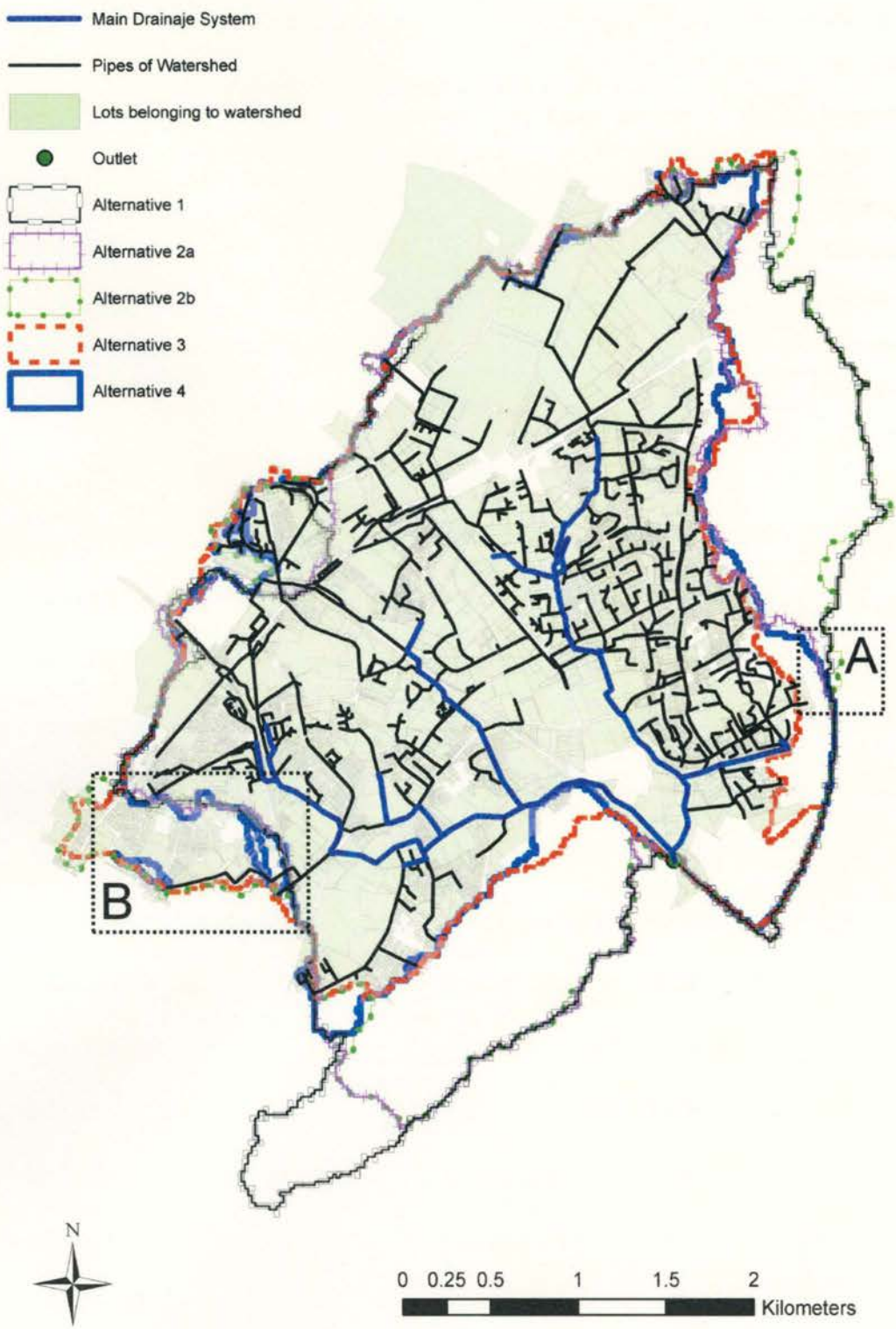

Figure 3.3. Parcels within the Aubinière watershed, the pipe system, and the watershed boundary implied by the four methods for representation of urban terrain.

3.4 Morphologic Properties

To compare the four methods of terrain representation, we first examine the geometric or morphological properties of the catchments when they are defined using both the lumped and semi-distributed approaches. In particular, we examine the basin areas, flow lengths, and slopes produced by the methods.

3.4.1 Area

Contributing area is perhaps the most important geometric property of a watershed because it determines the maximum volume of runoff that can be generated from a given rainfall event that falls over the area (Bedient and Huber 2002). Figure 3.3 shows the watershed boundaries that are computed by the four methods under the lumped approach along with the boundaries of the lots belonging to the watershed. These lots were identified with the methodology proposed by Rodriguez et al. (2003) in which all lots connected to a vector map of water flow along streets and the stormwater sewer network are considered to be part of the watershed. The differences between the watershed divides determined by the four methods are quite significant. The calculated contributing areas are 13.6 km^2 for method 1, 11.7 km^2 for method 2a, 14.0 km^2 for method 2b, 10.9 km^2 for method 3, and 10.4 km^2 for method 4. Method 4 produces the smallest basin area, and the other methods are up to 35% larger. When conduits are burned into the DEM, new connections are made with adjacent locations, and eventually more area is aggregated into the basin. This portion of land can contribute to the watershed area or to a flow path located outside the watershed. The main reason for the discrepancies in the watershed boundaries between methods 2a and 2b is the different depth adjustments used

by these methods. Larger burning depths tend to add more area because it is more likely for neighboring cells to drain into a lower cell. Therefore, although a large burning depth ensures that flow remains in known conduits, it can significantly affect the computation of the catchment area. The sink filling process also contributes to the different watershed areas. Because burned cells have a lower elevation for method 2b than method 2a, they are more likely to be filled to a lower elevation than the burned cells of method 2a. Thus, the flow directions generated by the methods can differ. An example of this is observed in the east side of the study area (window A in Figure 3.3), where the differences in the burning depth and subsequent filling cause the aggregation of a large portion of land to the watershed.

The divides computed using methods 3 and 4 are quite similar to each other and to the boundary defined by the lots, and the contributing areas in both cases are relatively close to 10.5 km^2, which is the area computed using the lots. Notice, however, that the computational complexity of method 3 is much less than method 4. Window B in Figure 3.3 also illustrates a problem with method 4, which is the need to assume inlet locations. In this window, one can see two small subcatchments that are isolated from the main watershed. These isolated catchments occur because no street intersections are identified along the pipe in window B, so no inlets are identified and flow cannot enter the pipe system. This is probably unrealistic given that the length of the pipe is more than 500 m. The burning methods do not share this problem because flow can enter at any point along the pipe's trench.

The methods can also be compared using the 28 subcatchment areas calculated using the semi-distributed approach described earlier. Figure 3.4 shows a scatter plot

comparing the areas obtained from methods 3 and 4; the correlation coefficient r is 0.44. This value is relatively far from 1, which implies a relatively poor correlation between the areas calculated using the two methods. However, the areas generated by methods 1, 2a, and 2b exhibit even less correlation with those produced by method 4. The respective values of r for these 3 methods are 0.04, -0.02, -0.01. Thus, the subcatchment areas produced by these methods are essentially uncorrelated with those produced by method 4. In all cases, the correlation is low because catchment areas are sensitive to small differences in the flow directions in grid cells located in the vicinity of subcatchment outlets. Figure 3.4 shows that many of the subcatchments defined by method 3 have small areas, in particular less than 5 ha. If the outlets were displaced a little bit from the original locations, larger catchments could be defined that would be more similar to those computed by method 4. Similar improvements could be achieved for the other methods, but the best outlet locations vary for each method and would need to be manually identified, making any direct comparison difficult.

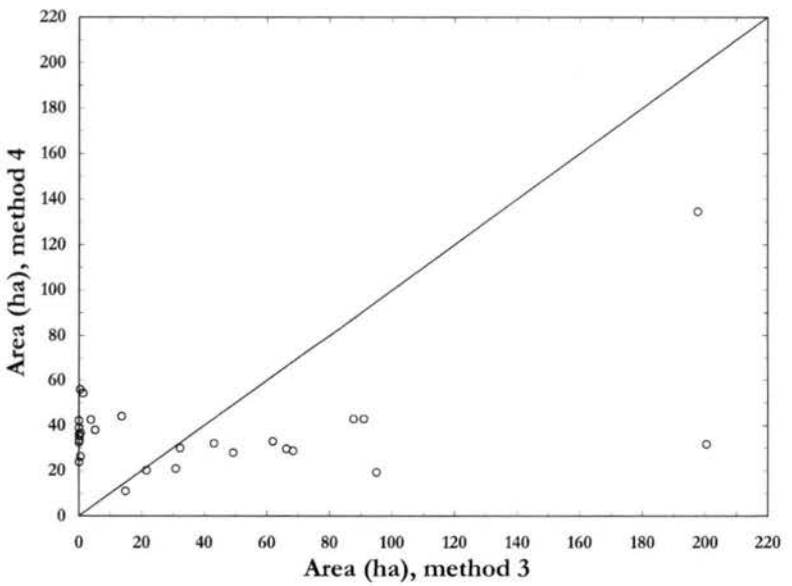

Figure 3.4. Comparison of the subcatchments area obtained using methods 3 and 4.

3.4.2 Flow length

Another fundamental property of a drainage network is the collection of flow paths or lengths from the points in the basin to the basin outlet. Rodríguez-Iturbe and Rinaldo (1997) stated, "When studying the structural characteristics of a drainage network and, most importantly, the implications of such a structure on the hydrologic response of a basin to any precipitation input, the arrangement of the flow paths from any point of the basin to the outlet are of the most crucial importance." Although this statement originally referred to natural watersheds, it is expected to be valid for urban watersheds as well. Indeed, Lhomme et al. (2004) showed the importance of a detailed description of flow paths in stormwater modeling, and Rodriguez et al. (2003, 2005) concluded that the morphology of the drainage system (i.e. the flow paths from each hydrologic element to the outlet) is of great importance in determining the shape of the hydrologic response.

The four methods can be evaluated by comparing their histograms of the flow length between points in the watershed and the watershed outlet. The flow distance histogram is computed by counting the number (or frequency) of grid cells whose flow distance to the outlet falls within specified intervals. In this study, we used an interval of 100 m to compute the histograms, which are shown in Figure 3.5. For the sake of clarity, these histograms are plotted using line charts rather than bar charts. Each part of Figure 3.5 compares the histograms of flow length for the entire watershed when the lumped and semi-distributed approaches are used in a given method. The histogram obtained from method 4 is shown in all the plots for comparison. The goodness-of-fit was evaluated using the modified coefficient of efficiency (*MCE*), defined as (Legates and McCabe, 1999):

$$MCE = 1 - \frac{\sum_{i=1}^{N} \left| f_{ref,i} - f_{sim,i} \right|}{\sum_{i=1}^{N} \left| f_{ref,i} - \overline{f}_{ref} \right|} \tag{3-2}$$

where $f_{ref,i}$=reference or "observed" frequency at distance interval i based on method 4; f_{sim}= simulated frequency at distance interval i using one of the other approaches; $\overline{f}_{ref}$ =average of the reference or "observed" frequencies; and N=number of distance intervals in the histogram. The *MCE* ranges from $-\infty$ to 1 and judges the performance of the simulated values in comparison to the variability of the observations (Legates and McCabe, 1999). A value of one indicates an exact match with the observations. If the value is zero, the simulation predicts the observed lengths with the same efficiency as the average of the observed values. Table 3.2 summarizes the resulting *MCE* values obtained for methods 1, 2a, 2b, and 3. Significant differences are observed between the methods from both Figure 3.5 and Table 3.2. When the lumped representations are used, method 2a (*MCE* = 0.607) and method 3 (*MCE* = 0.666) are the best at replicating the flow distance histogram of method 4. These two methods are also the best when the semi-distributed representations are used. However, the *MCE* value for method 3 improves when the semi-distributed representation is used (from 0.666 to 0.742) whereas the value for method 2a decreases slightly. When the semi-distributed approach is used, the flow paths within the 28 subcatchments differ for each of the methods but are the same as those of method 4 once the main drainage system is reached. Thus, one expects an improvement of the *MCE* if the flow distances are well represented at relatively small scales (i.e. in the subcatchments). The fact that method 2a does not improve its performance when the semi-distributed approach is used implies that the

errors in this method are primarily associated with streets and small conduits. It also suggests that method 3 is relatively more successful at representing the flow paths in the small conduits because its MCE increases when the semi-distributed approach is used.

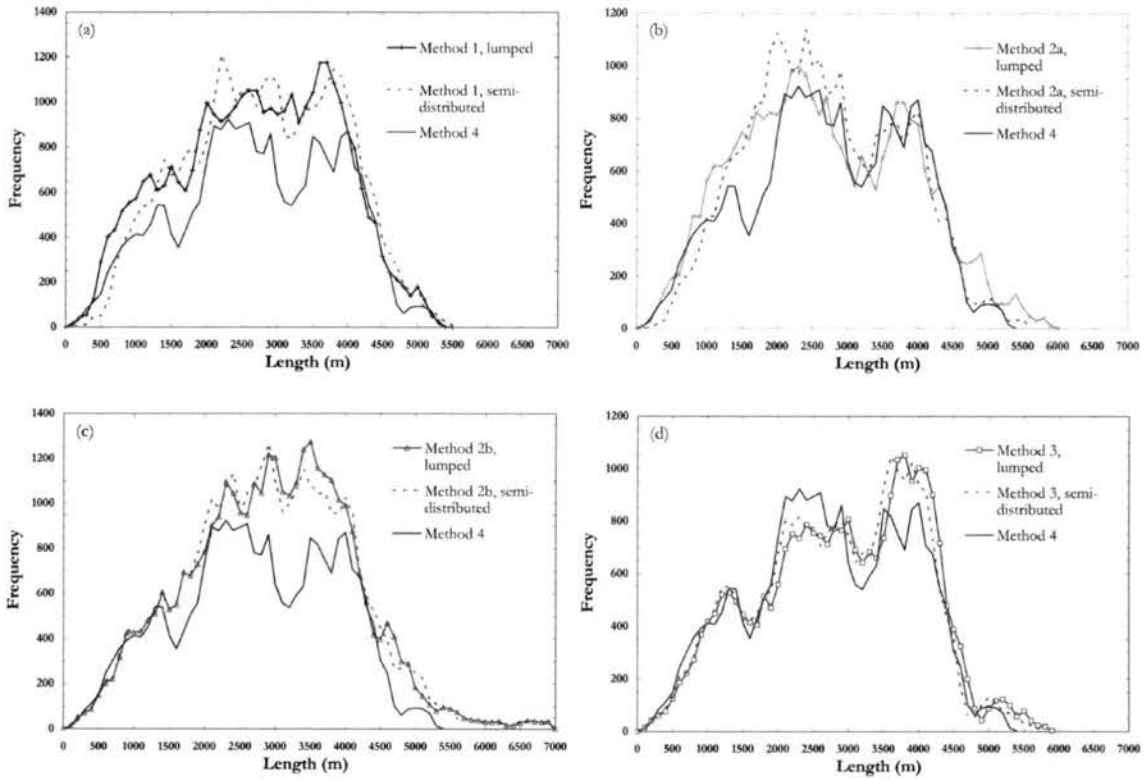

Figure 3.5. Flow length histograms obtained using the lumped and semi-distributed approaches, and comparison to the histogram derived from method 4. (a) shows results for method 1, (b) shows results for method 2a, (c) shows results for method 2b, and (d) shows results for method 3.

Table 3.2. Summary of MCE values between the flow length histograms generated by methods 1, 2a, 2b, and 3 and method 4, for the lumped and semi-distributed approaches.

Terrain Method	Lumped approach	Semi-distributed approach
1	0.441	0.402
2a	0.614	0.607
2b	0.381	0.395
3	0.666	0.742

It is interesting to note that these differences in the flow paths are not visible when only representative flow distance values are calculated for the entire watershed. Table 3.3 shows that it is not possible to identify method 3 as the closest one to method 4 when the maximum flow length, average flow length, median flow length, or standard deviation of flow lengths are compared for the entire watershed. However, when these attributes are calculated for the semi-distributed representations, differences arise and the representative lengths generated from method 3 are clearly the most similar to the ones computed from method 4. For example, Figure 3.6 compares the maximum flow length of each subcatchment for methods 3 and 4 when the semi-distributed approach is used. The correlation coefficient r is relatively low ($r = 0.48$), but it is much higher than for any other method, as shown in Table 3.4. This table also shows the values of r for the methods when the average flow length or median flow length is considered. The table shows that the results are consistent no matter which measure is used as the representative flow length.

Table 3.3. Characterization of flow lengths in the entire watershed for the different terrain representation methods.

Terrain Method	Maximum width (# cells and m^2)	Maximum flow length (m)	Average flow length (m)	Median flow length (m)	Standard deviation (m)
1	1,176 - 470,400	5,300	2,654	2,697	1,114
2a	997 - 398,800	5,840	2,648	2,538	1,192
2b	1,275 - 510,000	6,918	2,898	2,930	1,154
3	1,051 - 420,400	5,823	2,864	2,937	1,146
4	923 - 369,200	5,321	2,695	2,680	1,108

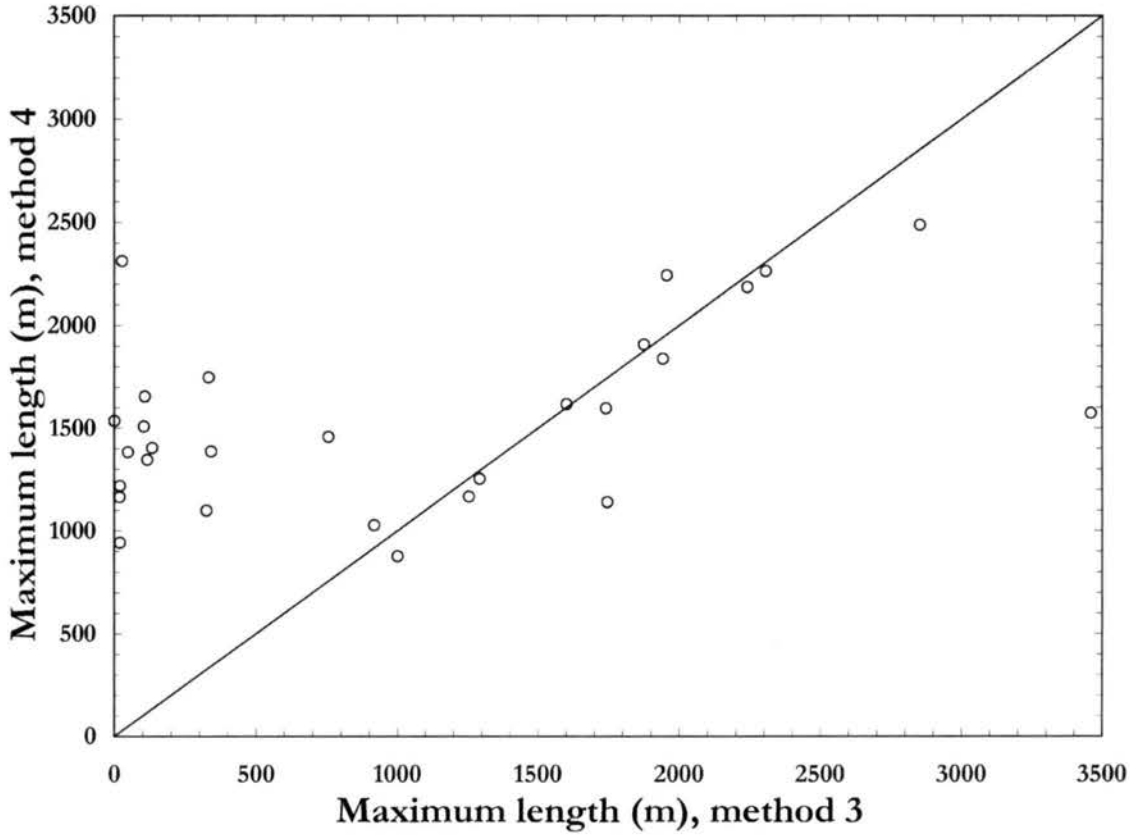

Figure 3.6. Comparison of each subcatchment's maximum length obtained using methods 3 and 4.

Table 3.4. Summary of the correlation coefficients r between the flow lengths generated by methods 1, 2a, 2b and 3 and method 4 for the 28 subcatchments in the semi-distributed representation.

Terrain Method	Average length	Median length	Maximum length
1	0.09	0.06	0.13
2a	0.17	0.15	0.11
2b	0.05	0.06	0.13
3	0.62	0.64	0.48

3.4.3 Slope

Watershed slopes were computed by dividing the difference in elevation between the upstream and downstream ends of the longest flow path by the total length of this flow path. Huber and Dickinson (1988) recommend this method for calculating the slope when building a SWMM model for a catchment with simple geometry, and a similar suggestion was made by Lhomme et al. (2004). Although the geometry is not simple for all the subcatchments, this approach is used in all cases for consistency. For methods 1, 2a, 2b and 3, the elevations were obtained directly from the corresponding DEM. In the case of method 4, the upstream elevation was obtained from the modified DEM, and the downstream elevation was obtained from the pipe or channel segment in the vector layer at the outlet. In contrast to the results for basin areas and flow lengths, the correlation coefficient obtained by comparing methods 3 and 4 (r = -0.2) is as poor as the values obtained when comparing the other methods to method 4 (r = 0.02 for method 1, r = 0.18 for method 2a, and r = 0.22 for method 2b). This poor correlation is due to the lack of agreement in the subcatchment boundaries that was pointed out earlier. Figure 3.4 and Figure 3.6 show several subcatchments with very small areas and small lengths. These subcatchments plotted close to the y axis in both of these figures, which allowed reasonable correlations to arise. However, the slopes calculated for these catchments are not necessarily small, so they distribute throughout the slope scatter plot, reducing the correlations. Figure 3.7 shows a scatter plot comparing the slopes generated by methods 3 and 4. In this figure, black points correspond to subcatchments larger than 5 ha, and white points correspond to subcathments smaller than 5 ha. Interestingly, if the black point at the top of the plot were removed, the rest of the black points follow a roughly

linear trend with an r value of 0.63.

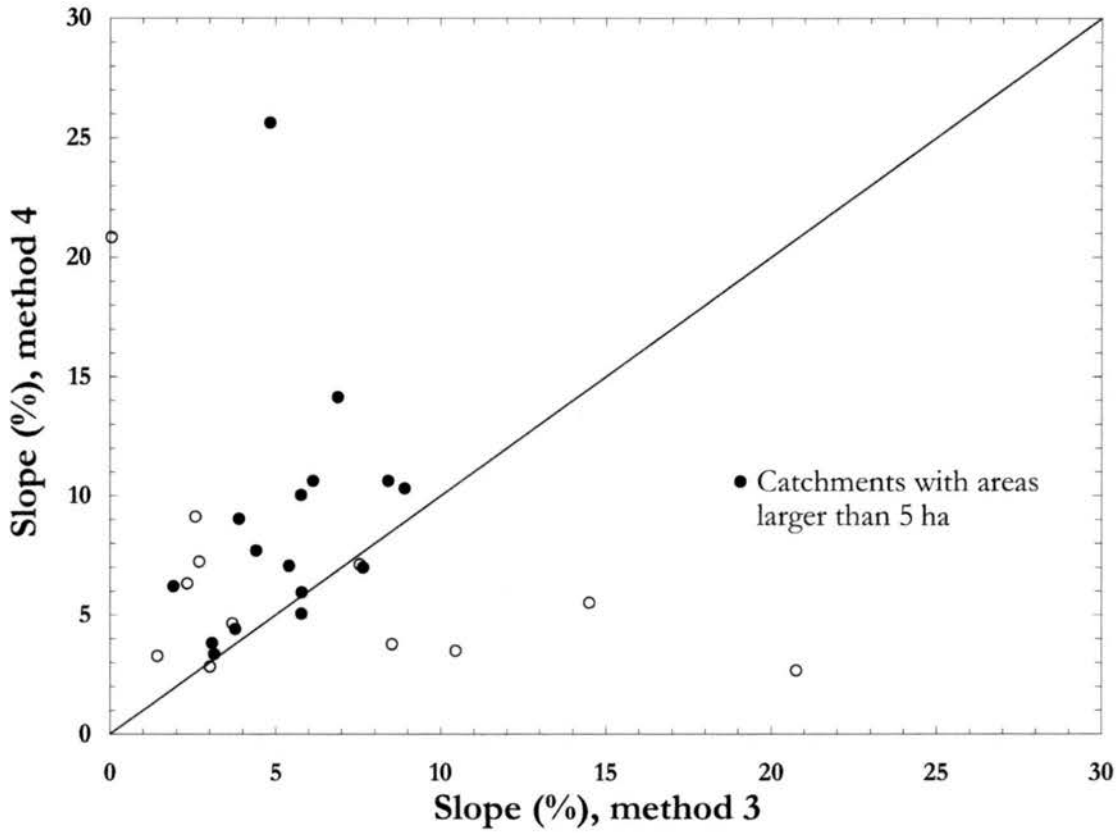

Figure 3.7. Comparison of subcatchments slopes obtained using methods 3 and 4.

3.5 Effects on Stormwater Modeling

In this section, we examine how the basin morphologies produced by the four methods affect stormwater modeling results. The catchments defined under the semi-distributed approach are used here to develop semi-distributed models in SWMM5 (Rossman, 2008), which is one of the more comprehensive models available for urban runoff in storm sewer pipes (Bedient and Huber 2002). The same major drainage system is used in all the models, so no differences are introduced by the hydraulic routing in the

pipe system. Hereafter, the models developed based on methods 1, 2a, 2b, 3 and 4 are referred as models 1, 2a, 2b, 3 and 4, respectively.

3.5.1 Modeling in SWMM

SWMM generates runoff from rainfall over a subcatchment using a non-linear reservoir method, which performs the overland flow routing as well. The subcatchment is represented as a rectangular plane, which is characterized by its area, width, slope, and imperviousness. The routing method is applied separately for the pervious and impervious subareas, and then the outflow rates are added. This technique couples the spatially-lumped continuity equation and Manning's equation to produce a non-linear differential equation for the water depth:

$$\frac{dh}{dt} = i_e - \frac{WS^{1/2}}{An}\left(h - d_p\right)^{5/3} \tag{3-3}$$

where A=subcatchment surface area (m^2); h=water depth (m); t=time (s); i_e=effective rainfall (m/s); W=subcatchment width (m); n=Manning's roughness coefficient; d_p=depression storage (m); and S=subcatchment slope (m/m). Notice that the watershed area and slope both occur in the coefficient $B \equiv (WS^{1/2})/(An)$ in Eq. (3-3). Furthermore, this coefficient includes the width, and a good initial estimation of the width can be obtained by dividing the area by the maximum flow length of the catchment L_{max} (Huber and Dickinson 1988). Once the depth is calculated from this equation, the outflow discharge Q is computed using the Manning equation. A more detailed explanation of this method and the numerical solution is explained by Huber and Dickinson (1988).

Other parameters related to the generation of effective precipitation (i.e. infiltration parameters, d_p, and the imperviousness) are not studied here. For simplicity, we assume that these parameters are homogeneous within the entire study area, and we only focus on the effects of the different methods for representing urban terrain. Table 3.5 shows the parameter values used in the model.

Table 3.5. Physical characteristics used in the stormwater model.

Property	Value	Property	Value
Imperviousness	30%	% of impervious area without depression storage	25%
Roughness coefficient, impervious areas	0.013	Maximum infiltration rate	76.2 mm/hr
Roughness coefficient, pervious areas	0.24 %	Minimum infiltration rate	6.6 mm/hr
Depression storage, pervious areas	3.8 mm	Infiltration decay coefficient	4 hr^{-1}
Depression storage, impervious areas	2 mm		

3.5.2 Uncalibrated scenario

Four storms were used to test the implications of the methods for representing urban terrain. The first is a long rainfall event of 5 mm/hr for 5 hours, and the second is a nearly instantaneous pulse of 60 mm/hr for 1 minute, which is the minimum rainfall interval allowed in SWMM. We also considered both a small real storm (4.2 mm) and a large real storm (42.5 mm) that occurred in the study area. The small storm started May 20th, 2007, and lasted for 160 minutes; the large storm started the same day at 10:55 pm and lasted for 13 hours. Hereafter, the long synthetic storm will be called storm 1, the

short synthetic storm will be called storm 2, the minor real storm will be called storm 3, and the major real storm will be called storm 4.

As with the morphologic properties, the discharges simulated by models 1, 2a, 2b and 3 were compared to the discharges simulated by model 4. In particular, the following quantities were computed and compared: maximum discharge (Q_{max}), average discharge ($Q_{average}$), time to peak (T_{max}), lag time (*Lag-t*), runoff duration (T_R), and runoff volume (V_R). To avoid simulating extremely long periods of time, V_R is calculated up to the time when the discharge goes below a nominal value of 0.01 m^3/s for storms 1, 3 and 4, and 0.005 m^3/s for storm which has a smaller magnitude. T_R corresponds to the time at which V_R is reached.

Table 3.6 shows the values of these quantities for each of the four models and each of the four storms. This table shows that the geometric differences implied by the different terrain processing methods result in significant differences in the hydrologic response. In general, the results from model 3 are more similar to those from model 4, which is not surprising given the fact that these methods produced the most geometrically similar basins. This is especially noticeable for Q_{max}, T_{max} and V_R, which are often the most important results from a stormwater model and are typically used to evaluate model performance (e.g., Aronica and Cannarozzo, 2000; Rodriguez et al., 2003; Lhomme et al., 2004; and Barco et al., 2008). Only Q_{max} for storms 3 and 4 is better reproduced by a model (model 2a) other than model 3. All the values of *Lag-t* and T_R for model 4 are also better reproduced by model 3 than any other model.

Table 3.6. Summary of the hydrologic simulations using different models and storms, uncalibrated semi-distributed modeling.

Terrain method	Storm 1						Storm 2					
	Q_{max} (m^3/s)	$Q_{average}$ (m^3/s)	T_{max} (hh:min)	Lag-t (hh:min)	T_R (hh:min)	V_R (x1000m^3)	Q_{max} (m^3/s)	$Q_{average}$ (m^3/s)	T_{max} (hh:min)	Lag-t (hh:min)	T_R (hh:min)	V_R (x1000m^3)
1	5.30	1.06	5:00	1:32	23:30	90.07	0.05	0.02	2:07	4:08	12:27	0.83
2a	4.86	1.25	4:53	1:13	18:15	82.06	0.06	0.02	2:14	3:59	11:03	0.74
2b	5.69	1.35	4:41	1:16	19:53	96.30	0.06	0.02	1:58	4:04	12:00	0.90
3	4.53	1.24	4:17	1:10	17:08	76.31	0.06	0.02	1:41	3:49	10:23	0.69
4	4.22	1.32	3:31	1:02	15:02	71.39	0.06	0.02	1:43	3:32	9:41	0.67

Continuation

Terrain method	Storm 3						Storm 4					
	Q_{max} (m^3/s)	$Q_{average}$ (m^3/s)	T_{max} (hh:min)	Lag-t (hh:min)	T_R (hh:min)	V_R (x1000m^3)	Q_{max} (m^3/s)	$Q_{average}$ (m^3/s)	T_{max} (hh:min)	Lag-t (hh:min)	T_R (hh:min)	V_R (x1000m^3)
1	0.99	0.15	2:31	3:16	19:04	10.52	12.98	1.47	5:14	1:27	29:26	155.83
2a	1.10	0.17	2:26	2:36	14:55	9.15	14.32	1.57	5:12	1:12	25:03	141.21
2b	1.27	0.19	2:29	2:43	16:26	10.97	16.18	1.74	5:12	1:14	26:34	166.73
3	1.06	0.17	2:26	2:28	13:55	8.47	14.88	1.54	5:12	1:10	24:01	133.50
4	1.15	0.19	2:27	2:09	12:04	8.16	14.36	1.53	5:12	1:02	22:17	122.37

Figure 3.8a through Figure 3.8d show the hydrographs simulated at the outlet using the four storms. The differences in the watershed areas have a significant impact on the hydrographs. This is particularly visible in Figure 3.8a, which is the response to the long pulse of rainfall. In this case, the peak discharge at equilibrium is given by the watershed areas multiplied by the effective precipitation. It is also interesting to note that the response of model 1 is much slower than the one simulated by model 2b, which has a similar total area. Because of this slower response, the discharges simulated by model 1 are the smallest ones for a considerable period of time before reaching the time of equilibrium, despite the large catchment area. When real storms such as storms 3 and 4 are used, model 1 tends to underestimate the largest peaks (more than any other model) and overestimate the minimum discharges, as seen in Figure 3.8c and Figure 3.8d. In contrast, model 2b, which has the largest watershed area and a fast response, overestimates the largest peaks (more than any other model). This observation is significant because it suggests that a reliable calibration of the overland flow parameters for a wide spectrum of storm events may be much more difficult if a less reliable terrain representation is used in building a model.

The overall ability of the models to reproduce the results from model 4 was evaluated using the *MCE*, which was used earlier to compare the flow distance histograms. Table 3.7 shows that the *MCE* values for model 3 are the closest to 1.0 for all the storms, and all the values for model 3 are larger than 0.91. The similarity of the responses of models 3 and 4 to storm 2 in particular is worth noting (Figure 3.8b). All the hydrographs in Figure 3.8b have two peaks, which is due to the contribution of a catchment that is directly connected to the watershed outlet. These results show that the differences in

subcatchment characteristics that were documented earlier in this paper have a significant effect on the hydrologic simulations based on these characteristics. It is interesting to note that results of model 3 is quite similar to the results of model 4 even though large discrepancies were observed between the subcatchment slopes of these two methods. This agrees with previous research (e.g., Zaghloul, 1983; Wan and James, 2002) showing that the hydrologic results are less sensitive to slope than the other geometric characteristics. It also follows from the fact that largest differences in the slopes generated by methods 3 and 4 occur for subcatchments with small areas, which have a minor impact on the overall hydrologic response. Table 3.6 and Table 3.7 also show that model 2a is the second most similar model to model 4, which is consistent with the fact that method 2a is the second best in reproducing the subcatchment areas and flow lengths of method 4. Finally, it is not clear whether model 1 or 2b is better. *MCE* values for model 1 are higher for storms 1 and 4, but they are lower for storms 2 and 3. This result emphasizes the need to use a realistic depth when burning the streets and pipes.

Table 3.7. Summary of MCE values between the discharges generated by different storms using models 1, 2a, 2b and 3 and model 4, uncalibrated semi-distributed modeling.

Model	Storm 1	Storm 2	Storm 3	Storm 4
1	0.811	0.639	0.723	0.771
2a	0.894	0.701	0.862	0.878
2b	0.775	0.692	0.769	0.726
3	0.946	0.913	0.918	0.924

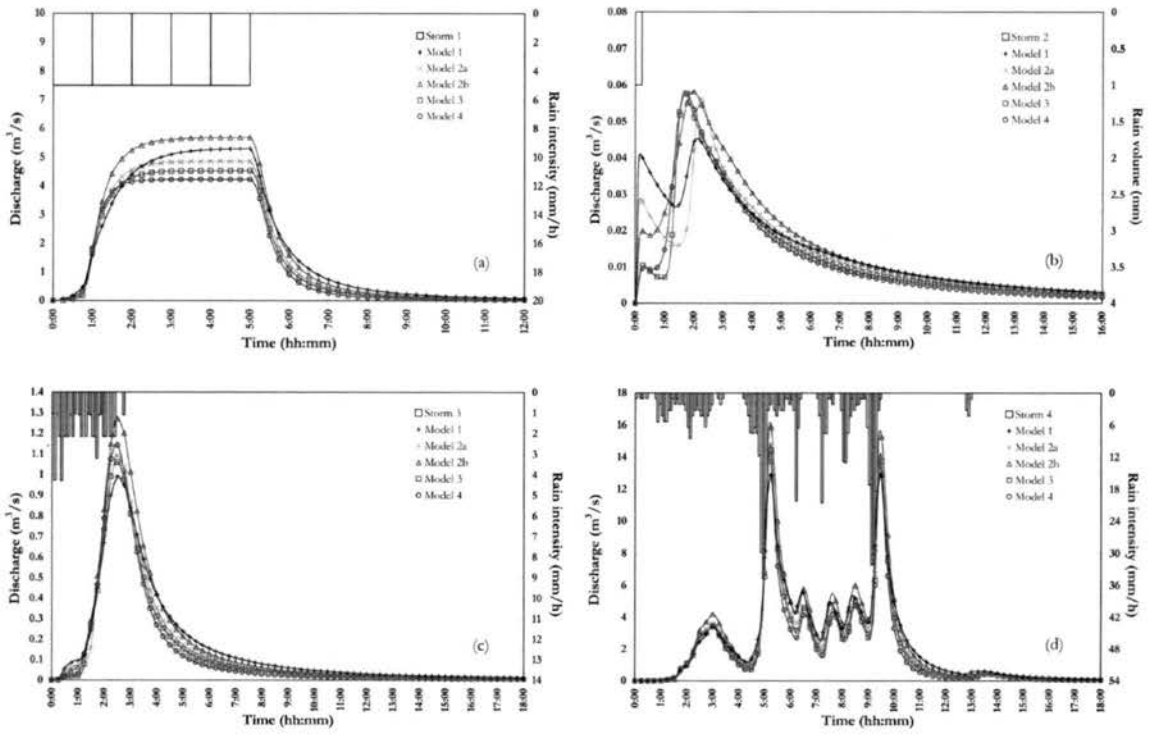

Figure 3.8. Hydrographs at the watershed's outlet for the uncalibrated semi-distributed models produced by the different terrain representation methods. (a) storm 1, constant pulse of 5 mm/h, (b) storm 2, 60 mm/hr pulse for one minute, (c) storm 3, minor storm, (d) storm 4, major storm.

3.5.3 Calibrated scenario

The previous sections demonstrated that the terrain representation methods produced significant differences in the subcatchment and watershed geometry and that these differences produce significant changes in the hydrologic responses when the rest of the model parameters are the same. In this section, we examine whether the errors that are introduced by the terrain processing methods are still significant after the model is calibrated to reproduce an observed hydrograph. Eq. (3-3) shows that equivalent changes may be produced by varying any of the characteristics grouped in the coefficient *B*. Three of these parameters (*S*, *W*, and *A*) were obtained from the terrain representations

and are considered to be known. Thus, one might consider n as the parameter with most uncertainty and use it as the calibration parameter. Alternatively, if n were considered known as well, one could introduce a calibration parameter α by redefining $B \equiv \alpha(WS^{1/2})/(An)$ and obtain similar result to those shown in this section.

Models 1, 2a, 2b and 3 were calibrated to replicate the response produced by model 4 to storm 2. The calibration aimed to improve the *MCE* value as much as possible. Storm 2 was used because it is close to the instantaneous unit hydrograph, which is the response function of the watershed to a unit pulse of excess rainfall and can be used to build responses to longer, more complex storms (Chow et al. 1988). Table 3.8 summarizes the key outputs for each of the calibrated models when they are applied not only to storm 2 (the calibration storm) but also to the rest of the storms, which might be other events requiring forecasts based on that calibration. Overall, the errors for Q_{max} and V_R are reduced after calibration for all the storms and models. Such an improvement is not clearly observed for the other quantities. Values of T_R generated by model 2b for storms 1 and 4 (the larger events) are significantly higher than for any other model. Calibration of this model reduces the large discharges generated by the uncalibrated model, and the larger runoff volumes produced by the calibrated model have to be released for a long time. Again, model 3 generates values of Q_{max}, T_{max}, *Lag-t*, and V_R that are closest to the values obtained using model 4. Only for storm 4 is the Q_{max} simulated by model 3 worse than the values produced by the other models.

Table 3.8. Summary of the hydrologic simulations using different models and storms, calibrated semi-distributed modeling.

	Storm 1 Calibrated						Storm 2 Calibrated					
Model	Q_{max} (m^3/s)	$Q_{average}$ (m^3/s)	T_{max} (hh:min)	Lag-t (hh:min)	T_R (hh:min)	V_R (x1000m^3)	Q_{max} (m^3/s)	$Q_{average}$ (m^3/s)	T_{max} (hh:min)	Lag-t (hh:min)	T_R (hh:min)	V_R (x1000m^3)
1	5.08	1.07	4:59	1:26	22:16	86.13	0.06	0.02	1:40	3:36	11:18	0.82
2a	4.59	1.01	5:00	1:20	21:17	77.70	0.07	0.02	1:40	3:36	10:20	0.71
2b	4.97	0.27	5:00	2:06	92:58	91.95	0.06	0.02	1:48	3:44	10:35	0.73
3	4.46	1.04	4:57	1:10	20:17	75.61	0.06	0.02	1:43	3:32	9:44	0.67
4	4.22	1.32	3:31	1:02	15:02	71.39	0.06	0.02	1:43	3:32	9:41	0.67

Continuation

	Storm 3 Calibrated						Storm 4 Calibrated					
Model	Q_{max} (m^3/s)	$Q_{average}$ (m^3/s)	T_{max} (hh:min)	Lag-t (hh:min)	T_R (hh:min)	V_R (x1000m^3)	Q_{max} (m^3/s)	$Q_{average}$ (m^3/s)	T_{max} (hh:min)	Lag-t (hh:min)	T_R (hh:min)	V_R (x1000m^3)
1	1.04	0.16	2:22	2:58	17:53	10.03	13.74	1.47	9:26	1:22	28:31	150.68
2a	1.08	0.15	2:25	2:40	16:14	8.53	14.68	1.37	5:09	1:16	27:32	135.33
2b	1.19	0.15	2:25	2:46	17:12	9.48	14.55	0.37	5:11	1:51	121:32	160.91
3	1.11	0.17	2:26	2:17	13:16	8.33	15.25	1.28	5:11	1:09	28:40	132.18
4	1.15	0.19	2:27	2:09	12:04	8.16	14.36	1.53	5:12	1:02	22:17	122.37

Figure 3.9a through Figure 3.9d show the hydrographs simulated for the four storms after the model calibration. Once the calibration is done, all the hydrographs are more similar to the ones produced by model 4. This is also observed in Table 3.9, which shows an improvement in the *MCE* values for all the models and storms after calibration. Similar to the uncalibrated case, model 3 has the best performance followed by model 2a, while models 1 and 2b produce similar results. In most cases, the performance of the calibrated versions of models 1, 2a, and 2b remains below the performance of the uncalibrated version of model 3. The exception is storm 2 where the *MCE* value for the calibrated model 2a (0.915) is comparable to the value for the uncalibrated model 3 (0.913). In this case, however, the performance of the calibrated model 2a is still worse than the performance of the calibrated model 3 (0.979). Thus, calibration is not enough to completely overcome the errors originated in the representation of the urban terrain.

Table 3.9. Summary of MCE values between the discharges generated by different storms using models 1, 2a, 2b and 3 and model 4, calibrated semi-distributed modeling.

Model	Storm 1 Calib.	Storm 2 Calib.	Storm 3 Calib.	Storm 4 Calib.
1	0.856	0.775	0.802	0.816
2a	0.933	0.915	0.894	0.906
2b	0.856	0.916	0.885	0.823
3	0.961	0.979	0.961	0.940

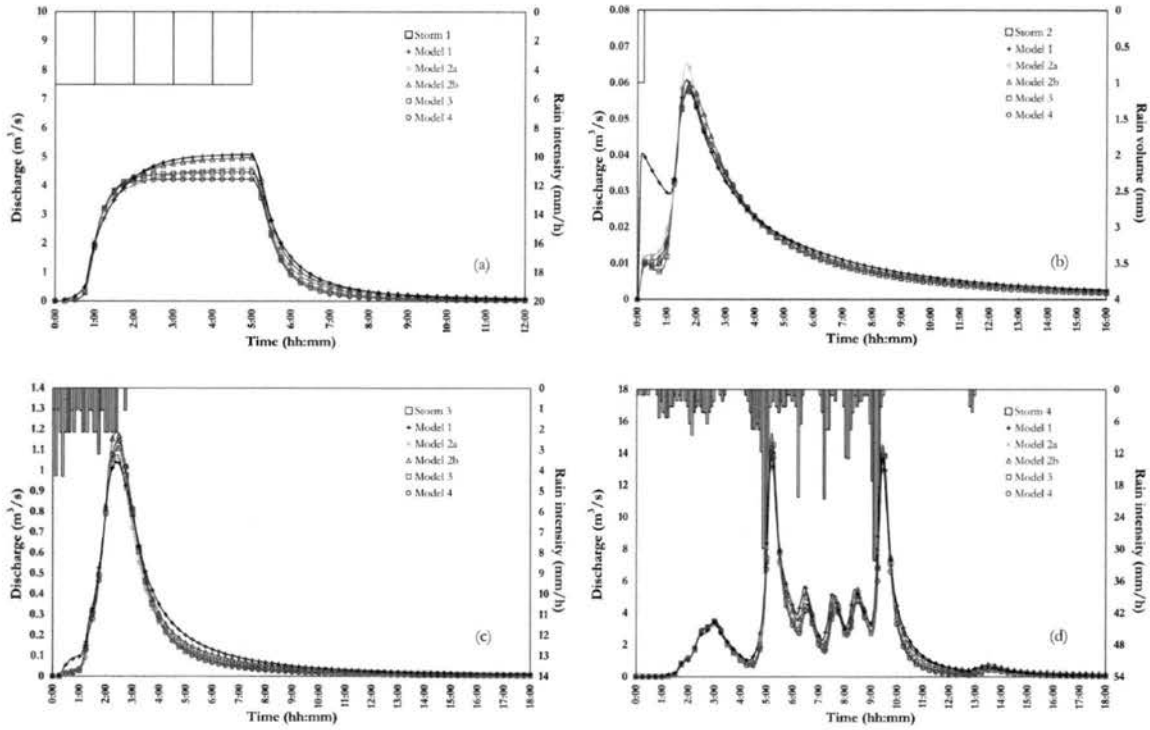

Figure 3.9. Hydrographs at the watershed's outlet for the calibrated, semi-distributed models produced by the different terrain representation methods. (a) storm 1, constant pulse of 5 mm/h, (b) storm 2, 60 mm/hr pulse for one minute, (c) storm 3, minor storm, (d) storm 4, major storm.

3.6 Conclusions

In this paper, we studied the performance of different methods to represent artificial conduits in DEMs that are used in stormwater modeling. These methods differ in their complexity and the amount of required data. The most detailed method (method 4), which explicitly describes the entire pipe system as a vector layer, is used as the reference to which the other methods are compared. This representation is assumed to be the most accurate given that the connectivity, elevations, and lengths of the pipes are known and included in the layer. The only major assumption in this method is the locations of the inlets. Based on the comparisons of the methods, we make the following key

conclusions:

1. The method used to process urban DEMs can have significant impacts on the watershed boundary and thus on basic watershed characteristics. Differences are easily introduced into the flow directions, which can ultimately affect the watershed boundary, area, flow lengths, and slope. These differences are observed when the methods are applied to the entire study watershed and when applied to 28 individual subcatchments. For instance, the *MCE* values for the flow length histograms generated by different methods range between 0.381 and 0.614 when the entire watershed is characterized by the processed DEMs and between 0.402 and 0.742 when the major drainage system is described explicitly in advance.

2. If one "burns" the DEM by reducing the elevation of cells that contain known conduits by a constant amount, the choice of the elevation adjustment can have significant implications on the resulting watershed characteristics. For example, the area of the entire watershed is 11.7 km^2 when elevation adjustments of 1 m and 2 m are used for the streets and pipes, respectively (i.e. method 2a), but the area is 14.0 km^2 when 2 m and 5 m adjustments are used for streets and pipes, respectively (method 2b). For the entire watershed and for the 28 subcatchments, the smaller, more realistic elevation adjustments usually give areas that are more similar to method 4 in which each pipe is represented explicitly and flow enters the pipe system at assumed inlet locations.

3. We also developed a methodology that uses the local pipe depths when making the elevation adjustments (method 3). When compared against method 4, method 3 is found to be superior to using the raw DEM (method 1) or making a constant elevation adjustment at all conduit locations (methods 2a and 2b). Method 3 is expected to become

increasingly advantageous as more conduits have flow traveling in a different direction than the flow on the surrounding surface. It should be noted that method 3 requires more information to implement (local pipe elevations) than the methods 1 and 2.

4. The urban terrain representation method also affected the results from a semi-distributed hydrologic model. The effects on the timing and amounts of peak flows as well as other model outputs are generally less significant than the effects on morphologic properties, but they are still appreciable. For example, differences up to 30% are observed in the peak discharges. When comparing against the results based on method 4, the results from method 3 had the best performance.

5. Calibration of the roughness parameter to reproduce the hydrologic response of a single event is unable to overcome the errors introduced by the DEM processing method. Even after the models were calibrated to reproduce the hydrograph for a particular storm from method 4, they still exhibited noticeable deviations from the results of method 4 for other storms. After calibration, the performance of all the models improved for multiple events, but methods 1 and 2 did not improve enough to overcome the performance level of the uncalibrated model based on method 3. These results again suggest the benefit of using local pipe elevations when burning the DEM if available.

Overall, this study showed that conduits that will not be modeled explicitly in a stormwater model should still be incorporated to some degree in the definition of the urban terrain. By doing so, the resulting geometric properties are expected to represent better the flow paths within the subcatchments and thus the accumulation of discharge in the system.

3.7 Acknowledgments

The authors thank the city of Nantes, France, for providing the GIS data (© Nantes – Métropole, 2003). The authors thank also Dr. John Labadie (Colorado State University) for his help in using Arc GIS and Arc Hydro. This research was made possible by the support of Region Pays de la Loire (Project MEIGEVILLE), and the generous financial support from the Harold H. Short endowed fund for the Civil Infrastructure System Laboratory at Colorado State University.

3.8 References

Aronica, G., Cannarozzo, M., 2000. Studying the hydrological response of urban catchments using a semi-distributed non-linear model. Journal of Hydrology 238(1-2), 35-43.

Barco, J., Wong, K.M., Stenstrom, M.K., 2008. Automatic calibration of the U.S. EPA SWMM model for a large urban catchment. Journal of Hydraulic Engineering 134(4), 466-474.

Bedient, P.B., Huber, W.C., 2002. Hydrology and Floodplain Analysis, 3rd Ed. Prentice-Hall, Upper Saddle River, NJ, p. 763.

Beffa C., 1998. Two-dimensional modelling of flood hazards in urban areas. Proceedings of the 3rd International Conference on Hydroscience and Engineering, Cottbus/Berlin, Germany.

Blackwell, P.R., Wells, G., 1999. DEM resolution and improved surface representation. Proceedings of the 19th annual ESRI user conference, San Diego, CA.

http://gis.esri.com/library/userconf/proc99/proceed/papers/pap629/p629.htm

Chow, V.T, Maidment, D.R., Mays, L.W., 1988. Applied Hydrology. McGraw-Hill, NY, p. 572.

Djokic, D., Maidment, D.R., 1991. Terrain analysis for urban stormwater modelling. Hydrological Processes 5(1), 115-124.

Doan, J.H., 2000. Hydrologic model of the Buffalo Bayou using GIS. In: Maidment, D.R., Djokic, D. (Eds), Hydrologic and Hydraulic Modeling Support with Geographic Information Systems. ESRI, Redlands, CA, pp. 113-143.

Elgy, J., Maksimovic, C., Prodanovic, D., 1993. Matching standard GIS packages with urban storm drainage simulation software. In: Kovar, K., Nachtnebel, H.P. (Eds), HydroGIS 93: Applications of Geographic Information Systems in Hydrology and Water Resources (Proceedings of the Vienna Conference, April, 1993), IAHS Publication No. 211, pp. 151-160.

Elliott, A.H., Trowsdale, S.A., 2007. A review of models for low impact urban stormwater drainage. Environmental Modelling & Software 22(3), 394-405.

Garbrecht, J., Ogden, F.L., DeBarry, P.A., Maidment, D.R., 2001., GIS and distributed watershed models. I: data coverages and sources. Journal of Hydrologic Engineering 6(6), 506-514.

Greene, R.G., Cruise, J.F., 1995. Urban watershed modeling using geographic information system. Journal of Water Resources Planning and Management 121(4),

318-325.

Hankin, B., Waller, S., Astle, G., Kellagher, R., 2008. Mapping space for water: screening for urban flash flooding. Journal of Flood Risk Management 1(1), 13-22.

Huber, W.C., Dickinson, R.E., 1988. Storm Water Management Model, Version 4: User's Manual. EPA/600/3-88/001a (NTIS PB88-236641/AS). U.S. Environmental Protection Agency, Athens, Ga.

Hunter, N.M., Bates, P.D., Neelz, S., Pender, G., Villanueva, I., Wright, N.G., Liang, D., Falconer, R.A., Lin, B., Waller, S., Crossley, A.J., Mason, D.C., 2008. Benchmarking 2D hydraulic models for urban flooding. Proceedings of the Institution of Civil Engineers-Water Management 161(1), 13-30.

Jordan J.G., and Grimison, E., 2001. Using GIS to analyze and model a closed stormwater basin in Ocala, Florida. In: Brashear, R.W., Maksimovic, C. (Eds), Urban Drainage Modeling, Proceedings of the Specialty Symposium of the World Water and Environmental Resources Congress. ASCE, Reston, VA.

Laurenson, E.M., Mein, R.G., 1995. RORB: Hydrograph synthesis by runoff routing. In: Singh, V.P. (Ed), Computer Models of Watershed Hydrology. Water Resources Publications, Highlands Ranch, CO, 151-164.

Laurenson, E.M., Mein, R.G., Nathan, R.J., 2007. RORB Version 6 Runoff Routing Program, User Manual. Monash University and Sinclair Knight Merz Pty Ltd, Clayton, Australia.

Legates, D.R., McCabe Jr., G.J., 1999. Evaluating the use of "goodness-of-fit" measures in hydrologic and hydroclimatic model validation. Water Resources Research 35(1), 233-241.

Lhomme, J., Bouvier, C., Perrin, J. L., 2004. Applying a GIS-based geomorphological routing model in urban catchments. Journal of Hydrology 299(3-4), 203-216.

Maksimovic, C., Prodanovic, D., 2001. Modelling of urban flooding-breakthrough or recycling of outdated concepts. In: Brashear, R.W., Maksimovic, C. (Eds), Urban Drainage Modeling, Proceedings of the Specialty Symposium of the World Water and Environmental Resources Congress. ASCE, Reston, VA.

Mark, O., Weesakul, S., Apirumanekul, C., Aroonnet, S.B., Djordjević, S., 2004. Potential and limitations of 1D modelling of urban flooding. Journal of Hydrology 299(3-4), 284-299.

MUSIC Development Team, 2005. MUSIC User Guide, Version 3.0. Cooperative Research Centre for Catchment Hydrology, Melbourne, Australia.

Nie, L., Schilling, W., Killingtveit, A., Saegrov, S., Selseth, I., 2002. GIS based urban drainage analyses and their preliminary applications in urban stormwater

management. In: Strecker, E.W., Huber, W.C. (Eds), Proceedings of the 9th International Conference on Urban Drainage, Sept. 8-13. ASCE Publication, Reston, VA [CD-ROM].

Olivera, F., Furnans, J., Maidment, D.R., Djokic, D., Ye, Z., 2002. Drainage systems. In: Maidment, D.R. (Ed), Arc Hydro, GIS for Water Resources. ESRI, Redlands, CA, pp. 55-86.

Pomeroy, C.A., Roesner, L.A., Coleman II, J.C., Rankin, E., 2008. Protocols for studying wet weather impacts and urbanization patterns, Report 03WSM3. Water Environment Research Foundation, Alexandria, VA.

Rodriguez, F., Andrieu, H., Zech, Y., 2000. Evaluation of a distributed model for urban catchments using a 7-year continuous data series. Hydrological Processes 14(5), 899-914.

Rodriguez, F., Andrieu, H., Creutin, J.D., 2003. Surface runoff in urban catchments: morphological identification of unit hydrographs from urban databanks. Journal of Hydrology 283(1-4), 146-168.

Rodriguez, F., Cudennec, C., Andrieu H., 2005. Application of morphological approaches to determine unit hydrographs of urban catchments. Hydrological Processes 19(5), 1021-1035.

Rodriguez, F., Andrieu, H., Morena, F., 2008. A distributed hydrological model for urbanized areas – Model development and application to case studies. Journal of Hydrology 351(3-4), 268-287.

Rodríguez-Iturbe I., Rinaldo A., 1997. Fractal River Basins: Chance and Self-Organization. Cambridge University Press, New York, pp. 547.

Rossman, L.A., 2008. Storm Water Management Model User's Manual Version 5.0. EPA/600/R-05/040, U.S. Environmental Protection Agency, Water Supply and Water Resources Division, National Risk Management Research Laboratory, Cincinnati, OH.

Ryan, C., 2005. CatchmentSIM User Guide, a Stand-alone GIS Based Terrain Analysis System. Cooperative Research Centre for Catchment Hydrology, Melbourne, Australia.

Schmitt, T.G., Thomas, M., Ettrich, N., 2004. Analysis and modeling of flooding in urban drainage systems. Journal of Hydrology 299(3-4), 300-311.

Selvalingam, S. Liong, S.Y., Manoharan, P.C., 1987. Application of RORB model to a catchment in Singapore. Water Resources Bulletin 23(1), 81-90.

Smith, M.B., 1993. A GIS-based distributed parameter hydrologic model for urban areas. Hydrological Processes 7(1), 45-61.

Smith, M.B., Vidmar, A., 1994. Data set derivation for GIS-based urban hydrological modeling. Photogrammetric Engineering and Remote Sensing 60(1), 67-76.

U.S. Army Corps of Engineers (USACE-HEC), 2006. HEC-HMS Hydrologic Modeling System User's Manual, Version 3.1.0. Hydrologic Engineering Center, Davis, CA.

Wan, B., James, W., 2002. SWMM calibration using genetic algorithms. In: Strecker, E.W., Huber, W.C. (Eds), Proceedings of the 9th International Conference on Urban Drainage, Sept. 8-13. ASCE Publication, Reston, VA [CD-ROM].

Zaghloul, N.A., 1983. Sensitivity analysis of the SWMM runoff-transport parameters and the effects of catchment discretization. Advances in Water Resources 6(4), 214-223.

Zech, Y., Sillen, X., Debources, C., Van Hauwaert, A., 1994. Rainfall-runoff modelling of partly urbanized watersheds: comparison between a distributed model using GIS and other models sensitivity analysis. Water Science and Technology 29(1-2), 163-170.

Zech, Y., Escarmelle, A., 1999. Use of high-resolution geographical databases for rainfall-runoff relation in urbanised areas. Water Science and Technology, 39(9), 87-94.

4. A Morpho-climatic Instantaneous Unit Hydrograph Model for Urban Catchments Calculated from Digital Elevation Models

Abstract: Stormwater models are valuable tools in urban planning as well as stormwater system design and management. Although the hydraulic simulation of pipes and channels in these models is often quite sophisticated, the hydrologic simulation of the flow contributing to the hydraulic elements is frequently greatly simplified. Hydrologic simulation of urban catchments is made particularly complex due to the presence of features such as streets, small pipes, and channels. In this study, we develop a new model called the U-McIUH (Urban Morpho-climatic Instantaneous Unit Hydrograph), which defines the IUH as the probability density function of the travel time from a random location in the urban terrain to the outlet. Flow paths are extracted from a specially processed digital elevation model that incorporates streets, pipes, and channels, and travel times are computed in each cell using the average wave celerity from kinematic wave theory. These expressions depend on the upstream contribution of flow and the excess rainfall intensity, so they incorporate the so-called climatic dependence of the IUH, which is the dependence of the unit hydrograph on the rainfall intensity. Rainfall pulses of different intensities are convoluted with their respective IUH and superimposed to generate the response to a given storm event. The application of the model to a real

catchment provides good reproduction of observed hydrographs, suggesting that the U-McIUH is able to capture some significant hydrologic properties of the catchment. The model is studied by analyzing the effects of (1) the upstream contribution of flow on the travel time formulation, (2) the variation of flow velocities within the urban catchment, (3) the non linear dependence of the IUH on the rainfall intensity (i.e. the climatic dependence), and (4) the spatial distribution of imperviousness. Overall, these results suggest that the presence of artificial elements in urban watersheds has a significant role in determining the travel times and thus the hydrologic response of the watershed.

.

4.1 Introduction

Stormwater models are valuable tools for the prediction of discharges, the assessment of downstream impacts associated with land-use changes, as well as the design of different elements of the stormwater system. As summarized by Zhao (2001) and Zoppou (2001), most of these models provide a detailed description of the sewer system hydraulics, yet they still rely on very simplistic parameterizations of the upstream runoff formation and concentration (Rodriguez et al., 2003). In these models, the watershed is divided into subcatchments in which a hydrologic method (e.g., a unit hydrograph or a linear or non-linear reservoir) is used to accumulate the flow that discharges into the major elements of the drainage system. The subcatchment is often conceptualized as a simple geometric shape or reservoir that neglects the actual spatial configuration, and the conduits or channelized elements contained in each subcatchment (i.e. streets, small pipes, and small streams) are neglected. However, Rodriguez et al. (2003 and 2005), Lhomme et al. (2004), and Gironás et al. (2009) demonstrated that these elements play an important role in directing flow within subcatchments and using an existing stormwater model found that their representation has a significant impact on the response of urban subcatchments.

Distributed models have been developed in recent years to address the difficulties of the more traditional methods. The spatial capabilities of geographic information systems (GISs) have allowed the integration of different layers of spatial information in building these models. The first distributed stormwater models operating on grid-cells were built in the early 1990s. Smith (1993) developed a distributed model in which the catchment was represented as a cascade of cells. Continuity and Manning's equations were used to

compute discharges from overland flow and time-shift routing was used to compute storm sewer flows assuming full-pipe flow velocities. Zech et al. (1994) developed a stormwater model using a digital elevation model (DEM) grid in which the water budget was computed at each cell and pipes were also represented by cells. Flows at the outlet were calculated by adding the contribution from the cells based on the travel times. Overland flow and pipe velocities were computed using a semi-empirical expression and Manning's equation, respectively. Later, Rodriguez et al. (2000) tested the model by comparing it to a lumped model. Aronica and Cannarozzo (2000) and Lhomme et al. (2004) proposed models in which the hydrograph at the catchment's outlet corresponded to the sum of the elementary responses of portions of the catchment, which were represented by means of linear reservoirs and/or linear channels.

Maidment (1993) and Maidment et al. (1996) explicitly incorporated the spatial structure of the catchment in the identification of the unit hydrograph (UH). Maidment et al. (1996) used the geomorphic features of a rural catchment (i.e. the cells' slopes and the drainage network derived from the DEM) in the definition of the UH by generating a spatially-distributed velocity field. Similar studies in rural catchments include those by Kilgore (1997), Saghafian et al. (2002), Martínez et al. (2002), Noto and La Loggia (2007), Cleveland et al. (2008), and Du et al. (2009). The use of geomorphologic features to identify the UH in urban catchments has been much less explored. Several studies (e.g., Zhang et al., 2001; Turner-Gillespie et al., 2003; Smith et al., 2005; Javier et al., 2007) have applied the Network Model (Morrison and Smith, 2001) to study floods in urban catchments. This model divides the catchment into hillslope and channel components, which are characterized by constant overland flow and constant channel

flow velocities that are used to determine the travel time from each cell to the outlet. Although the UH is not computed explicitly in this model, Smith et al. (2005) showed its equivalence with the geomorphologic instantaneous unit hydrograph (GIUH) formulation, developed by Rodríguez-Iturbe and Valdés (1979) and extended by Rodríguez-Iturbe and Rinaldo (1997). Melesse and Graham (2004) developed a spatially-distributed travel time method that was applied to evaluate different imperviousness scenarios. This formulation considered a field of spatially-distributed hillslope and channel velocities. They did not define a UH from the time-area relationship, but computed discharges by adding the runoff generated by cells having the same travel time to the outlet. Recently, Kute and Stuart (2008) used a simpler version of this method, but they explicitly generated a UH to characterize the hydrologic response of the watershed. Finally, Rodriguez et al. (2003, 2005) developed a method based on the morphology of the catchment, in which the IUH was obtained by adding the runoff generated by a unit of effective precipitation over the hydrologic elements based on the travel times. Flow paths along streets and pipes with known properties were explicitly identified in a vector layer, and velocities along them were computed using the Manning's equation, while a constant velocity was used for overland flow. The non-linearity of the IUH was handled by generating IUHs for different returns periods

The available methods to determine the distributed unit response all include at least one of three significant drawbacks. The linear theory of the UH states that the instantaneous unit hydrograph (IUH) of a catchment is unique, and the response to a storm event is obtained using the principles of proportionality and superposition. However, evidence of non-linearity in the rainfall-runoff response has been observed in

both urban catchments (Hossain et al., 1978) and rural catchments (Saghafian et al., 2002 and Saghafian, 2006). A second problem is the omission or simplification of flow in pipes, which can be the main component of the drainage network in small to mid-sized urban catchments. Finally, the velocities in hillslope cells are typically assumed to be constant or independent of the amount of overland flow that is entering the cell. In their formulation, Maidment et al. (1996) defined the velocity in the cell also as a function of the contributing area to take into account the velocity increase observed downstream in river systems. Lhomme et al. (2004) addressed this issue by incorporating the upstream area into an empirical expression for the velocity. Nonetheless, this aspect should be formally considered in a hydrologic model for urban catchments. Rodriguez et al. (2003, 2005) addressed the first two issues, but some aspects in their formulation can be further improved. In particular, they considered the nonlinear dependence on intensity between storms but not within each storm, and they identified the streets and pipes in a vector layer that is separate from the DEM. This approach requires relatively sophisticated algorithms to produce the hydrologic response and may not be necessary to adequately characterize the basin response (Gironás et al., 2009).

This paper develops an Urban Morpho-climatic Instantaneous Unit Hydrograph (U-McIUH), which aims to overcome these drawbacks. Non-linearity in the rainfall-runoff response is modeled by including a dependence on the rainfall intensity. The role of the streets and pipes in directing the flow within the catchment is considered through the application of a more realistic representation of the urban terrain. Finally, the effect of upstream contribution on the travel time in hillslope cells is formally incorporated through a more physically-based expression. In the model, the catchment is represented

by a raster of grid-cells that incorporates the surface topography and the artificial features that are typical of urban areas. Each cell of this terrain is identified as a hillslope, street, pipe, or channel. Flow paths from each cell to the outlet are identified from the terrain, and the travel times in each cell are computed with closed form expressions obtained from kinematic wave theory. These expressions vary with the type of cell and incorporate the climatic dependence through the rainfall intensity. The travel times are aggregated along each flow path to calculate the total travel time from each cell to the outlet, and the IUH is obtained by generating the probability density function (PDF) of the travel times to the outlet. The model executes this routine for each excess rainfall pulse, so that a different IUH is obtained and convoluted with each rainfall pulse. The structure of the paper is as follows. In the next section, the model formulation is presented. Then, we introduce the study area and the associated dataset in the section "Study site". The testing of the model is presented in the section "Performance of the model", while the section "Characteristics of the U-McIUH model" explores the method's characteristics and capabilities. The last section of the paper comprised a summary the main conclusions.

4.2 Description of the Model

4.2.1 The geomorphoclimatic instantaneous unit hydrograph

Rodríguez-Iturbe and Valdés (1979) and Gupta et al. (1980) introduced the GIUH theory, which uses the spatial structure of the basin to identify the IUH. In the theory, the IUH is defined as the PDF of the travel time to the catchment outlet, i.e. the probability that a rainfall drop chosen at random from the input has reached the outlet at time t. In

this study, we reinterpret the IUH as the PDF of the travel time to the catchment outlet for a perturbation in the flow. With this slight revision, the IUH describes the travel time of the flood wave instead of individual water particles. An implicit or explicit approach can be adopted to define the GIUH (see Lee and Yen, 1997 and Liu et al., 2003 for a detailed discussion). In the implicit approach, Horton's laws are used to characterize the organization of the flow paths. In the explicit approach, the individual flow paths from each location in the catchment to the outlet are defined using a DEM. The explicit approach is more appropriate for urban catchments, given the complexity of the flow paths, their possible deviation from Horton's laws, and the increasing availability of drainage system data (Rodriguez et al., 2003). The approach also facilitates the use of spatially-variable flow velocities in artificial conduits within the subcatchment.

Rodríguez-Iturbe et al. (1982) extended the GIUH to the geomorphoclimatic instantaneous unit hydrograph (GcIUH), which incorporates climatic data (i.e. the excess rainfall intensity and duration) in the identification of the IUH. With this addition, the original formulation departed from the linearity assumptions because the IUH becomes variable for different rainfall inputs. Rodriguez et al. (2003 and 2005) observed a strong dependence of the shape of the IUH in urban catchments on the return period of the rainfall event. Therefore, a morphoclimatic approach is more suitable than a purely morphologic approach in identifying the IUH in urban catchments (as suggested by Rodriguez et al. (2005), the term "morphological" is used here instead of "geomorphological" because artificial conduits are a major portion of the urban drainage network).

4.2.2 Urban terrain representation

A detailed description of the flow paths is of great importance in determining the hydrologic response in urban catchments (Lhomme et al., 2004; Rodriguez et al., 2003; Rodriguez et al., 2005, Gironás et al., 2009). In this study, we use the method proposed by Gironás et al. (2009) to pre-process urban DEMs for the generation of urban terrains. In this method, the streets and pipes are "burned" into the DEM by reducing the elevation of the cells where these artificial conduits are located. Unlike the more common approach in which a constant depth is subtracted, the method uses the local conduit depths when making the elevation adjustments. This approach allows the flow in the conduits to have different directions than the flow on the ground surface. The data required for implementing the method are the raw DEM and vector layers representing conduits (i.e. streets, pipes, and channels) with the planar and vertical coordinates of the upstream and downstream ends of each element. After processing the DEM, the post-processing routines available in Arc Hydro are used to fill pits, compute the local slopes, and generate the flow directions using the direction of steepest descent.

The methodology for the terrain representation also generates a second raster with the classification of each cell in the catchment. Thus, cells representing overland flow (hillslopes) and flow in conduits (streets, pipes, and open channels) can be easily identified. If both a street and a pipe occur in a cell, it is labeled a pipe. Similarly, if a street or a pipe occurs together with a channel, the cell is identified as a channel. The raster file that identifies the cell classifications is linked to other raster files containing the geometrical attributes of the conduits (i.e. slopes and other geometric properties). This approach allows the U-McIUH to use the actual values of these properties when

calculating the hydrologic behavior of the conduit in each cell. In the case of a hillslope cell, all the required geometric attributes can be determined directly from the DEM.

4.2.3 Excess rainfall

The U-McIUH depends on the excess rainfall rate as described earlier. Thus, although this study focuses on the travel times in a subcatchment, a method is needed to partition total rainfall into excess rainfall and losses. Two losses are considered here: an initial abstraction (including depression storage and interception) and infiltration. The initial abstraction *IA* is constant over the catchment and must be filled completely prior to the occurrence of infiltration and runoff (Table 4.1 contains a complete list of symbols used in this paper). The infiltration capacity is represented by a simplified version of the Horton model (Viessman and Lewis, 1995) where the initial and final infiltration rates are the same and equal to a constant infiltration capacity f_c, which is a property of the soil. Perrin et al. (2001) used an equivalent approach to successfully represent losses in a peri-urban catchment in Ecuador. In reality, the infiltration capacity is expected to depend on the antecedent moisture conditions. Because the U-McIUH will be applied to individual events, an event-dependent calibration parameter C is used to account for the antecedent moisture.

The impervious area is also included in this simple model for excess rainfall. In a cell j of area A_j, the imperviousness H_j is defined as the ratio A_j^I / A_j, where A_j^I is the impervious area of the cell. It is assumed that all rainfall occurring on the impervious area becomes runoff. Thus, after the initial abstraction occurs, the excess rainfall intensity produced by the cell j at a time i ($E_{j,i}$) is computed as:

$$E_{j,i} = \begin{cases} I_i H_j & \text{if } I_i \le f_c / C \\ (1 - H_j)\left(I_i - \dfrac{f_c}{C}\right) + I_i H_j & \text{if } I_i > f_c / C \end{cases} \tag{4-1}$$

where I_i is the rainfall intensity. $E_{j,i}$ is computed for all the cells in the urban terrain including those classified as conduits, and this spatially distributed field is used to generate the different IUHs.

Table 4.1. Comprehensive list of nomenclature used in this study

Nomenclature			
A	Area (L^2)	Q_u	Upstream inflow to conduits (L^3 T^{-1})
A^I	Impervious area (L^2)	q	Discharge in a plane per unit width (L^2 T^{-1})
A_c	Cross-sectional flow area in conduits (L^2)	q_L	Uniform lateral inflow to a conduit (L^2 T^{-1})
A_u	Contributing area (L^2)	q_u	Upstream inflow to a plane per unit width (L^2 T^{-1})
B	Bottom width of rectangular conduits (L)	R	Total # of cells in a flow path
C	Infiltration parameter	r	Identification for cells in a flow path
D	Diameter (L)	S	Slope (L/L)
d	Water depth in conduits (L)	T	Travel time from a cell to the outlet (T)
E	Excess rainfall intensity (L T^{-1})	t	Time (T)
$\overline{E}$	Spatially averaged depth of an excess rainfall pulse (L)	t_L	Travel time in conduits (T)
f_c	Infiltration rate (L T^{-1})	t_{max}	Time to peak (T)
H	Total imperviousness	u	identification of precipitation intervals
H_u	Total imperviousness of contributing area A_u	V	Velocity, defined for hillslopes, streets, pipes and channels (L T^{-1})
$H(x)$	Imperviousness function (L^2)	v	identification of discharge intervals
$h(t)$	Unit hydrograph for an excess-rainfall duration Δt	$W(x)$	Width function (L^2)
I	Rainfall intensity (L T^{-1})	y	Flow depth in a plane (L)
i	Time interval identification	z	Side slope (H/V) for vertical curb conduits
IA	Initial abstraction (L)	α_h	Kinematic wave parameter for overland flow
j	Cell identification	α_c	Kinematic wave parameter for flow in conduits
K_s	Hydraulic conductivity at natural saturation (L T^{-1})	B_h	Kinematic wave parameter for overland flow
L	Length of conduits (L)	β_c	Kinematic wave parameter for flow in conduits
$L_{T,L}$	Total vector length of conduits (L)	Δt	duration of an excess rainfall pulse (T)
$L_{T,\ell}$	Total length of conduits from raster (L)	Δx	grid cell size (L)
ℓ	Flow length across a grid cell (L)	ϕ	Parameter for correction of conduit lengths
N_T	Total number of cells in the catchment	λ	Dimensionless inflow ratio in a plane relating q_u to E
n	Manning's roughness coefficient, defined for hillslopes, streets, pipes and channels	λ_c	Dimensionless inflow ratio in a conduit relating Q_u to q_L
n_P	n for pervious areas	τ	Travel time in a cell (T)
n_I	n for impervious areas		
$\underline{n}_t$	# of cells with common values of $T = t$		
Q	Discharge (L^3 T^{-1})		

4.2.4 Overland flow representation

Overland flow is simulated using a travel time for each cell that is derived from kinematic wave theory. Kinematic wave was selected for travel time computations for both hillslope and conduit cells due to its extensive use in small to mid-size urban drainage systems (Overton and Meadows, 1976; Singh, 2001; Xiong and Melching, 2005) where shallow flows and short and fairly steep prismatic conduits are commonly found (Pilgrim and Cordery, 1993; ASCE, 1996; Singh, 1996). For hillslope cells, it is assumed that the equilibrium in each individual cell is always reached before the end of a rain pulse. Rodríguez-Iturbe et al. (1982) tested this hypothesis for subcatchments of order 1 in natural watersheds (instead of hillslope grid cells) and showed its validity. Given the small size of a grid cell, it is very likely that equilibrium will be reached for a given rainfall pulse intensity and duration, and this approximation has been widely used to represent overland flow and travel time in hillslope cells (Muzik, 1996; Kilgore, 1997; Melesse and Graham, 2004; Du, 2009).

In a typical basin, many hillslope cells are linked together with flow being transferred from upslope hillslope cells to downslope hillslope cells. This connectivity is addressed by using an expression for the time of equilibrium that depends not only on the precipitation over the cell but also on the upstream contribution of flow. Using kinematic wave theory, Wong (1995) derived an expression for the wave-celerity-based travel time τ for a rectangular plane subjected to a uniform excess rainfall pulse of intensity E and with a constant upstream inflow per unit width q_u. This expression, which is also an expression for the time to equilibrium, can be written:

$$\tau = \left(\frac{\ell E^{1-\beta_h}}{\alpha_h} \right)^{1/\beta_h} \left[(\lambda+1)^{1/\beta_h} - \lambda^{1/\beta_h} \right] \tag{4-2}$$

where ℓ is the flow length across the plane and $\lambda \equiv q_u / (E\ell)$ is a dimensionless inflow relating q_u and the excess rainfall produced per unit width. α_h and β_h are parameters that relate the discharge per unit width $q = E\ell + q_u$ to the flow depth y as follows:

$$q = \alpha_h y^{\beta_h} \tag{4-3}$$

Using Manning's equation, the discharge-depth parameters are $\alpha_h = S^{0.5}/n$ and $\beta_h = 5/3$, where S is the slope of the plane and n is Manning's resistance coefficient. Eq. (4-2) becomes:

$$\tau = 6.99 \left(\frac{n\ell}{\sqrt{S}} \right)^{0.6} E^{-0.4} \left[(\lambda+1)^{0.6} - \lambda^{0.6} \right] \tag{4-4}$$

where τ is in min, S in m m^{-1}, ℓ in m, and E in mm h^{-1}.

If the upstream inflow to the plane is zero ($q_u = \lambda = 0$), Eq. (4-4) reduces to the traditional kinematic wave expression of τ for a rectangular plane of length ℓ and slope S (Bedient and Huber, 2002)

$$\tau = 6.99 \left(\frac{n\ell}{\sqrt{S}} \right)^{0.6} E^{-0.4} \tag{4-5}$$

Eq. (4-5) or similar expressions that do not consider the effects of upstream flow on the computation of travel times have been used in previous DEM-based models for urban areas (e.g. Zech et al., 1994; Melesse and Graham, 2004; Kute and Stuart, 2008). The effect of the upstream contribution on the travel time of a hillslope cell will be evaluated later in this work.

Generalizing the nomenclature to allow variations in time and between cells, we

obtain $\tau_{j,i}$ the travel time at a hillslope cell j for an excess rainfall pulse $E_{j,i}$ at time i as:

$$\tau_{j,i} = 6.99\left(\frac{n_j \ell_j}{\sqrt{S_j}}\right)^{0.6} E_{j,i}^{-0.4}\left[(\lambda_j + 1)^{0.6} - \lambda_j^{0.6}\right] \tag{4-6}$$

where j is an index of cells and i is an index of times. In this expression, the slope S_j and the flow length ℓ_j in the grid cell j are obtained from the processed urban terrain, n_j is assumed to be a function of the landuse, and $E_{j,i}$ is obtained using Eq. (4-1). $\ell_j = \Delta x$ (the grid resolution) when the downstream flow is vertical or horizontal, and $\ell_j = \Delta x\sqrt{2}$ when the flow is in the diagonal direction. In Eq. (4-6), we have assumed that λ_j is constant in time. In reality, this dimensionless ratio would change as the relative contributions of upstream flow and local flow change. To simplify the method, we use a temporally invariant "effective" value of λ_j by first assuming that precipitation is homogeneous over the catchment. In this case, the upstream discharge is dependent on the contributing area (Rodríguez-Iturbe et al., 1992, Rodríguez-Iturbe and Rinaldo, 1997). In addition, because impervious areas play a major role in the generation of runoff in urban areas, we neglect the contribution of flow from the pervious areas. Note that these assumptions are only applied for the purpose of obtaining the value of λ_j (not for the method as a whole). Under these assumptions, λ_j is the ratio between the total impervious area contributing to cell j and the impervious area of the cell itself:

$$\lambda_j = \frac{H_{u,j} A_{u,j}}{H_j A_j} \tag{4-7}$$

where $A_{u,j}$ is the contributing area for cell j, $H_{u,j}$ is the total imperviousness of the contributing area $A_{u,j}$, and H_j is the imperviousness of cell j. The final expression for

travel time in hillslope cells, $\tau_{j,i}$, is obtained by substituting Eq. (4-7) in Eq. (4-6):

$$\tau_{j,i} = 6.99\left(\frac{n_j \ell_j}{\sqrt{S_j}}\right)^{0.6} E_{j,i}^{-0.4}\left[\left(\frac{H_{u,j}A_{u,j}}{H_j A_j}+1\right)^{0.6} - \left(\frac{H_{u,j}A_{u,j}}{H_j A_j}\right)^{0.6}\right] \tag{4-8}$$

The units of Eq. (4-8) are the same as those in Eq. (4-4), and the areas A_j and $A_{u,j}$ are defined in m^2. This expression depends on E, so the climatic dependence of the IUH identified by Rodríguez-Iturbe et al. (1982) is partially incorporated for the hillslope cells (it will be addressed similarly for the conduit cells). In this respect, the Mc-IUH relaxes the linearity assumption used in UH theory. However, because the dimensionless ratio λ_j does not vary temporally during a storm in response to the actual flows entering each grid cell at each time, the method still remains simpler both in its theory and in its computation than full kinematic wave routing.

4.2.5 Conduit flow representation

Travel times in cells representing conduits are also computed using kinematic wave theory. We consider three types of conduit elements: streets (represented as gutters), pipes, and channels. Wong (2003) derived the following expression for the wave's travel time t_L in a conduit of length L:

$$t_L = \left(\frac{L}{\alpha_c q_L^{\beta_c - 1}}\right)^{1/\beta_c}\left[(\lambda_c + 1)^{1/\beta_c} - \lambda_c^{1/\beta_c}\right] \tag{4-9}$$

where α_c and β_c are parameters relating the discharge in the conduit Q to the cross-sectional flow area A_c in the expression $Q = \alpha_c A_c^{\beta_c}$. λ_c is a dimensionless ratio relating the upstream inflow Q_u to the uniformly distributed lateral inflow q_L:

$$\lambda_c \equiv \frac{Q_u}{q_L L} \tag{4-10}$$

Eq. (4-9) is in the same form as Eq. (4-2), and it is consistent with the travel time formula proposed by Lee and Yen (1997). In order to adapt Eq. (4-9) so that it can be used in a grid cell formulation, we need to estimate the conduit length that should be associated with each conduit cell. An obvious choice for L would be ℓ_j obtained from the grid cell dimension. However, this approach would overestimate the length of a conduit that traverses multiple cells unless the conduit is directly aligned with the grid or the diagonal direction. This bias can be quantified by measuring a factor ϕ, which is the ratio of the total length measured from the raster representing these conduits using ℓ ($L_{T,\ell}$) and the true total length of the conduits belonging to the drainage system ($L_{T,L}$):

$$\phi \equiv \frac{L_{T,\ell}}{L_{T,L}} \tag{4-11}$$

The conduit length L in a cell j could then be estimated by ℓ_j multiplied by $1/\phi$. Note that this approach is still an approximation because the same value of ϕ is used throughout the system (irrespective of the local pipe orientation).

A second consideration in adapting Eq. (4-9) to a grid cell is the value for q_L. This variable is calculated as the flow produced by the excess rainfall in the cell $E_{j,i}A_j$ divided by the conduit flow length ℓ_j/ϕ. This approach implies that cells identified as conduits are able to generate runoff, and the travel time depends on the excess rainfall rate (like the hillslope cells). Finally, like hillslopes, λ_c is computed using the ratio of the upstream and local impervious areas (see Eq. (4-7)). From Eq. (4-9), we obtain the final expression for the travel time in a conduit cell j at time i, $\tau_{j,i}$, as:

$$\tau_{j,i} = \frac{\ell_j}{\phi}\left[\frac{1}{\alpha_{c,j}(E_{j,i}A_j)^{\beta_{c,j}-1}}\right]^{1/\beta_{c,i}}\left[\left(\frac{H_{u,j}A_{u,j}}{H_jA_j}+1\right)^{1/\beta_{c,j}} - \left(\frac{H_{u,j}A_{u,j}}{H_jA_j}\right)^{1/\beta_{c,j}}\right] \tag{4-12}$$

where the notation of $\alpha_{c,j}$ and $\beta_{c,j}$ implies that the values of the kinematic wave parameters for conduits vary depending on whether the cell j represents a street, pipe, or channel. These parameters will be calculated using Manning's equation for each conduit type.

Flow in street grid cells is modeled using a gutter geometry because gutters typically convey the flow. Assuming a gutter section with a vertical curb and a side slope (H/V) of z, the kinematic wave parameters are (Wong and Zhou, 2006):

$$\alpha_c = \frac{\sqrt{S}}{n}\left[\frac{z}{2(1+\sqrt{1+z^2})^2}\right]^{1/3} \tag{4-13}$$

$$\beta_c = 4/3 \tag{4-14}$$

Substituting Eq. (4-13) and (4-14) into Eq. (4-12) and allowing n, S, and z to vary between cells, gives the following expression for $\tau_{j,i}$:

$$\tau_{j,i} = \frac{0.86}{\phi}\left(\frac{n_j}{\sqrt{S_j}}\right)^{3/4}\frac{\ell_j}{(E_{j,i}A_j)^{1/4}}\left(\frac{1+\sqrt{1+z_j^2}}{\sqrt{z_j}}\right)^{1/2}\left[\left(\frac{H_{u,j}A_{u,j}}{H_jA_j}+1\right)^{3/4} - \left(\frac{H_{u,j}A_{u,j}}{H_jA_j}\right)^{3/4}\right] \tag{4-15}$$

The units are min for $\tau_{j,i}$, m m^{-1} for S_j, m for ℓ_j, mm h^{-1} for $E_{j,i}$ and m^2 for A_j and $A_{u,j}$.

Pipes are assumed to have a circular cross-sectional shape and a flow depth d below the limit of $d/D = 0.87$. For these conditions, the kinematic wave parameters are (Wong and Zhou, 2003):

$$\alpha_c = 0.501\frac{D^{1/6}\sqrt{S}}{n} \tag{4-16}$$

$$\beta_c = 5/4 \tag{4-17}$$

Substituting Eq. (4-16) and (4-17) in Eq. (4-12) and allowing for variability of n, S and D between grid cells gives:

$$\tau_{j,i} = \frac{0.59}{\phi}\left(\frac{n_j}{\sqrt{S_j}}\right)^{4/5}\frac{\ell_j}{(E_{j,i}A_j)^{1/5}D_j^{2/15}}\left[\left(\frac{H_{u,j}A_{u,j}}{H_jA_j}+1\right)^{4/5}-\left(\frac{H_{u,j}A_{u,j}}{H_jA_j}\right)^{4/5}\right] \tag{4-18}$$

Units are the same as those of Eq. (4-15) and D is calculated in m.

Channels sections are approximated as wide and rectangular with width B. The kinematic wave parameters in this case are (Wong and Zhou, 2006):

$$\alpha_c = \frac{\sqrt{S}}{nB^{2/3}} \tag{4-19}$$

$$\beta_c = 5/3 \tag{4-20}$$

Wong and Zhou (2006) also give the values of these parameters for other channel sections, which could be used if the channels are not well-approximated as wide and rectangular. Substituting Eq. (4-19) and (4-20) into Eq. (4-12) and allowing n, S and B to vary between grid cells, gives:

$$\tau_{j,i} = \frac{6.99}{\phi}\ell_j\left(\frac{n_j}{\sqrt{S_j}}\right)^{3/5}\left(\frac{B_j}{E_{j,i}A_j}\right)^{2/5}\left[\left(\frac{H_{u,j}A_{u,j}}{H_jA_j}+1\right)^{3/5}-\left(\frac{H_{u,j}A_{u,j}}{H_jA_j}\right)^{3/5}\right] \tag{4-21}$$

Units are the same as those of Eq. (4-15), and B has units of m.

4.2.6 Instantaneous unit hydrograph and convolution

To compute the total travel time T_j of the wave going from each cell j to the outlet, we add the travel times along the R_j cells belonging to the flow path starting at that cell. The

travel time in each cell is obtained using Eqs. (4-8), (4-15), (4-18) and (4-21), depending on the classification of each cell on the path. Thus, T_j is given by:

$$T_j = \sum_{r \in R_j} \tau_r \tag{4-22}$$

Note that both τ and T_j depend on the excess rainfall rate. Following the definition proposed by Rodríguez-Iturbe and Valdés (1979) and Gupta et al. (1980), the IUH corresponds to the PDF of the travel times, $f(T_j)$. From the IUH, Chow et al. (1988) derived $h(t)$, which is the UH for an excess rainfall duration Δt as:

$$h(t) = \frac{1}{\Delta t} \int_{t-\Delta t}^{t} f(T_j)\, dT = \frac{F(t) - F(t-\Delta t)}{\Delta t} \tag{4-23}$$

where $F(t)$ is the cumulative probability of the travel time for points within the catchment and Δt has the same units as T_j. In the right side of Eq. (4-23), $F(t) - F(t-\Delta t)$ is equivalent to $P(t-\Delta t \le T \le t)$ which can be estimated as $\underline{n}_t / N_T$, where $\underline{n}_t$ is the number of cells whose travel time to the outlet is in the range [t-Δt t], and N_t is the total number of cells in the catchment. Note that $\underline{n}_t$ depends on the excess rainfall rate. Thus, the UH for a pulse of duration Δt is calculated as:

$$h(t) = \frac{1}{\Delta t} \frac{\underline{n}_t}{N_T} \tag{4-24}$$

Finally, Q_v, the flow rate at the v^{th} time interval of length Δt, is given by the discrete convolution between the rainfall pulses and the corresponding UHs calculated from Eq. (4-24):

$$Q_v = A \sum_{i=1}^{v} \overline{E}_i h_{v-i+1} \tag{4-25}$$

where A is the area of the catchment, h is the UH corresponding to the i^{th} excess rainfall pulse and $\overline{E}_i$ is the spatially averaged excess rainfall depth of the i^{th} pulse, which is computed as:

$$\overline{E}_i = \frac{\Delta t}{N_T} \sum_{j \in N_T} E_{j,i} \tag{4-26}$$

In Eq. (4-25), if A is in m^2 and P_u is in mm, the units of Q are l s^{-1}. Note that we are convoluting a UH derived from a spatially-distributed excess rainfall field with the spatially-averaged excess rainfall depth. This quasi-linear approach was proposed by Muzik (1996) and has been used by others (e.g., Lee and Yen, 1997; Hall et al., 2001; Lee et al., 2008). It allows incorporation of the climatic-dependence of the IUH and thus the nonlinear response of catchments to excess precipitation.

4.3 Study Site

The U-McIUH method was studied by simulating a series of events in the Gohard and Aubinière catchments, which are located in the metropolitan area of Nantes, France. The Gohard catchment has an area of 163.7 ha and an overall imperviousness of 30.8%. It is a subcatchment of the Aubinière catchment, whose area is 10.9 km^2 and overall imperviousness is 31.7%. The Aubinière catchment is situated close to the Atlantic coast at an average elevation of 27 m. The region has an oceanic climate, and the total annual precipitation is around 800 mm (Gironás et al., 2009). The soils are loams and sandy loams (Rodriguez et al., 2008). The Gohard catchment contains single- and multi-family housing, commercial areas, and industrial zones and has been used previously to develop and test hydrologic models (Rodriguez et al., 2003, 2005 and 2008). The available data

include a DEM with a resolution of 20 m, an imperviousness raster with the same resolution, and layers delineating streets, storm sewer pipes, and natural channels. These layers include all the information required to define the urban terrain and apply the model. Figure 4.1 shows the boundaries of the Gohard and Aubinière catchments, the drainage systems, and the locations of the outlets. The boundaries of the catchments were obtained from the processed urban terrain.

The Gohard catchment was used to test the U-McIUH model because it has reliable discharge records. Three years (2001 – 2003) of rainfall and discharge records were discretized into a 5-min time steps. This short time step usually allows adequate representation of rapid changes in the runoff hydrographs (Bedient and Huber, 2002). Table 4.2 summarizes the beginning time, total precipitation, duration, and maximum intensity for the 17 events that were used in the evaluation of the U-McIUH. Note that the maximum rainfall intensity for these events ranges from about 2 mm/hr to about 36 mm/hr, the total precipitation ranges from less than 2 mm to more than 48 mm, and the storm duration ranges from less than 1 h to nearly 40 h. Thus, a relatively diverse range of rainfall events is included in this set. Base flow, which is typically small or nonexistent at the event time scale, was removed from observed discharge hydrographs using the straight line method (Viessman and Lewis, 1995). The Gohard has no open channels, so this component of the U-McIUH is not tested here. Later in this paper, the model will be applied to the entire Aubinière, which does include channels. The results for the larger catchment cannot be compared to observations because no reliable discharge data are available at the outlet of the Aubinière.

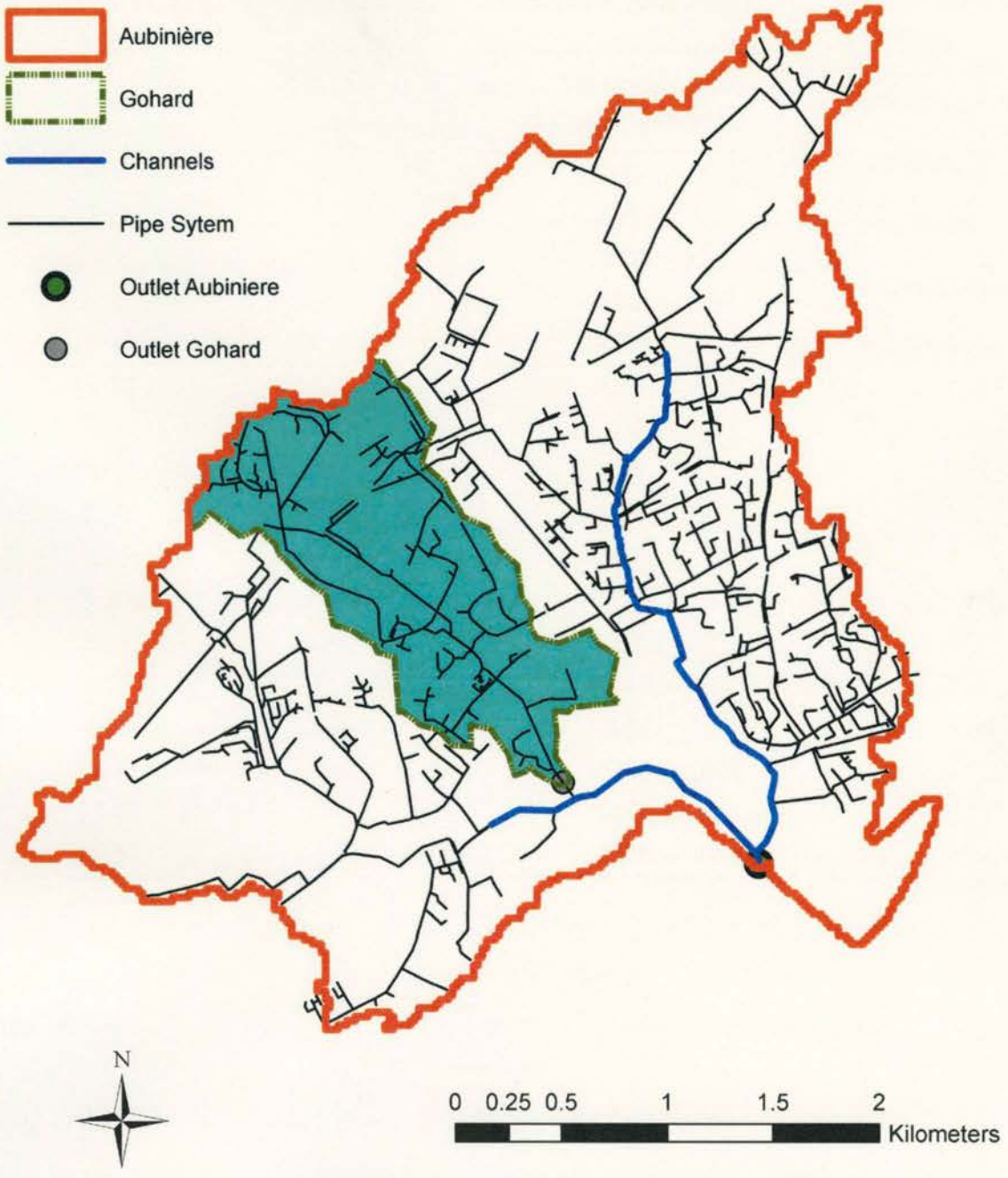

Figure 4.1. Study area including the Gohard and Aubinière catchments. The Gohard catchment is used to test the model performance and both catchments are used to study the properties of the model.

Table 4.2. Storm events that were simulated with the U-McIUH. The first five storms were used for calibration.

Storm event	Beginning date (dd-mm-year)	Beginning time (hh:mm)	Total Precipitation (mm)	Duration (hr)	Maximum intensity (mm/h)
1	03-Sept-2001	10:30	2.24	2.50	3.36
2	28-Sept-2001	21:35	3.66	4.33	2.76
3	02-Oct-2001	20:55	12.70	3.33	13.31
4	06-Oct-2001	3:35	5.33	13.42	6.82
5	07-Oct-2001	14:30	16.20	4.83	36.24
6	31-Jan-2002	19:15	5.20	8.17	3.82
7	13-Feb-2002	14:05	10.54	11.17	6.00
8	17-Apr-2002	18:10	1.80	0.92	6.05
9	01-Jul-2002	9:30	3.89	7.33	2.14
10	09-Jul-2002	3:35	10.14	7.75	7.37
11	02-Aug-2002	5:20	10.50	6.50	7.18
12	26-Aug-2002	5:15	22.00	18.75	4.82
13	24-Oct-2002	3:25	48.33	39.83	29.87
14	24-May-2003	7:25	7.53	10.08	15.82
15	30-Nov-2003	17:45	13.40	15.33	15.60
16	13-Dec-2003	15:15	5.2	4.67	3.60
17	20-Dec-2003	11:00	8.34	8.17	4.88

4.4 Performance of the Model

The raw DEM including both catchments was processed to generate the urban terrain according to the method previously summarized, and the U-McIUH was developed using this information. Flow direction, accumulation, length, and slope raster files were obtained from the urban terrain. The flow accumulation and imperviousness raster files were used in Eq. (4-7) to generate the raster file with values of λ_j. The saturated hydraulic conductivity K_s was measured at a depth of 0.2 m under natural conditions at a

nearby location and found to be 46.8 mm h^{-1} (Rodriguez et al., 2008). This value is used as an estimate of f_c. Values of n at hillslope cells were generated as the imperviousness weighted average of the roughness coefficients for pervious and impervious areas (n_P and n_I, respectively):

$$n_j = n_I H_j + n_P(1 - H_j) \tag{4-27}$$

Initial values of $n_P = 0.2$ and $n_I = 0.015$ were obtained from the literature (Novotny, 2003; Akan and Houghtalen, 2003). Preliminary values for the roughness coefficients for streets (n = 0.0161) and pipes (n = 0.0152) were obtained from a previous study in the area (Rodriguez et al., 2003), and a preliminary value of n = 0.15 for the channels was determined from the literature (Chin, 2006), typical of brush and irregular channels. For conduit cells, the pipe diameters D, channel widths B, and slopes S, were determined from the complementary raster files generated from the original vector representations of the conduits. A constant side slope z = 25 was assumed for the street gutters, which was adopted from typical ranges given in the literature (Nicklow, 2001). To estimate the length correction factor ϕ, we computed values of $L_{T,L}$ = 14 827 m and $L_{T,\ell}$ = 22 002 m in the Gohard catchment, and $L_{T,L}$ = 86 185 m and $L_{T,\ell}$ = 126 649 m in the Aubinière catchments. Using Eq. (4-11), we obtain an average value of ϕ = 1.475, which we used in both catchments.

The five rainfall events available in year 2001 were used to manually calibrate the model. We adopted n_P as the calibration variable for hillslope cells due to the difficulties in estimating its value. Likewise, n was used for calibration of street and pipe cells. n for channels was not calibrated due to the absence of channels in the Gohard. The

calibration aimed to maximize the value of the modified coefficient of efficiency (MCE), which is defined as (Legates and McCabe, 1999):

$$\mathrm{MCE} = 1 - \frac{\sum_{v} \left| Q_{obs,v} - Q_{sim,v} \right|}{\sum_{v} \left| Q_{obs,v} - \overline{Q}_{obs,v} \right|} \tag{4-28}$$

where $Q_{obs,v}$ is the observed discharge, $Q_{sim,v}$ is the simulated discharge, $\overline{Q}_{obs,v}$ is the average of the observed discharges, and v indicates each time interval belonging to the period of simulation. A value of one indicates an exact match with the observations, and a value of zero implies that the simulation predicts the observed discharges with the same efficiency as $\overline{Q}_{obs,v}$. In addition to the MCE, the ratio between the observed and simulated peak discharges $Q_{\max}^{obs} / Q_{\max}^{sim}$, the ratio of the observed and simulated volumes V^{obs} / V^{sim}, and the error between the observed and simulated time to peak $\left| t_{\max}^{obs} - t_{\max}^{sim} \right|$ were calculated for all events. In the end, the calibrated value of the pervious surface roughness was n_P = 0.1, and calibrated values of n for the streets and pipes were 0.0289 and 0.0242, respectively. These values are in the upper part of the range of typical values proposed by the literature (e.g., Bedient and Huber, 2002) and may suggest the presence of obstacles in the gutters (tires on parked cars) and sediments and/or tree roots in some of the pipes.

Because the U-McIUH is an event-based model, values of *IA* and *C* were adjusted for each storm (Table 4.3). These parameters depend on the soil moisture conditions at the beginning of an event and could eventually be estimated through a continuous formulation of the model. Values of *IA* for all the storms ranged between 0.2 mm and 1.1 mm, with an average of 0.61 mm. These values agree with those summarized by Huber

and Dickinson (1988) for European catchments. Values of C ranged between 2.9 to 29.3, with an average of 13.7. These values imply an average effective infiltration rate (f_c/C) of 5 mm h^{-1}, a rate quite lower than K_s reported by Rodriguez et al. (2008). However, the same authors estimated a value of K_s = 0.025 mm h^{-1} at a depth of 1.5 m using an exponential decay model to represent the compaction effect on the soil. This rate is substantially lower than K_s near the surface and may explain the values obtained for f_c/C. Also, compaction of urban soil can significantly reduce its infiltration capacity (Gregory et al., 2006). Furthermore, the effective infiltration rates obtained are in the range defined for modeling purposes for soils similar to the one in the study area (Viessman and Lewis, 1995; Huber and Dickinson, 1988). Figure 4.2 shows the observed and simulated hydrographs for the calibration period.

The calibrated model was then tested using the 12 storm events in 2002 and 2003. In this second period of application, the parameters IA and C were still adjusted for each storm to account for the changing antecedent moisture conditions, but the roughness values were not changed from the values calibrated using 2001 data. Figure 4.3 compares the simulated and observed hydrographs. Overall, the simulated and observed flows are quite similar. The timing of the peak, recession times, and overall hydrograph shapes are all well predicted by the model. Table 4.3 summarizes the events and the values of the comparison criteria. The simulation start times given in Table 4.3 identify the zero times in Figure 4.2 and Figure 4.3. Among all the events, the MCE ranges between 0.52 and 0.82, with half of the storms having efficiencies greater than 0.75. The average values for the calibration and validation periods are 0.70 and 0.72, respectively. The lowest MCE values were obtained for events 5 and 13, in which Q_{max} was greatly

overestimated. During these particularly intense events, it is likely that the pipe system surcharged or simply flooded, causing flow conditions to differ from those assumed by the model. If these two events were not considered in the analysis, the average MCE improves to 0.75. A low MCE (0.55) was also obtained for event 8. Observed flows for that event show a second, smaller peak after the main one, which is not well simulated (Figure 4.3). However, the computed hydrograph is consistent with the structure of the storm event, which has only one peak. Underestimation of a later secondary peak is also observed for events 3, 6, 7, 12, 15, 16, 17, but a subset of these (events 7, 8, 15, and 17) show an overestimation of the preceding peak. Thus, some storage or flow detention in the system may not be adequately simulated by the model. Furthermore, this difference might also be due to the existence of base flow that was not properly removed from the observed hydrographs. Events 15, 16 and 17 have the highest base flows among the 12 events. Overall, the prediction of the peak discharges is reasonably good, with an average $Q_{\max}^{obs} / Q_{\max}^{sim}$ ratio of 0.86, and the average error for the volume (7%) is also fairly low. The model also does well in predicting the response time of the catchment and its dependence on the different pulse's intensities. The error in estimating t_{max} is 5 min or less in 11 out of the 17 events, and the maximum error is 15 min. The extremely large error in predicting t_{max} for event 6 is explained by the fact that two very similar peaks separated by 2 h and 35 min are observed for this event (Figure 4.3). The model predicts a slightly larger first peak, while the observations suggest a higher second peak. The larger of the two discharges is used to calculate t_{max}. This issue also affects the comparison of the peak discharges. $Q_{\max}^{sim}$ = 355.8 l/s is simulated at a time of 2.08 h, and $Q_{\max}^{obs}$ = 286.6 l/s occurs at 4.66 h. If one compares Q^{sim} and Q^{obs} at a consistent time of

4.66 h, Q^{obs}/Q^{sim} = 1.02. Overall, the model generates good results in spite of the simple representation of the excess rainfall and the absence of a hydraulic module to explicitly route the flows.

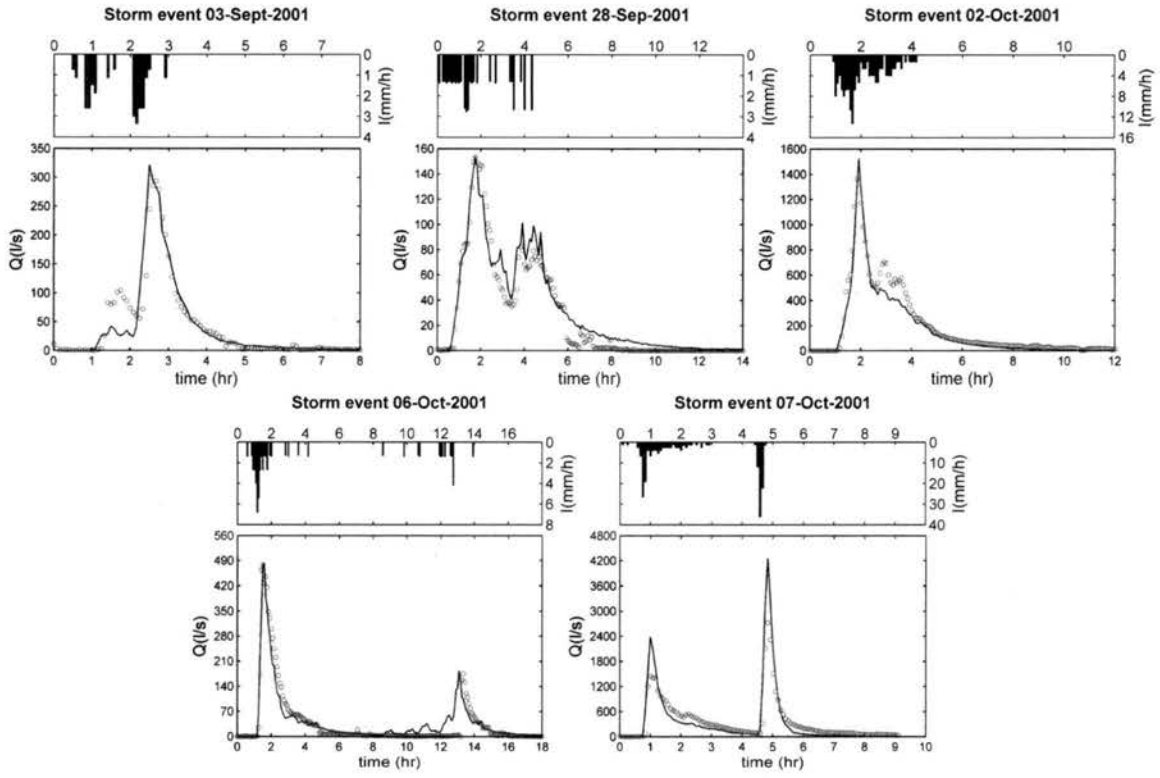

Figure 4.2. Comparison of the observed (circles) and simulated (lines) flows for the calibration events, which occurred in 2001.

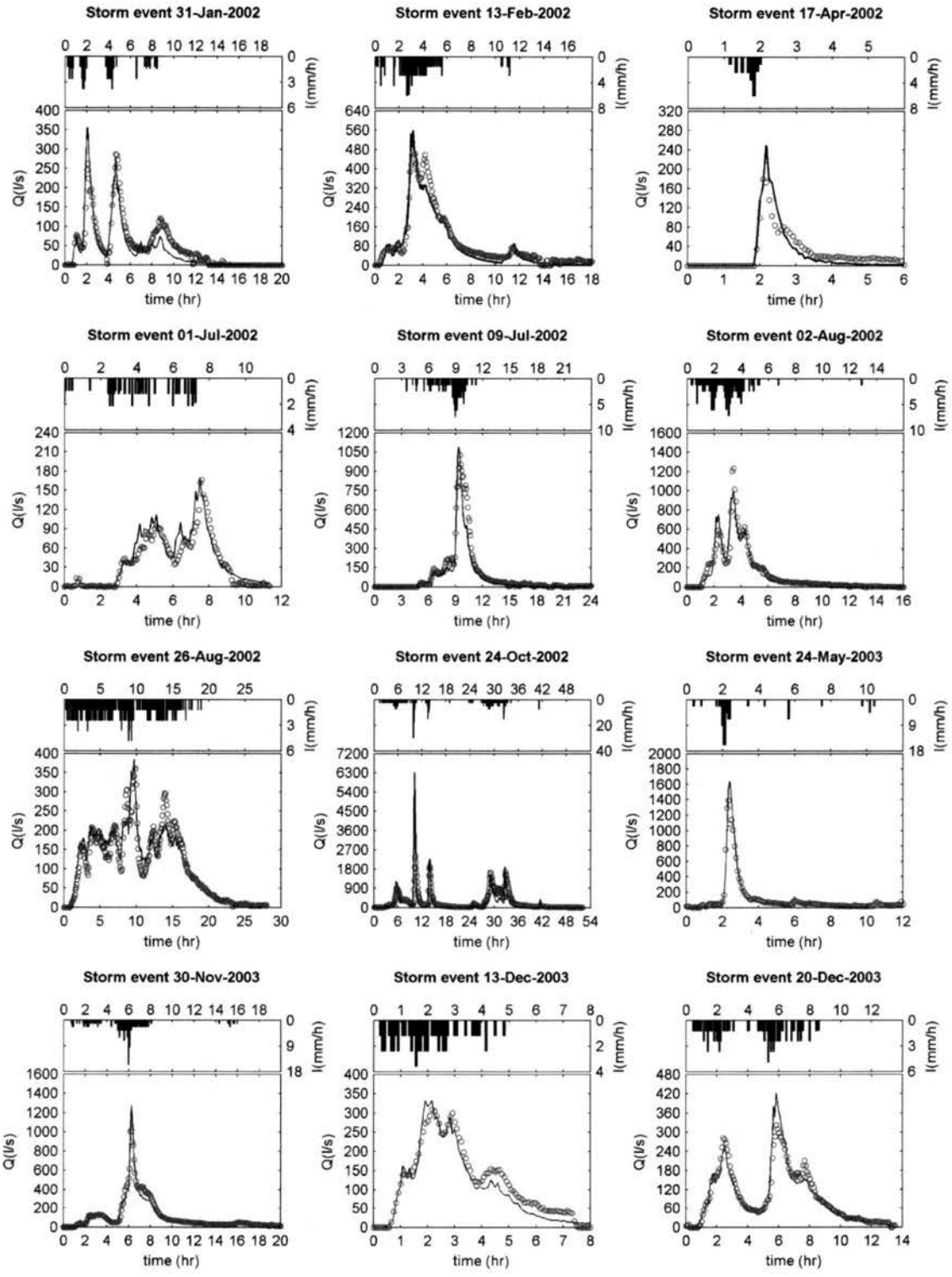

Figure 4.3. Comparison of the observed (circles) and simulated (lines) flows for the second period of application (2002-2003).

Table 4.3. Summary of the performance of the model. The first five events were used for calibration.

Storm event	Simulation start (hh:mm)	Duration of simulation (h)	*IA* (mm)	*C*	MCE	$\frac{Q_{\max}^{obs}}{Q_{\max}^{sim}}$	$\frac{V^{obs}}{V^{sim}}$	$\lvert t_{\max}^{obs} - t_{\max}^{sim} \rvert$ (hh:mm)
1	10:00	8	0.6	23.40	0.73	0.91	1.02	0:10
2	21:30	14	0.5	11.70	0.77	1.00	0.85	0:00
3	20:00	12	0.3	5.85	0.82	0.90	1.20	0:05
4	3:00	18	1.1	14.63	0.65	0.99	0.92	0:05
5	14:30	9	0.8	2.93	0.52	0.64	1.00	0:00
6	19:00	20	0.5	18.72	0.63	0.81	1.19	2:35
7	14:00	18	0.6	10.40	0.74	0.84	1.17	0:00
8	17:00	6	1.1	15.60	0.55	0.72	1.10	0:05
9	9:30	11.5	1	29.25	0.71	0.99	0.90	0:05
10	0:00	24	0.5	11.70	0.78	0.94	1.28	0:10
11	5:00	16	0.5	15.60	0.81	1.23	1.10	0:00
12	5:00	28	0.8	11.70	0.78	0.93	1.00	0:10
13	2:00	52	0.8	11.70	0.52	0.38	1.19	0:15
14	7:00	12	0.2	4.25	0.75	0.85	1.02	0:05
15	17:00	20	0.4	4.68	0.78	0.80	1.16	0:00
16	15:00	8	0.5	23.40	0.73	0.93	1.13	0:15
17	10:30	13.5	0.2	16.71	0.82	0.76	1.01	0:00

4.5 Characteristics of the U-McIUH Model

The U-McIUH model allows every cell in the subcatchment to have a different imperviousness and travel time, which is also climatic dependant. These characteristics contrast with methods previously used to represent the hydrologic response of urban areas. In this section, we compare the U-McIUH results to those produced under four assumptions used in other approaches. First, previous methods have neglected the effects of upstream flow on the travel times in hillslope cells (e.g., Rodriguez et al., 2003;

Melesse and Graham, 2004; Rodriguez et al., 2005; Kute and Stuart, 2008), so we examine how the modified travel times affect the simulated hydrographs. Second, previous methods have assumed that the velocity is constant within each cell classification (e.g. Zhang et al., 2001; Turner-Gillespie et al., 2003; Smith et al., 2005; Javier et al., 2007). Additionally, Rodriguez et al. (2003 and 2005) assumed a constant overland flow velocity. Thus, we examine the variability of velocity between and within these element classifications. Third, previous methods have assumed that the response of the basin is linear with respect to excess precipitation thus neglecting quicker travel times for higher flow rates (e.g. UDFCD, 2001; Akan and Houghtalen, 2003; Lhomme et al., 2004; Kute and Stuart, 2008), so we examine the modification of the IUH for different excess precipitation rates. Fourth, previous methods, particularly those based on semi-distributed representations of the catchment, have neglected explicit representations of the patterns of imperviousness (e.g., Aronica and Cannarozzo, 2000; Zhao, 2001; Zoppou, 2001), so we examine the change in the hydrologic response when the observed pattern is included. Lastly, we incrementally transforme the spatial structure of the basin into the U-McIUH to illustrate the combined effects of these various issues on the hydrologic response. The Aubinière catchment is used in this analysis (in addition to the Gohard) because two channels are part of its drainage system. Storm 11 is selected because its average intensity and duration are typical but its intensity varies through time. Unless noted otherwise, excess rainfall parameters IA = 0.5 mm and C = 15.6 (the parameters of Storm 11) are used for comparing responses to this storm.

4.5.1 Sensitivity of travel times in hillslope cells to the upstream contribution

The U-McIUH model incorporates the effect of upstream contributions on the computation of travel times in cells. Figure 4.4 illustrates the effect of the upstream contribution on the travel time of a typical cell, for instance a hillslope cell (β = 5/3). This figure plots values of the ratio of Eq. (4-4) and Eq. (4-5) for different values of λ. Eq. (4-4) corresponds to the travel time formulation for hillslope cells used in the model, while Eq. (4-5) corresponds to the traditional kinematic-wave-based formulation that neglects upstream inflows. No other assumption regarding the geometry of the cell is necessary given that the ratio of Eq. (4-4) and Eq. (4-5) is only function of λ. For a cell receiving an upstream discharge equal to the discharge produced by the rainfall over the cell ($\lambda = 1$), τ reduces to almost 50% of the τ of a cell with no upstream contribution. This reduction quickly increases as the value of λ increases and then tends to stabilize. This large deviation from 1 confirms that the travel time is highly sensitive to the contribution of upstream flows.

The effects of these different formulations are further studied by analyzing the simulated responses of the Gohard and Aubinière catchments to Storm 11. Figure 4.5a and Figure 4.5b show major differences in the IUHs generated when Eq. (4-4) and Eq. (4-5) are used to define travel times in hillslope cells. The time base is much longer and the peak flow is significantly lower when the upstream contribution of flow is neglected in calculating the travel times. Discrepancies are less important in the rising part of the hydrograph, which is more controlled by the faster flows in conduit cells and isolated hillslope cells that are directly connected to them. Neglecting the contribution of upstream flows also results in lower peaks and longer values of time base when the Storm

11 is simulated (Figure 4.5c and Figure 4.5d). One could calibrate the model based on Eq. (4-5) by reducing the value of n. However, and as shown in Figure 4.5d, that would negatively affect the timing of the peaks. The results may explain the findings of Melesse and Graham (2004). They had to define very small hillslope areas and represent the majority of the flow using channels because large hillslope areas resulted in slower travel times, which affected the performance of the model. Moreover, our study supports the finding by Lhomme et al. (2004) who concluded that slope and the upstream contributing area are the main morphologic parameters needed to characterize the "hydraulic pattern" (i.e. velocity) of the drainage system.

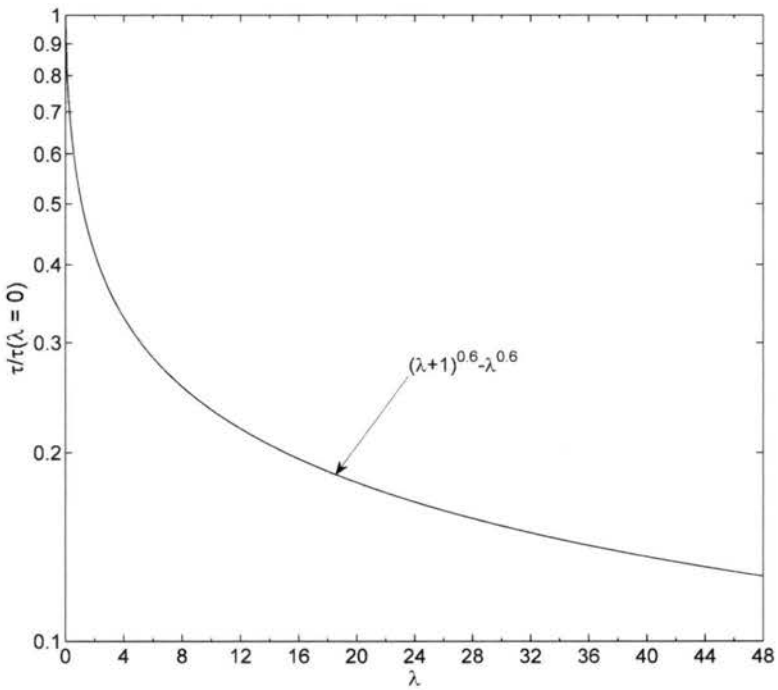

Figure 4.4. Sensitivity of the ratio of τ and τ when $\lambda = 0$ to different values of λ.

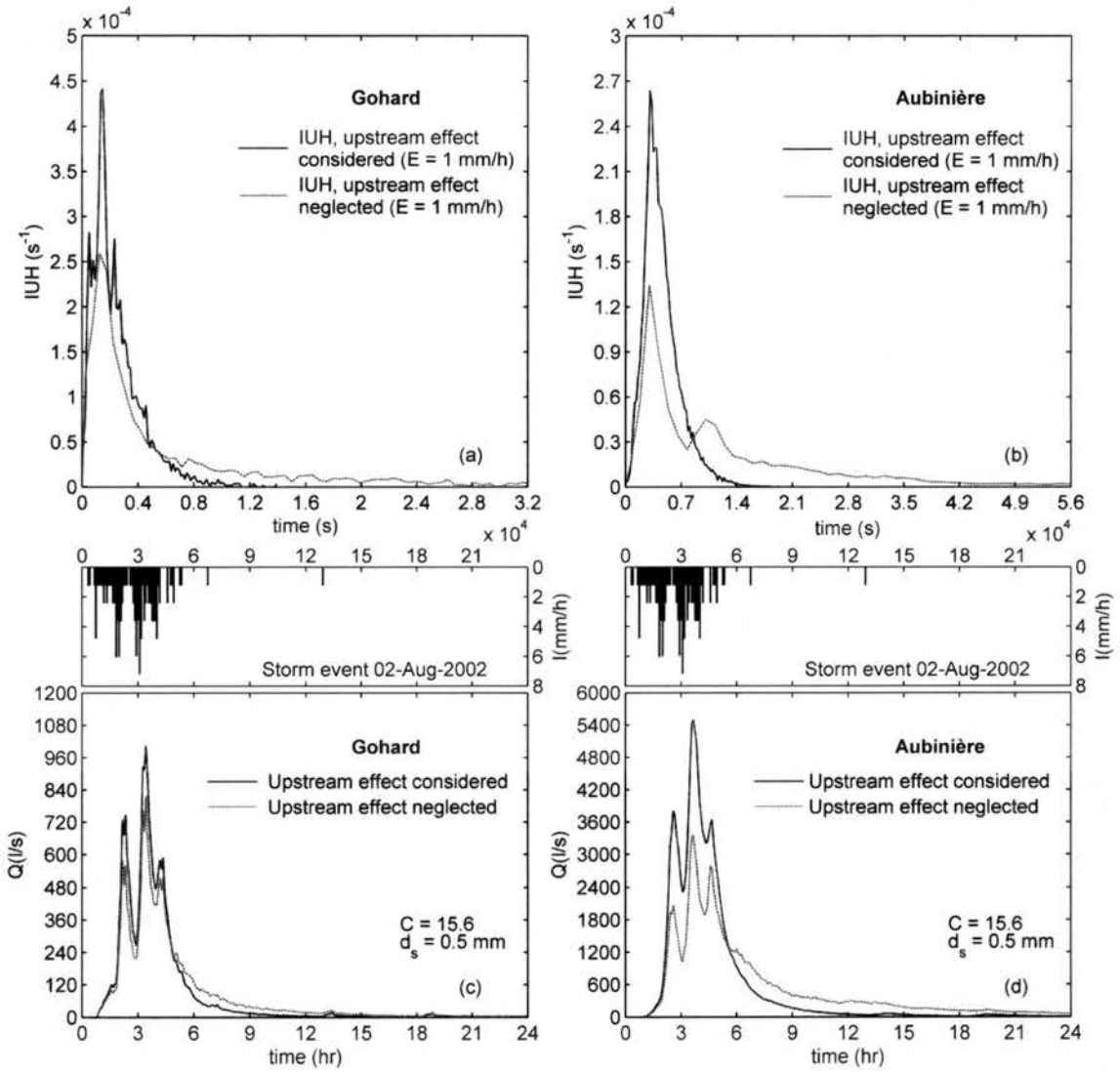

Figure 4.5. Effect of the upstream contribution of flow in the travel time formulation for hillslope cells on the IUH and hydrologic response of the catchment. (a) Comparison of the IUH for E = 1 mm/hr generated at the Gohard catchment when upstream effects are considered and neglected in the computation of travel times, (b) same for the Aubinière catchment, (c) comparison of the response to Storm 11 when upstream effects are considered and neglected in the computation of travel times in the Gohard catchment, (d) same for the Aubinière catchment.

4.5.2 Variability of travel times between and within cell classifications

The U-McIUH model distinguishes between hillslope, street, pipe, and channel cells, and it allows varying travel times within each of these cell classifications. We now examine the impact of the variability in travel times on the simulated hydrologic response. Figure 4.6 shows the cumulative distribution functions (CDFs) of the travel times simulated in each of the four types of cells. The CDFs were generated in the Aubinière catchment using a rainfall pulse of I = 10 mm h^{-1} and parameters C = 15.6 and IA = 0. Overall, travel times in the conduit cells are 10 to 80 times shorter than the travel times in the hillslope cells. This difference agrees with those from previous studies (Zhang et al., 2001; Turner-Gillespie et al., 2003; Smith et al., 2005; Javier et al., 2007). Travel times are around 4 to 8 times shorter in pipe cells than street cells. Variability is observed for among the travel times for a given classification. In fact, most of the CDFs span about one order of magnitude of travel time. In absolute terms, the hillslopes exhibit the widest range because their travel times are the largest on average and they are more sensitive to inflow contribution as represented by the parameter λ (Figure 4.4). Cells located upslope have small values of λ and thus large travel times, while cells located downslope have larger values of this parameter implying much lower travel times. The CDF for the channel cell travel times also indicates a wide range of variability. The shape of this CDF occurs because some cells near the outlet have very low slopes and thus very large travel times.

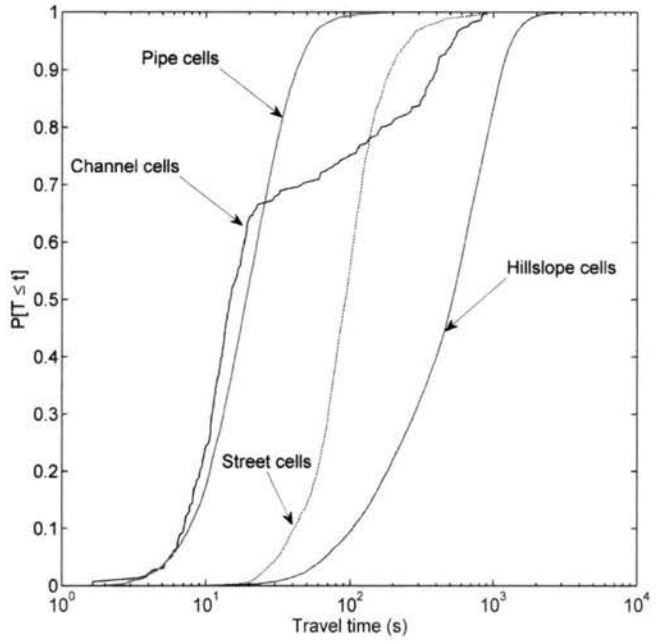

Figure 4.6. Cumulative distribution function (CDF) of travel times in different types of cells obtained using a 5 min rainfall pulse with an intensity of 10 mm/h over the Aubinière catchment. Excess rainfall parameters C = 15.6 and IA = 0 were used.

The impact of distinguishing between the different elements can be further studied by analyzing the hydrologic behavior as we successively incorporate each element classification into the characterization of the catchment. In this analysis, we use four different representations of the two catchments to generate both the IUH for an excess precipitation rate of 1 mm/h and the response to Storm 11. In the first representation, we identify all the catchment cells as channel cells and assume B_j = 1.6 m (the smallest width for a real channel in the Aubinière catchment) for all cells that were not originally defined as channel cells. In the second representation, we distinguish the hillslope cells while all other cells (i.e. the conduit cells) remain identified as channels. Next, we also distinguish the pipe cells, and finally we distinguish the street cells to include all four element classifications. Figure 4.7a and Figure 4.7b show the resulting IUHs and

illustrate how the final IUH is a combination of the rapid response of conduit cells and a slower recession that is more affected by the flow in hillslope cells. For the Gohard catchment, the IUHs produced by assuming only channels and by including channels and hillslopes share a short portion of the rising limb but then become very different when hillslope cells are incorporated. The peak flow decreases, and the time to peak and the time base increase. A major modification of the IUH is observed when pipes replace the channels (there are no channels in the Gohard). In this particular case, the peak flow increases and is more pronounced, and the time to peak decreases. Despite the shorter time to peak, the time base does not change, and the shape of the falling limb tends to be similar to the one produced by the channel-hillslope scenario. Finally, the replacement of the remaining channel cells with the streets has almost no effect in the shape of the IUH. Differences in travel times in pipe and street cells (4 to 8 times according to Figure 4.6) seem not to affect the shape of the response. This insensitivity may be due to the hierarchy used in the terrain representation, which defines as a pipe cell a cell crossed by both streets and pipes. Thus, a traditional drainage network in which pipes are under streets is mainly represented by a set of relatively isolated street cells and a cascade of pipe cells. The IUH of the Aubinière catchment exhibits similar changes as more elements are distinguished in the model. However, the IUHs for the initial scenario (only channels) and the final scenario are much more alike. This is because the existence of the channels in this catchment controls the flow in the rising limb. The effect of the pipes is observed in the spikiness of the peak flow while the hillslope cells affect the recession. Simulations with Storm 11 (Figure 4.7c and Figure 4.7d) produce faster recessions and higher peaks under the only-channels scenario, in spite of the larger peak flow of the IUH

for both catchments when pipes are included. This is explained by the consistently higher discharges of the IUHs that include only channels. This analysis suggests that it is important to distinguish overland and conduit flow at least. However, it is only with the inclusion of flow in pipes that spikiness and fast responses are observed.

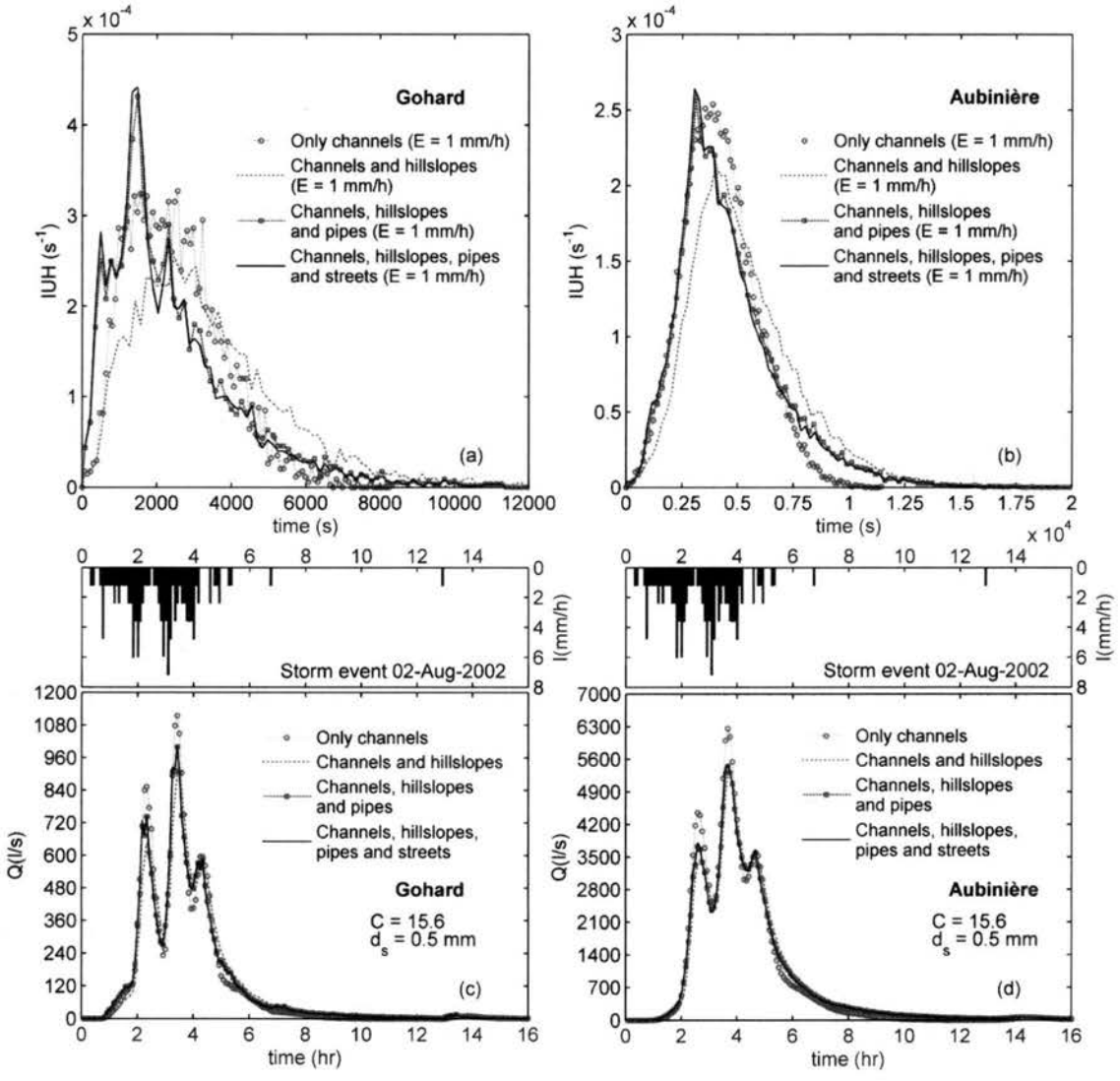

Figure 4.7. Effect of distinguishing different element types on the IUH and the hydrologic response to a storm. (a) Channel, hillslope, pipe and street cells are successively incorporated in the calculation of the IUH for E = 1 mm/h over the Gohard catchment, (b) same for the Aubinière catchment, (c) comparison of the response to Storm 11 when channel, hillslope, pipe and street cells are successively incorporated in the model of the Gohard catchment, (d) same for the Aubinière catchment.

4.5.3 Effect of the non-linearity in the response to excess precipitation

The U-McIUH model confronts the non-linearity of the runoff response by producing IUHs that depend on E. We explore this dependence by comparing the IUHs generated in both catchments using values of E = 1, 2, 5, 10, 20 and 40 mm h^{-1} (Figure 4.8a and Figure 4.8b). Larger intensities reduce the travel times particularly in hillslope cells, which increases the peak discharge of the IUH while reducing the time to peak and the time base. Comparing the IUHs for E = 1 mm h^{-1} and E = 40 mm h^{-1}, for example, the peak flow is about 3 times larger, while the time to peak is 60% shorter for the higher excess rainfall rate. We further explored the effects of the non-linearity by comparing the results of the U-McIUH model to an application of a constant IUH for the entirety of Storm 11 (Figure 4.8c and Figure 4.8d). In this experiment, the IUH generated by a pulse of E = 1 mm h^{-1} (the average E of the non-zero pulses of storm 11) was used for all excess precipitation intensities. The response generated by the constant IUH exhibits much less variability in the flow than the response of the U-McIUH. It also exhibits lower peak flows than the response from the U-McIUH. Note that the variability in flow produced by the U-McIUH is also found in the observations shown in Figure 4.3. A calibration of the constant IUH method would likely improve the simulation of this storm. However, in order to match the peak flows for these high intensities, the peak flows for other lower intensity events would likely be overestimated. This brief analysis confirms the findings by Rodriguez et al. (2003) and suggests that the nonlinearity in the response to excess precipitation can have a significant effect on the hydrologic response of an urban catchment.

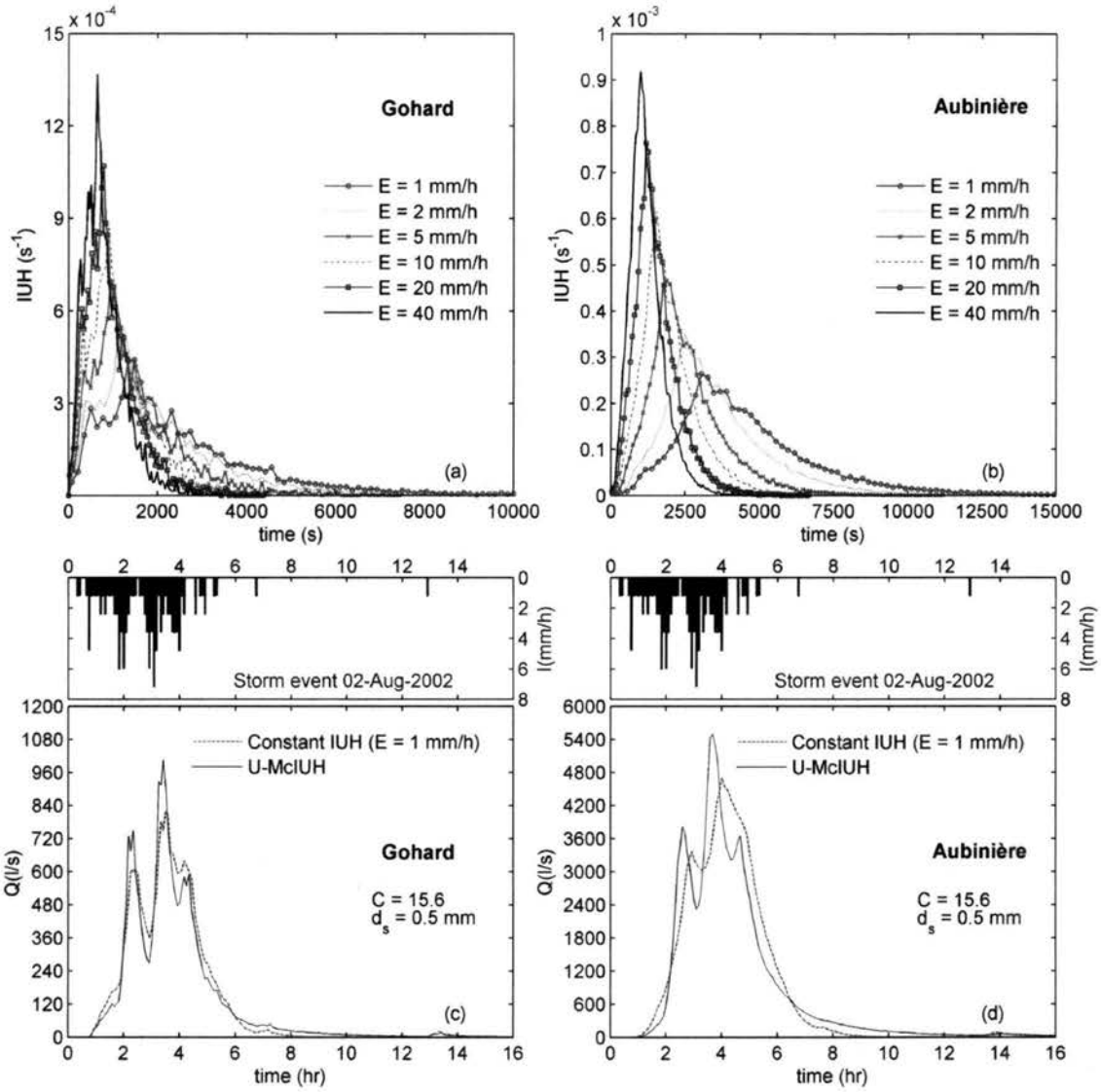

Figure 4.8. Implications of the dependence of the travel times on the excess precipitation rate. (a) IUH for different excess rainfall intensities for the Gohard catchment, (b) same for the Aubinière catchment, (c) comparison of the response to Storm 11 using the U-McIUH and a constant IUH in the Gohard catchment, (d) same for the Aubinière catchment.

4.5.4 Sensitivity to patterns of imperviousness within the catchment

The Mc-IUH also includes an explicit representation of the imperviousness pattern in the catchment. The imperviousness affects the model through E, n, and λ (Eq. (4-8)).

Hence, the imperviousness distribution affects not only the runoff generation but also the velocity of flow. The effects of the imperviousness distribution were evaluated by comparing the results from the real imperviousness pattern to results produced by a uniform distribution with an equivalent total impervious area. First, we consider the effects of imperviousness on the IUH for a given E (Figure 4.9a and Figure 4.9b). In this case, the imperviousness only affects the shape of the IUH through n and λ. The differences between the IUHs are relatively minor, especially in the Gohard catchment. One reason for these similarities is that the real imperviousness pattern is relatively uniform in both catchments. However, the sensitivity that is observed can be explained by λ. Eq. (4-6) shows that the travel time is less sensitive to λ when λ is large (i.e. in the downstream direction). Hence, the effects of imperviousness through λ are most important in the upstream areas of the catchment. As a result, the differences in the IUHs are more evident in the recession limbs of the hydrographs, which are more influenced by the most upstream hillslope cells where values of λ tend to be smaller. In a second step, we also incorporate the effect of the imperviousness pattern through the spatial variation of E. Figure 4.9c and Figure 4.9d show the IUHs generated by a rainfall pulse of I = 1 mm h^{-1} over the catchments using values of $IA = 0$ and $C = 15.6$ and the different patterns of imperviousness. The differences here are more noteworthy and again more significant in the falling limb, which is slower for the real imperviousness distribution in both catchments. This analysis illustrates how small values of E over pervious cells generate slower flows that delay the overall response. Figure 4.9e and Figure 4.9f show the effects of these changes when a real event is simulated. Minor differences in the hydrographs are observed, with the recession limb being the most affected. Thus, in this case, the

spatial pattern of imperviousness does not produce major differences in the hydrologic response of the catchments, but the U-McIUH provides a framework whereby proposed or real imperviousness patterns could be analyzed.

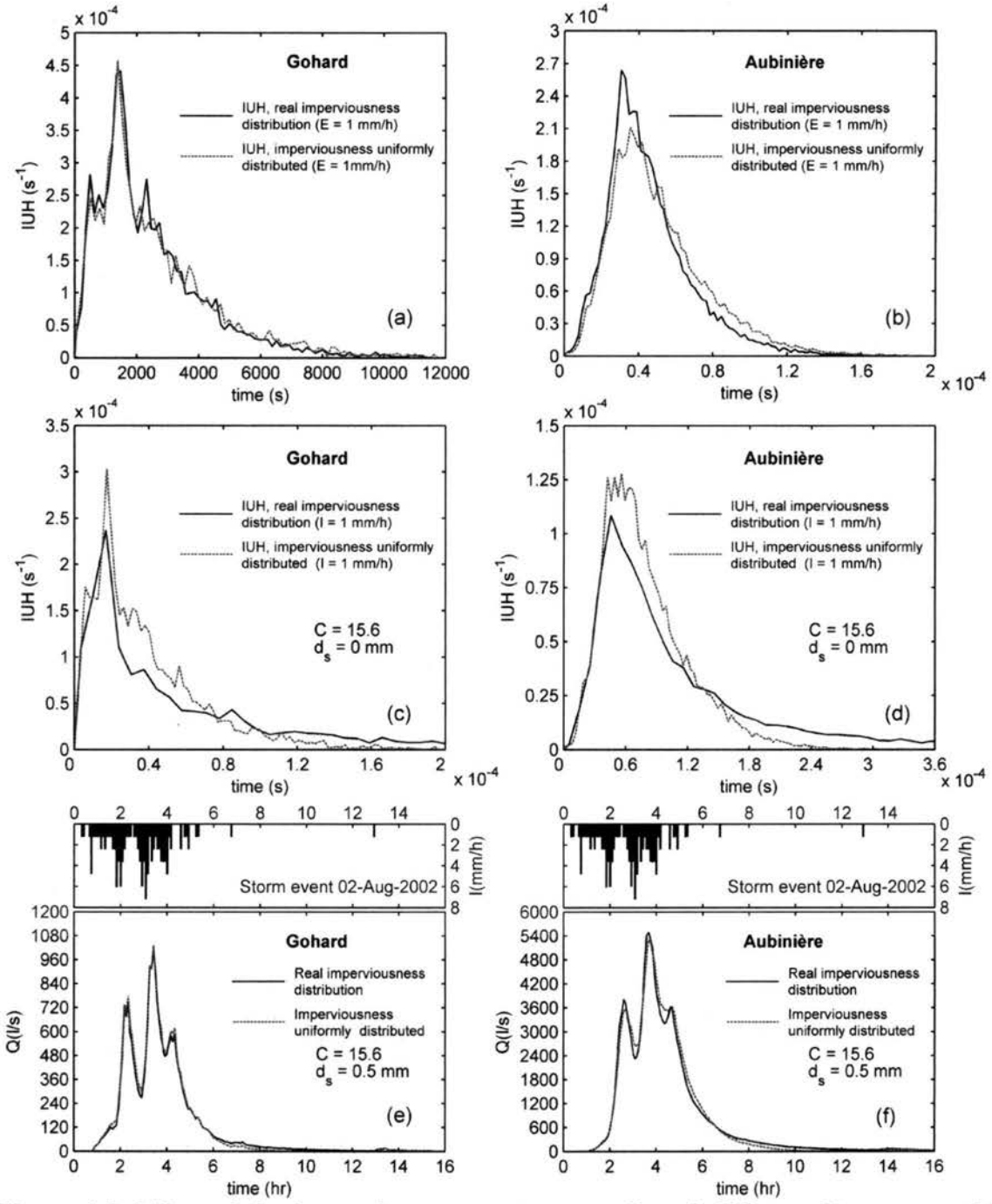

Figure 4.9. Effect of the imperviousness pattern on the rainfall-runoff response. (a) Comparison of the IUH for the real and an assumed homogeneous imperviousness pattern for the Gohard catchment when E = 1 mm/h, (b) same for the Aubinière catchment, (c) comparison of the IUH for the real and an assumed homogeneous imperviousness pattern for the Gohard catchment when I = 1 mm/h and infiltration is included in the analysis using a infiltration parameter C = 15.6, (d) same for the Aubinière catchment, (e) comparison of the hydrologic response to Storm 11 when the real and homogeneous impervious patterns are used in the Gohard catchment, (f) same for the Aubinière catchment.

4.5.5 From the morphology of the catchment to the hydrologic response

In this section, we summarize the transformation of the spatial structure of the basin into the U-McIUH. The spatial structure of the basin can be characterized using the width function, $W(x)$, which is the portion of the basin area at a flow distance x from the outlet (Rodríguez-Iturbe and Rinaldo, 1997). $W(x)$ incorporates some essential characters of the hydrologic response because the travel time from each point in the basin is related to the flow distance that must be traversed (Rodríguez-Iturbe and Rinaldo, 1997). We extend this concept to consider the fact that impervious areas are dominant in the production of runoff in urban areas. For this purpose, we define the imperviousness function, $H(x)$, which corresponds to the portion of the total impervious area at a flow distance x from the outlet. Hence, $H(x)$ represents the spatial distribution of the runoff generation if one ignores the runoff production from pervious areas. $H(x)$ also allows for the description of the two-dimensional spatial variability of the imperviousness in a one-dimensional function. Figure 4.10a shows both the $W(x)$ and $H(x)$ functions for the Aubinière catchment, which were extracted from the modified terrain. $W(x)$ was computed by summing the area located at different flow distances x from the outlet. $H(x)$ was computed by summing only the impervious areas located at different flow distances x from the outlet. Figure 4.10a also shows the imperviousness function that is obtained if all the cells have an imperviousness of H = 31.7%, which is the average imperviousness for the entire catchment. The similarity of these two curves confirms our earlier assertion that the imperviousness is relatively homogeneous within the Aubinière.

By defining flow velocities one can transform the spatial scale of $H(x)$ into a temporal scale and generate an IUH. This rescaling process assumes that all precipitation on

pervious areas is completely infiltrated. Eq. (4-22), which was used to obtain the travel time from cell j, T_j, can be expressed in terms of the flow length ℓ_r and velocity V_r in each of the R_j cells belonging to the flow path:

$$T_j = \sum_{r \in R_j} \frac{\ell_r}{V_r} \tag{4-29}$$

Following the idea of Rinaldo et al. (1995), we rescale $H(x)$ by incorporating different levels of complexity in the definition of V_r. The basic transformation is generated by assuming a constant velocity for all the cells. Figure 4.10b shows the resulting IUH after the transformation into a PDF of $H(x)$ and the rescaling using $V_r = 0.5$ m s^{-1}. The PDF is simply obtained by normalizing $H(x)$ by the total impervious area and the Δx used, in this case the grid resolution of 20 m. As expected, the IUH has exactly the same shape as $H(x)$ and is not skewed to the left. Secondly, we distinguished overland and channel flows (representing all the flow in conduits), as suggested by Morrison and Smith (2001). For this analysis, let V_h = 0.05 m s^{-1} and V_c = 1.85 m s^{-1} denote the average velocity in hillslope and channel cells, respectively. These values were estimated using the median travel times for hillslope and channel cells shown in Figure 4.6 and an average flow length of 24 m. The resulting IUH shows that different dynamic characterization of hillslopes and channels, even through average velocities, drastically enhances the positive skewness of the response (Figure 4.10c). The shape of the IUH smoothes when average velocities characterizing the four types of cells are used in the space-time rescaling (Figure 4.10d). Velocities in pipes (V_p = 1.2 m s^{-1}) and streets (V_s = 0.27 m s^{-1}) were also obtained from Figure 4.6. The time to peak increases because V_s and V_p are smaller than V_c. The final level of complexity considers the spatially varied velocity field used by U-

McIUH, in which travel times are defined for each cell (Figure 4.10e). Two IUH corresponding to rainfall intensities of I = 1 mm h^{-1} and I = 10 mm h^{-1} are shown to illustrate the climatic dependence of the travel times. The addition of the velocity field is comparable to the inclusion of dispersion within the catchment for the identification of the IUH carried out by Rinaldo et al. (1995). Because average velocities used previously were obtained from Figure 4.6 (i.e. I = 10 mm h^{-1}), one can compare the IUHs in Figure 4.10d and Figure 4.10e. The final IUH is similar but even smoother, and its falling limb extends for longer. This analysis shows that the key properties of spatially defined UH formulation for urban areas are the non-linearity of the response and the differences in the flow dynamics of the components of the drainage network.

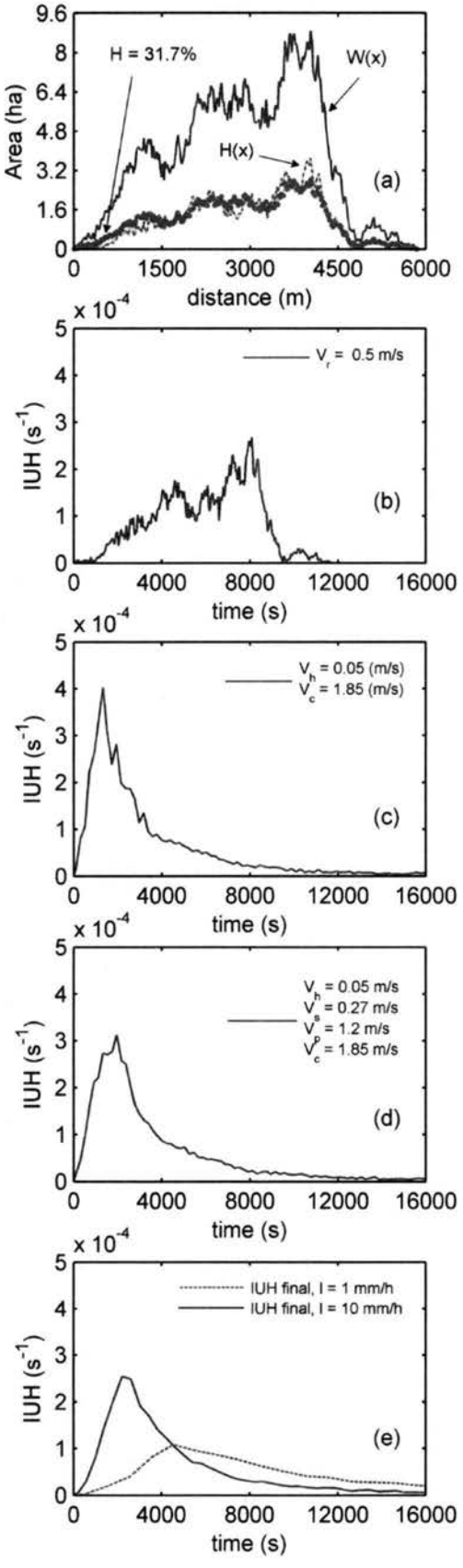

Figure 4.10. Transformation of the spatial structure of the Aubinière catchment into the U-McIUH. (a) The width function, $W(x)$, the imperviousness function, $H(x)$, and the imperviousness function assuming a constant imperviousness distribution of 31.7%, (b) transformation of $H(x)$ into an IUH using a constant flow velocity V_r= 0.5 m/s for all the cells, (c) transformation of $H(x)$ into an IUH using V_h = 0.05 m/s and V_c = 1.85 m/s, (d) transformation of $H(x)$ into an IUH using the previous velocities as well as V_p = 1.2 m/s and V_s = 0.27 m/s, (e) transformation of $H(x)$ into U-McIUHs using the full model for intensities I =1 mm/h and I = 10 mm/h.

4.6 Summary and conclusions

In this paper, we have developed and tested a new hydrologic model for urban catchments denoted as the U-McIUH (Urban Morpho-climatic Instantaneous Hydrograph). The model is based on the explicit representation of the GIUH, which defines the IUH as the PDF of the travel times from each cell in a raster representation of the catchment to the outlet. The urban terrain is represented by a single raster file that incorporates the pathways defined by different elements that are typically observed in urban drainage systems (hillslopes, streets, pipes, and channels). Additional raster files are used to store the known attributes of these elements. The flood wave travel times in each cell are defined using closed expressions from kinematic wave theory (Wong, 1995; Wong, 2003). These expressions depend on the hydraulic element represented by each cell, the properties of the hydraulic element, the excess rainfall intensity, and the upstream contribution of flow. By including the excess rainfall intensity in the travel time calculation, the model includes a so-called climatic dependence of the IUH (i.e. faster travel times associated with higher excess rainfall rates). However, the relative contribution of upstream flow is assumed to be temporally constant when calculating the travel times and is estimated using the upstream impervious area. In this way, the U-McIUH remains simpler than a full kinematic wave routing method. Using this quasi-linear approach, spatially-averaged rainfall pulses of different intensities are convoluted with their respective IUHs to generate the response to storm events.

The model was tested by applying it to the Gohard catchment. Five rainfall events were used to calibrate the roughness coefficients, and then the model was applied to an additional 12 events. The maximum rainfall intensity for these events ranged from about

2 mm/hr to about 36 mm/hr. An average MCE value of 0.71 was obtained including both periods of application. The average absolute error was 14% for the discharge rates and 7% for the total hydrograph volumes. The error in the estimated time to peak was 5 min or less in 11 out of the 17 events. Overall, the model does well in predicting the timing of response of the catchment and its dependence on different pulse intensities. In a certain cases, the model was unable to capture some apparent storage or detention in this basin. Further testing is necessary to determine whether this behavior results from a weakness in the model or if it is due to an unrepresented feature of this particular basin. Also, the model testing did not include the representation of channels because the Gohard does not include any channels.

A detailed analysis was made to compare the results produced by the U-McIUH to the results produced using assumptions made in previously-used methods. Based on this analysis, we make the following conclusions:

1. The effect of the upstream contribution of flow on the travel time in a grid cell can be substantial. The effect is larger for hillslope cells than for the other element types and it is more important for downslope cells where the contribution of flow from upstream relative to the locally produced flow is large. The resulting changes in the travel time can significantly alter the shape of the IUH for a given excess rainfall rate and the overall response to a storm.

2. The variability of travel times between different types of cells and within a given type of cell can be substantial. For example, the travel times in the conduit cells were 10 to 80 times shorter than the travel times in the hillslope cells for the case considered. In addition, the travel times within each element type were observed to vary over about one

order of magnitude. When considering the impact of these differences on the IUH for a given excess rainfall rate and the response to a selected storm, we found that distinguishing overland and conduit cells creates the most significant modifications in the hydrologic behavior and thus is probably the most important distinction to include. However, distinguishing pipes produces spiky and fast responses that are seen in the observed flow rates.

3. The faster travel times produced by higher excess rainfall rates also has a substantial impact on the hydrologic behavior of the basin. This nonlinearity was observed to produce a higher peak flow and a shorter time to peak for the IUH when it was produced with a higher excess rainfall rate. Ultimately, this modification in the IUH produced more variability and higher peak flows in the simulated responses to a real storm.

4. For the case considered, using the observed spatial pattern of imperviousness did not produce a significantly different hydrologic response than using a uniform pattern of imperviousness. However, the real imperviousness pattern was shown to be relatively homogeneous. Mathematically, the spatial pattern of the imperviousness affects not only the runoff generation but also the velocity of flow. Thus, it remains possible that a more heterogeneous pattern of imperviousness would substantially alter the hydrologic response of the catchment. The U-McIUH provides a framework whereby different imperviousness patterns could be analyzed.

Overall, the results demonstrate that an explicit representation of the urban morphology including the spatial structure of the catchment, the different elements contained in the catchment, and the associated impacts on the travel times can produce

benefits in the simulation of the hydrology response. Potential directions for future research include: (1) the development of an improved runoff generation component that allows for continuous rather than event-based simulation, (2) further testing of the U-McIUH in catchments with different sizes and varying degrees of pipes, streets, and channels, (3) using of the spatial capabilities of the model to evaluate the effects of different spatial patterns of imperviousness as well as anthropogenic changes in the basin composition and structure.

4.7 Acknowledgment

The authors thank the city of Nantes for providing the GIS data (Nantes – Métropole, 2003). This research was made possible by the support of Region Pays de la Loire (Project MEIGEVILLE), and the generous financial support from the Harold H. Short endowed fund for the Civil Infrastructure System Laboratory at Colorado State University.

4.8 References

Akan, A.O., Houghtalen, R.J., 2003. Urban Hydrology, Hydraulics, and Stormwater Quality. John Wiley and sons Inc., Hoboken, NJ, p.373.

American Society of Civil Engineering (ASCE), 1996. Technical Engineering and Design Guides as Adapted From the US Army Corps of Engineers, No. 19: Flood-Runoff Analysis. ASCE Press, NY, p. 176.

Aronica, G., Cannarozzo, M., 2000. Studying the hydrological response of urban catchments using a semi-distributed non-linear model. Journal of Hydrology 238(1-2), 35-43.

Bedient, P.B., Huber, W.C., 2002. Hydrology and Floodplain Analysis, 3rd Ed. Prentice-Hall, Upper Saddle River, NJ, p. 763.

Chin, D.A., 2006. Water-Resources Engineering, Second ed. Prentice-Hall, Upper Saddle River, NJ, 962.

Chow, V.T, Maidment, D.R., Mays, L.W., 1988. Applied Hydrology. McGraw-Hill, NY, p. 572.

Cleveland, T.G., Thompson, D.B., Fang, X., He, X., 2008. Synthesis of unit hydrographs from a digital elevation model. Journal of Irrigation and Drainage Engineering 134(2), 212-221.

Du, J., Xie, H., Hu, Y., Xu, Y., Xu, C-Y., Development and testing of a new storm runoff routing approach based on time variant spatially distributed travel time method, Journal of Hydrology (2009), doi: 10.1016/j.jhydrol.2009.02.033.

Gironás, J., Niemann, J.D., Roesner, L.A., Rodriguez, F., Andrieu, H., 2009. Evaluation of methods for representing urban terrain in stormwater modeling. Journal of Hydrologic Engineering. *In press.*

Gregory, J.H., Dukes, M.D., Joseph P.H, Miller, G.L., 2006. Effect of urban soil compaction on infiltration rates. Journal of Soil and Water Conservation 61(3), 117-124.

Gupta, V.K., Waymire, E., Wang, C.T., 1980. A representation of an instantaneous unit hydrograph from geomorphology. Water Resources Research 16(5), 855-862.

Hall, M.J., Zaki, A.F., Shahin, M.M.A., 2001. Regional analysis using the geomorphoclimatic instantaneous unit hydrograph. Hydrology and Earth System Sciences 5(1), 93-102.

Hossain, A., Rao, A.R., Delleur, J.W., 1978. Estimation of direct runoff from urban watersheds. Journal of the Hydraulics Division-ASCE 104(2), 169-188.

Huber, W.C., Dickinson, R.E., 1988. Storm Water Management Model, Version 4: User's Manual, EPA/600/3-88/001a (NTIS PB88-236641/AS). U.S. Environmental Protection Agency, Athens, Ga.

Javier J.R.N., Smith J.A., Meierdiercks K.L., Baeck M.L., Miller A.J., 2007. Flash flood forecasting for small urban watersheds in the Baltimore metropolitan region. Weather and Forecasting 22(6), 1331-1344.

Kilgore, J.L., 1997. Development and evaluation of a GIS -based spatially distributed unit hydrograph model. MS Thesis, Virginia Polytechnic Institute and State University, Blacksburg, VA., p. 118.

Kute, A., Stuart, N., 2008. Predicting GIS-based spatially distributed unit hydrograph from urban development scenarios. WaPUG Spring Meeting, 3 Jun 2008, Coventry, UK.

Lee K.T., Yen, B.C., 1997. Geomorphology and kinematic-wave-based hydrograph derivation. Journal of Hydraulic Engineering 123(1), 73-80.

Lee K.T., Chen, N.C., Chung, Y.R., 2008. Derivation of variable IUH corresponding to time-varying rainfall intensity during storms. Hydrological Sciences Journal 53(2), 323-337.

Legates, D.R., McCabe Jr., G.J., 1999. Evaluating the use of "goodness-of-fit" measures in hydrologic and hydroclimatic model validation. Water Resources Research 35(1), 233-241.

Lhomme, J., Bouvier, C., Perrin, J. L., 2004. Applying a GIS-based geomorphological routing model in urban catchments. Journal of Hydrology 299(3-4), 203-216.

Liu, Y.B., Gebremeskel, S., De Smedt, F., Hoffmann, L., Pfister, L., 2003. A diffusive transport approach for flow routing in GIS-based flood modeling. Journal of Hydrology 283(1-4), 91–106.

Maidment, D.R., 1993. Developing a spatially distributed unit hydrograph by using GIS. In: Kovar, K., Nachtnebel, H.P. (Eds.), Application of Geographic Information Systems in Hydrology and Water Resources, Proceedings of the Vienna Conference, Vienna. IAHS Publ. 211, pp.181-192.

Maidment, D.R., Olivera, F., Calver, A., Eatherall, A., Fraczek, W., 1996. Unit hydrograph derived from a spatially distributed velocity field. Hydrological Processes 10(6), 831-844.

Martínez, V. García, A.I., Ayuga, F., 2002. Distributed routing techniques developed on GIS for generating synthetic unit hydrographs. Transactions of the ASAE 45(6), 1825-1834.

Melesse, A.M., Graham, W.D., 2004. Storm runoff prediction based on a spatially

distributed travel time method utilizing remote sensing and GIS. Journal of the American Water Resources Association 40(4), 863-879.

Morrison, J.E., Smith, J.A., 2001. Scaling properties of flood peaks. Extremes 4(1), 5–22.

Muzik, I., 1996. Flood modelling with GIS-derived distributed unit hydrographs. Hydrological Processes 10(10), 1401-1409.

Nicklow, J.W., 2001. Design of stormwater inlets. In: Mays, L.W. (Ed), Stormwater Collection Systems Design Handbook. McGraw-Hill, New York, pp. 5.1-5.42.

Noto, L.V., La Loggia, G., 2007. Derivation of a distributed unit hydrograph integrating GIS and remote sensing. Journal of Hydrologic Engineering 12(6), 639-650.

Novotny, V., 2003. Water Quality, Diffuse Pollution and Watershed Management. John Wiley and Sons Inc., Hoboken, NJ, p. 864.

Overton, D.E., Meadows, M.E., 1976. Stormwater Modeling. Academic Press Inc, New York, p. 358.

Perrin, J.L., Bouvier, C., Janeau, J.L., Ménez, G., Cruz, F., 2001. Rainfall/runoff processes in a small peri-urban catchment in the Andes mountains. The Rumihurcu Quebrada, Quito (Ecuador). Hydrological Processes 15(5), 843 – 854.

Pilgrim, D.H., Cordery, I., 1993. Flood Runoff. In: Maidment, D.R. (Ed), Handbook of Hydrology. McGraw-Hill, New York, pp. 9.1-9.42.

Rinaldo, A., Vogel, G.K., Rigon, R., Rodríguez-Iturbe, I., 1995. Can one gauge the shape of a basin? Water Resources Research 31(4), 1119-1128.

Rodriguez, F., Andrieu, H., Zech, Y., 2000. Evaluation of a distributed model for urban catchments using a 7-year continuous data series. Hydrological Processes 14(5), 899-914.

Rodriguez, F., Andrieu, H., Creutin, J.D., 2003. Surface runoff in urban catchments: morphological identification of unit hydrographs from urban databanks. Journal of Hydrology 283(1-4), 146-168.

Rodriguez, F., Cudennec, C., Andrieu H., 2005. Application of morphological approaches to determine unit hydrographs of urban catchments. Hydrological Processes 19(5), 1021-1035.

Rodriguez, F., Andrieu, H., Morena, F., 2008. A distributed hydrological model for urbanized areas – Model development and application to case studies. Journal of Hydrology 351(3-4), 268-287.

Rodríguez-Iturbe, I., Valdés, J.B., 1979. The geomorphologic structure of hydrologic response. Water Resources Research 15(6), 1409-1420.

Rodríguez-Iturbe, I., González-Sanabria, M., Bras, R.L., 1982. A geomorphoclimatic theory of the instantaneous unit hydrograph. Water Resources Research 18(4), 877-886.

Rodríguez-Iturbe, I., Ijjász-Vásquez, E.J., Bras, R.L., Tarboton, D.G., 1992. Power law distributions of discharge mass and energy in river basins. Water Resources Research 28(4), 1089-1093.

Rodríguez-Iturbe I., Rinaldo A., 1997. Fractal River Basins: Chance and Self-Organization. Cambridge University Press, New York, pp. 547.

Saghafian, B., 2006. Nonlinear transformation of unit hydrograph. Journal of Hydrology 330(3-4), 596-603.

Saghafian, B., Julien, P.Y., Rajaie, H., 2002. Runoff hydrograph simulation based on time variable isochrone technique. Journal of Hydrology 261(1-4), 193-203.

Singh, V.P., 1996. Kinematic Wave Modeling in Water Resources: Surface Water Hydrology. Wiley and Sons, New York.

Singh, V.P., 2001. Kinematic wave modelling in water resources: a historical perspective. Hydrological Processes 15(4), 671-706.

Smith, M.B., 1993. A GIS-based distributed parameter hydrologic model for urban areas. Hydrological Processes 7(1), 45-61.

Smith, J.A., Baeck, M.L, Meierdiercks, K.L., Nelson, P.A., Miller, A.J., Holland, E.J., 2005. Field studies of the storm event hydrologic response in an urbanizing watershed. Water Resources Research 41, W10413, doi:10.1029/2004WR003712.

Turner-Gillespie, D.F., Smith, J.A., Bates, P.D., 2003. Attenuating reaches and the regional flood response of an urbanizing drainage basin. Advances in Water Resources 26(6), 673–684.

Urban Drainage and Flood Control District (UDFCD), 2001. Urban storm drainage criteria manual. Revised August 2006, Denver, Colorado.
Available online: http://www.udfcd.org/downloads/down_critmanual.htm

Viessman, W., Lewis, L., 1995. Introduction to Hydrology (Fourth Edition). Addison-Wesley Educational Publishers, Inc., p. 760 pp.

Wong, T.S.W., 1995. Time of concentration formulae for planes with upstream inflow. Hydrological Sciences Journal 40(5), 663-666.

Wong, T.S.W., 2003. Comparison of celerity-based with velocity-based time-of-concentration of overland plane and time-of-travel in channel with upstream inflow. Advances in Water Resources 26(11), 1171–1175.

Wong, T.S.W., Zhou, M.C., 2003. Kinematic wave parameters and time of travel in circular channel revisited. Advances in Water Resources 26(4), 417–425.

Wong, T.S.W., Zhou, M.C., 2006. Kinematic wave parameters for trapezoidal and rectangular channels. Journal of Hydrologic Engineering 11(2), 173-183.

Xiong, Y., Melching, C.S., 2005. Comparison of kinematic-wave and nonlinear reservoir routing of urban watershed runoff. Journal of Hydrologic Engineering 10(1), 39-49.

Zech, Y., Sillen, X., Debources, C., Van Hauwaert, A., 1994. Rainfall-runoff modelling of partly urbanized watersheds: comparison between a distributed model using GIS and other models sensitivity analysis. Water Science and Technology 29(1-2), 163-170.

Zhang, Y., Smith, J.A., Baeck, M.L., 2001. The hydrology and hydrometeorology of extreme floods in the Great Plains of eastern Nebraska. Advances in Water Resources 24(9-10), 1037–1049.

Zhao, B., 2001. Computer models for stormwater system design. In: Mays, L.W. (Ed), Stormwater Collection Systems Design Handbook. McGraw-Hill, New York, pp. 21.1-21.23.

Zoppou, C., 2001. Review of urban storm water models. Environmental Modelling and Software 16(3), 195-231.

5. Summary, Conclusions and Recommendations

The research documented in this work has explored the applicability to urban settings of morphologic descriptors and the geomorphologic unit hydrograph theory, both originally developed for natural watersheds. Three main issues were addressed: (a) the applicability of morphologic functions to characterize urban watersheds and the impacts at different spatial scales of urbanization in the structure of natural watersheds, (b) the development and validation of a methodology to generate urban terrains that better incorporate the effect of artificial conduits on the extraction of morphologic information, and (c) the development and testing of a rainfall-runoff model based on the morpho-climatic instantaneous unit hydrograph theory. The model is identified from the morphologic description given by the urban terrain representation proposed in this study. Overall, the results show that the characterization of the morphology of urban watersheds is highly relevant to the evaluation of the impacts of urbanization and the development of better stormwater models that are more representative of the drainage structure. The following are the main conclusions from this work:

1. Morphologic relationships and properties can be used to identify impacts of urbanization on the geomorphology and the internal structure of natural watersheds. Because these relationships and properties are defined for a wide range of scales, they allow the identification of the spatial scales and thresholds at which these impacts occur or become significant. Several changes in the expected behavior of these

relationships and properties were observed when applied to a 10 km^2 urban catchment. This finding is relevant when building stormwater models intended to simulate and compare the pre- and post-development catchment response. These morphologic impacts should be incorporated into stormwater models through the redefinition of model parameters that characterize both the channelized and unchannelized portions of the catchment when the urbanized scenario is simulated. Finally, differences between the scaling exponents of the morphologic relationships for the urban watershed and the values typically observed in nature suggest that the topography extracted from urban raw DEMs of medium to high resolution (around 10 m) would not correspond to the topography of the previously existing undeveloped area. However, although the DEM reflects some of the features of urbanized landscapes, it is clear that many artificial conduits (e.g. streets, pipes, swales) cannot be resolved in such data.

2. Prior to this study, no clear evidence had been provided to validate the use of raw or processed DEMs (i.e. DEMs modified to incorporate artificial conduits) for the generation of urban terrain for stormwater modeling purposes. This research shows that the choice of terrain can have significant impacts on the identification of flow directions, which can ultimately affect the watershed boundary, area, flow lengths, and slope. The main source of error in representing the true flow paths within the drainage network is the assumption that flow in pipes is in the direction given by the surface topography. This error is considerably reduced when this assumption is discarded and a modification of the DEM based on the real elevation of the artificial conduits is used. Results show that the errors associated with the adoption of the

urban terrain into the hydrologic modeling can not be overcome through calibration. This becomes more noticeable when a wide range of storms with different characteristics are used, as it is typically the case of continuous models. Overall, it is concluded that, given their role in the accumulation of flow, artificial conduits that are not explicitly modeled with hydraulic methods in a stormwater model should be incorporated in the definition of the urban terrain when a semi-distributed or distributed stormwater model is used.

3. The new rainfall-runoff model developed for this research (the U-McIUH) represents a step forward in the definition of physically-based distributed hydrological models for urban areas. Until now, very few models that are strongly based on the morphology of the urban drainage system have been made available, and all of them have one or more limitation identified in this research. The U-McIUH fills an existing gap in the field of stormwater modeling by adapting the geomorphoclimatic instantaneous unit hydrograph theory to urban settings. Some of the most important contributions of this model are:
    a. A more thorough treatment of the flow in minor conduits and unchannelized portions of the watershed, which enhances the simulations of runoff accumulation that are traditionally used in conceptual models. This improved representation does not require a larger number of parameters to be calibrated. In fact, given that the travel times are directly derived from the morphology of the watershed, and that the roughness coefficients are assumed to be functions of the imperviousness, the calibration parameters for routing are limited to four values: the roughness coefficient for overland flow in pervious areas and the roughness coefficient for

flows in streets, pipes and channels.

b. A simplification of kinematic wave routing that considers the dependence of the unit hydrograph on rainfall intensity and the effect of upstream contributions on the travel times without explicitly solving the flow equation at each cell for each time step. This simplification reduces the complexity of the model computations while still producing reasonable model performance.

Data available for this research were relatively limited, particularly for the development, implementation and testing of the methodology to generate the urban terrain representation and the U-McIUH model. The model and all the findings of this work must be tested in other watersheds, located in different geographic and climatic areas, with different sizes and varying degrees of imperviousness and artificial channelization. The effects of urbanization on the geomorphology and internal structure of watersheds observed in this research may vary from one location to another. The distribution and degree of imperviousness may clearly affect these observations, so applications in other conditions are necessary to validate and characterize the results obtained. With respect to the terrain representation and the applicability of the U-McIUH, no major problems are expected to be detected in applications to other watersheds and locations. However, the formulation of travel times in channels or urban streams in the U-McIUH remains to be tested with real discharge data. It is possible that wide and long open channels can provide an extra storage capacity not considered in the current version of the model. If that is the case, a modification can be implemented in which an additional storage capacity is provided by means of a linear reservoir.

Finally, the research reported in this work opens future possibilities and applications.

The characterization of urban watersheds from a morphologic point of view provides an alternative to the common characterization based only on imperviousness. As one urban development with adequate stormwater control practices may have less impact than another one with the same imperviousness, one could expect that two urban developments with the same imperviousness but different morphological features may also have different impacts. Additionally, the morphological tools used in this research can be used to determine spatial distribution and integration of drainage solutions so that urbanization impacts are controlled at the scale at which they become more significant. On the other hand, the U-McIUH has many potential applications that deserve to be studied, other than those of traditional rainfall-runoff models. Some of them include:

a. Evaluation of the impacts associated with different spatial patterns of imperviousness. This topic has not been extensively studied mostly because the massive use of lumped and semi-distributed models that do not allow the detailed study of spatially varied imperviousness distributions. A better understanding of this issue will be of relevance for urban development planning and management.

b. Evaluation of the impacts associated with different degrees of channelization of urban watersheds. Additionally, the model can be used to explore different scenarios in which the largest portion of the drainage network corresponds to either artificial elements (streets, pipes and swales) or open streams.

c. Detection of maloperation in the drainage network. The strong relationship between the morphology of the drainage network and the discharges simulated by the model may allow the detection of the location of portions of the network that are not operating properly (e.g. broken or clogged pipes, excess of sediments).

In summary, this research moves our comprehension of urbanization and its impacts forward, and provides us with new tools and research opportunities to characterize and model them.

6. APPENDIX I. Matlab code of algorithm used to incorporate streets and pipes in the urban terrain

The following code is used in the generation of the urban terrain that incorporates artificial conduits separately defined as vector features (streets, pipes and urban streams). The purpose of this code is to properly incorporate artificial features in the definition of the urban terrain so that the flow paths are more accurately described. In the method, the streets and pipes are burned in the DEM by reducing the elevation of the cells where these artificial conduits are located. Unlike the traditional approach in which a constant depth is subtracted, the method uses the local streets and pipes depths when making the elevation adjustments, so that flow in conduits with different directions to those given by the surface topography are better depicted. The code corresponds to "method 3" defined in Chapter 3 "**Evaluation of Methods for Representing Urban Terrain in Stormwater Modeling**", and is also used to preprocess the terrain in the application of the U-McIUH model in Chapter 4 "**A morpho-climatic instantaneous unit hydrograph model for urban catchments calculated from digital elevation models**". The code is presented in the following pages.

Required data

(1) Network is a matrix with all the transport elements (conduits) identified through the x and y coordinates (planar location), and z (altitude) of the upstream and downstream ends of the transport element. It has 7 columns: identification, x_up, y_up, x_down, y_down, z_up, z_down. The coordinates must be in the same units of length.
(2) Raster_net_prop is the table with the properties of the raster file obtained after converting the features (pipes and streets) to raters. It has then 2 columns: identification of the element (ID), and the number of cells corresponding to that specific element.
(3) Raster_net is the raster with the conduits (numbers that represent the element). The size of this raster should be the same as the DEM raster. This raster file is obtained by transforming the feature (street or pipe) to a raster. The feature ID is used for this transformation. Therefore, the cell acquires a value equal to the largest ID if 2 or more conduits are defined in the cell. Cells with no conduits will have a value of -9999.
(4) The DEM of the area under study.
(5) Top: the top coordinate (in length dimensions) of the DEM.
(6) Left: the left coordinate (in length dimensions) of the DEM.

All the raster files must have the same resolution

Result

New_DEM is the matrix with the new DEM after the modification. Its size is the same as the original DEM. The matrix is also saved as a text file "New_DEM_after_pipes.txt"

```
function[New_DEM]=modification(network,raster_net_prop,raster_net,DEM,top,left)

%___________Section of the code to create just one table with all the information associated to each element_____________________
slopes=zeros(size(raster_net_prop,1),1);                                    % Definition of the array that will have the
                                                                            slopes of each element
data_to_raster=zeros(size(raster_net_prop,1),6);                            % Definition of the array that will have
                                                                            temporarily the extracted data from the
                                                                            % network matrix that correspond to the elements
                                                                            described in the raster_net_prop matrix


for i=1:size(raster_net_prop,1),                                            % The for cycle cover the complete list of
                                                                            elements defined in the raster_net_prop matrix
    j=1;                                                                    % With the while cycle we check all the elements
                                                                            defined in the network matrix, j accounts
    while network(j,1)~=raster_net_prop(i,1),                               % for each line in this array
        j=j+1;
        if j>size(network,1), break,end,                                    % The while ends in case the last row of the
                                                                            network matrix is reached
    end

    data_to_raster(i,1:6)=network(j,2:7);                                   % The useful information is stored in the
                                                                            data_to_raster matrix


    if raster_net_prop(i,2)==1,                                             % Computation of the slope based on the upstream
                                                                            and downstream elevations and the number of
        slopes(i,1)=(data_to_raster(i,5)-data_to_raster(i,6))/2;            % cells covered by each element. There are three
                                                                            cases: (1) if there is one cell, then the slope
    elseif raster_net_prop(i,2)>1,                                          % is given by the difference of the elevation
                                                                            divided by 2. (2) if there are N = 2 o more cells,
                                                                            the
        slopes(i,1)=(data_to_raster(i,5)-data_to_raster(i,6))/(raster_net_prop(i,2)-1); % slope is given by the difference in the
                                                                            elevation divided by N-1. Finally, any other case
    else                                                                    % implies a slope = 0
        slopes(i,1)=0;
    end

end

raster_net_prop2=[raster_net_prop data_to_raster slopes];                   % Three matrix are merged: the raster elements,
                                                                            their properties and the slope separately
                                                                            computed.

%_____________________________________________________________________________________________________________________________


%_________Section of the code to localize the nodes in the DEM and set up their elevations_____________________________________
```

```
position=zeros(size(raster_net_prop,1),4);                    % Position is a matrix that will storage the
                                                              position of the input and output junctions of the
                                                              elements
                                                              % Each junction is defined by two numbers
                                                              corresponding to the index of the raw and column
                                                              in the DEM matrix
raster_net_prop3=zeros(size(raster_net_prop,1),10);           % definition of a temporal matrix to be used in
                                                              building the new matrix raster_net_prop2 that does
                                                              not have elements defined outside the DEM

elevation=-9999*ones(size(DEM,1),size(DEM,2));                % Elevation is a matrix with the same size than
                                                              the DEM raster. Here is where we will storage the
                                                              depth of the pipe system
q=1;                                                          % q is defined to count for the conduit records in
                                                              which both upstream and downstream junctions are
                                                              inside the DEM records
for i=1:size(raster_net_prop2,1),                             % The for cycle covers all the conduits

% The IF condition is defined to eliminate any conduit that starts or ends outside the DEM. Note that elements starting right in any
of the borders of the DEM are eliminated as well. This is done since the algorithm look for data in each of the 8 directions. Once the
elements are eliminated, the matrix raster_net_prop2 is updated so it has exactly the same number of conduits than the matrix
position.

% IMPORTANT, THE IF CONDITION DEPENDING ON THE SIZE OF THE GRID CELL
    if (raster_net_prop2(i,3)-left)/20>1&&(top-raster_net_prop2(i,4))/20>1&&(raster_net_prop2(i,5)-left)/20>1&&(top-
    raster_net_prop2(i,6))/20>1&&(raster_net_prop2(i,3)-left)/20<=size(DEM,2)&&raster_net_prop2(i,4)-
    top<=size(DEM,1)&&(raster_net_prop2(i,5)-left)/20<=size(DEM,2)&&raster_net_prop2(i,6)-top<=size(DEM,1),

    position(i,1)=raster_net_prop2(i,1);                      % Identity of each conduit
    position(i,2)=ceil((raster_net_prop2(i,3)-left)/20);      % The next four lines transform from x,y
                                                              coordinates into rows and columns, with element
                                                              1,1 located in the top left corner.
    position(i,3)=ceil((top-raster_net_prop2(i,4))/20);       % DEPENDING ON THE SIZE OF THE GRID CELL It is
                                                              dividing by 20 since that is the resolution of the
                                                              DEM. Be careful If watersheds in south hemisphere
                                                              are used.
    position(i,4)=ceil((raster_net_prop2(i,5)-left)/20);
    position(i,5)=ceil((top-raster_net_prop2(i,6))/20);
    position(i,6)=q;                                          % q is a counting variable (the conduit list will
                                                              be sorted according to this variable to find zero
                                                              records)
    raster_net_prop3(i,1:9)=raster_net_prop2(i,1:9);
    raster_net_prop3(i,10)=q;

    q=q+1;
```

```
    elevation(position(i,3),position(i,2))=raster_net_prop2(i,7);

    elevation(position(i,5),position(i,4))=raster_net_prop2(i,8);
    end
end

clear q

position2=sortrows(position,6);


raster_net_prop3=sortrows(raster_net_prop3,10);
k=1;
while position2(k,6)<1,
    k=k+1;
end

position3=position2(k:size(position2,1),:);

raster_net_prop4=raster_net_prop3(k:size(raster_net_prop3,1),:);

position=sortrows(position3,1);

position=position(:,1:5);

raster_net_prop2=sortrows(raster_net_prop4,1);

raster_net_prop2=raster_net_prop2(:,1:9);

clear k;

a=min(position(:,2:5))

z=max(position(:,2:5))

%_____________________________________________________________________________________________

%____________Section of the code to interpolate the elevations between the junctions_____________

h=0;
e=0;
for i=size(raster_net_prop2,1):-1:1,


    record=0;
```

```
% Definition of the elevation in the matrix
elevation corresponding to the junctions.

% Clear q

% the conduit list is sorted according to q to
find zero records (both in position and
raster_net_prop2)

% small While cycle to find the zero records

% we eliminate the zero records (both in position
and raster_net_prop2)

% we resort the list of conduits according to the
ID
% we eliminate the auxiliary column for sorting

% we resort the list of conduits according to the
ID
% we eliminate the auxiliary column for sorting

% Deleting variable k

% Verification, these two number should be inside
the DEM dimensions

% Covering the entire table with all the raster
elements.
```

```
r=0;
if  raster_net_prop2(i,9)>0                                  % Making sure we are working with valid elements.
                                                             All the elements in the table should be valid
                                                             though
%_____________________________________________________________________________________________________

    if raster_net(position(i,3),position(i,2))==raster_net_prop2(i,1),   % This "IF" is used  when the beginning of the
                                                             conduit is not covered (hidden) by other conduit
                                                             so

        pos1_a=position(i,3);                                % the beginning can be identified. We keep the
                                                             same nomenclature so Pos1_a and Pos1_b will store
                                                             the
        pos1_b=position(i,2);                                % location where we are.
        pos2_a=pos1_a-1;                                     % pos2_a and pos2_b will store the rows above and
                                                             below to where we are
        pos2_b=pos1_a+1;                                     % pos3_a and pos3_b will store the columns above
                                                             and below to where we are

        pos3_a=pos1_b-1;
        pos3_b=pos1_b+1;
        temp1=raster_net(pos1_a,pos1_b);                     % temp1 stores the location in the raster net
                                                             where we are to be ready to move to the next cell
        temp2=raster_net_prop2(i,7);                         % temp2 stores the initial elevation of the
                                                             element identified.


        count=1;

        while r==0&&count<=raster_net_prop2(i,2),            % This "WHILE" cycle is used to always look for
                                                             the N-S-E-W neighbor with the same identity,
                                                             BEFORE check diagonals
            Position1=[1:4; zeros(2,4)]';                    % The matrix Position1 is defined. It will be used
                                                             to detect the furthest cell from the downstream
                                                             node. This cell is the one used for the next
            r=1;                                             % interpolation since it is assumed to be closer
                                                             to the upstream.

            j=0;
            k=0;
            if temp1==raster_net(pos2_a,pos1_b),             % The next four "if" conditions are used to find
                                                             the next element in the N-S-E-W neighborhood with
                                                             the same
                Position1(1,2)=1;                            % identification as the conduit we are working
                                                             with. Whenever we find something we also compute
                                                             and store
                Position1(1,3)=sqrt((position(i,5)-(pos2_a))^2+(position(i,4)-pos1_b)^2); %the distance from that new location to
                                                             the downstream junction (in matrix Position 1)
                j=j+1;
            end
```

```
if temp1==raster_net(pos2_b,pos1_b),
    Position1(2,2)=1;
    Position1(2,3)=sqrt((position(i,5)-(pos2_b))^2+(position(i,4)-pos1_b)^2);
    j=j+1;
end
if  temp1==raster_net(pos1_a,pos3_a),
    Position1(3,2)=1;
    Position1(3,3)=sqrt((position(i,5)-pos1_a)^2+(position(i,4)-(pos3_a))^2);
    j=j+1;
end
if temp1==raster_net(pos1_a,pos3_b),
    Position1(4,2)=1;
    Position1(4,3)=sqrt((position(i,5)-pos1_a)^2+(position(i,4)-(pos3_b))^2);
    j=j+1;
end

if j>0;                                                    % Here we look which one of any of the cells
                                                           located is the furthest from the outlet of the
                                                           conduit.
    P2 = sortrows(Position1,[2 3]);                        % Additionally we store in "count" the number of
                                                           cells we have worked with so that when all the
                                                           cells
    clear Position1                                        % associated to a element are used we can jump to
                                                           the next element
    count=count+1;
    r=0;
    j=0;
    raster_net(pos1_a,pos1_b)=0;                           % the cell founded is deleted so it is not
                                                           available for the next iteration
    switch P2(4,1)                                         % The switch command includes the four possible
                                                           cases (N-S-E-W). In each case the new location and
                                                           elevation are defined
        case 1                                             % elevation and stored in temp1 and temp2
                                                           respectively. Additionally, the elevation is
                                                           entered in the matrix
        if elevation(pos2_a,pos1_b)==-9999,                % "elevation" if no real elevation existed in that
                                                           position before.
            if temp2-raster_net_prop2(i,9)>raster_net_prop2(i,8)+0.01, %This if cycle is used so we do not have the
                                                           depth of the downstream junction before reaching
                                                           it. This
                elevation(pos2_a,pos1_b)=temp2-raster_net_prop2(i,9); %algorithm gives always an elevation between the
                                                           previous one (upstream) and the downstream end. We
                                                           add
            else                                           %0.01 m to avoid cases where [temp2-
                                                           raster_net_prop2(i,9)]-
                                                           raster_net_prop2(i,8)=0.0000000001 (positive)
                elevation(pos2_a,pos1_b)=1/8*(7*temp2+raster_net_prop2(i,8)); % Here is where we apply an
```

```
                                                                    interpolation when we reach the downstream
                                                                    elevation
    end
    temp1=raster_net(pos2_a,pos1_b);
    temp2=elevation(pos2_a,pos1_b);
    pos1_a=pos2_a;                                                  % In each case "pos1_a" and "pos1_b" store the new
                                                                    position, to be used in the next iteration
    pos1_b=pos1_b;
end,
case 2
if elevation(pos2_b,pos1_b)==-9999,
    if temp2-raster_net_prop2(i,9)>raster_net_prop2(i,8)+0.01, %This if cycle is used so we do not have the
                                                                    depth of the downstream junction before reaching
                                                                    it. This
        elevation(pos2_b,pos1_b)=temp2-raster_net_prop2(i,9); %algorithm gives always an elevation between the
                                                                    previous one (upstream) and the downstream end. We
                                                                    add
    else                                                            %0.01 m to avoid cases where [temp2-
                                                                    raster_net_prop2(i,9)]-
                                                                    raster_net_prop2(i,8)=0.0000000001 (positive)
        elevation(pos2_b,pos1_b)=1/8*(7*temp2+raster_net_prop2(i,8)); % Here is where we apply an
                                                                    interpolation when we reach the downstream
                                                                    elevation
    end
    temp1=raster_net(pos2_b,pos1_b);
    temp2=elevation(pos2_b,pos1_b);
    pos1_a=pos2_b;
    pos1_b=pos1_b;
end,
case 3
if elevation(pos1_a,pos3_a)==-9999,
    if temp2-raster_net_prop2(i,9)>raster_net_prop2(i,8)+0.01, %This if cycle is used so we do not have the
                                                                    depth of the downstream junction before reaching
                                                                    it. This
        elevation(pos1_a,pos3_a)=temp2-raster_net_prop2(i,9); %algorithm gives always an elevation between the
                                                                    previous one (upstream) and the downstream end. We
                                                                    add
    else                                                            %0.01 m to avoid cases where [temp2-
                                                                    raster_net_prop2(i,9)]-
                                                                    raster_net_prop2(i,8)=0.0000000001 (positive)
        elevation(pos1_a,pos3_a)=1/8*(7*temp2+raster_net_prop2(i,8)); % Here is where we apply an
                                                                    interpolation when we reach the downstream
                                                                    elevation
    end
    temp1=raster_net(pos1_a,pos3_a);
    temp2=elevation(pos1_a,pos3_a);
    pos1_a=pos1_a;
```

```
                    pos1_b=pos3_a;
                end,
                otherwise
                if elevation(pos1_a,pos3_b)==-9999,
                    if temp2-raster_net_prop2(i,9)>raster_net_prop2(i,8)+0.01, %This if cycle is used so we do not have the
                                                                                depth of the downstream junction before reaching
                                                                                it. This
                        elevation(pos1_a,pos3_b)=temp2-raster_net_prop2(i,9); %algorithm gives always an elevation between the
                                                                                previous one (upstream) and the downstream end. We
                                                                                add
                    else                                                        %0.01 m to avoid cases where [temp2-
                                                                                raster_net_prop2(i,9)]-
                                                                                raster_net_prop2(i,8)=0.0000000001 (positive)
                        elevation(pos1_a,pos3_b)=1/8*(7*temp2+raster_net_prop2(i,8)); % Here is where we apply an
                                                                                interpolation when we reach the downstream
                                                                                elevation
                    end
                    temp1=raster_net(pos1_a,pos3_b);
                    temp2=elevation(pos1_a,pos3_b);
                    pos1_a=pos1_a;
                    pos1_b=pos3_b;
                end,

            end
            pos2_a=pos1_a-1;                                                    % pos2_a and pos2_b will store the rows above and
                                                                                below to where we are (the new location)
            pos2_b=pos1_a+1;                                                    % pos3_a and pos3_b will store the columns above
                                                                                and below to where we are (the new location)
            pos3_a=pos1_b-1;
            pos3_b=pos1_b+1;

        end
        clear Position1
    end

% End of "WHILE" cycle that was used to give preference to the N-S-E-W neighbors.
% Next line are used to identify cells in the corners

%_____________________________________________________________________________________________________________

    Position2=[1:4; zeros(2,4)]';                                               % Exactly the same than before, but now we are
                                                                                looking at the four corners, instead of the
    if temp1==raster_net(pos2_a,pos3_a),                                        % N-S-E-W directions. Beside that, the process is
                                                                                totally the same. We use "Position2" instead
        Position2(1,2)=1;                                                       % Position1
        Position2(1,3)=sqrt((position(i,5)-(pos2_a))^2+(position(i,4)-(pos3_a))^2);
        k=k+1;
```

```
end
if temp1==raster_net(pos2_a,pos3_b),
    Position2(2,2)=1;
    Position2(2,3)=sqrt((position(i,5)-(pos2_a))^2+(position(i,4)-(pos3_b))^2);
    k=k+1;
end
if temp1==raster_net(pos2_b,pos3_a),
    Position2(3,2)=1;
    Position2(3,3)=sqrt((position(i,5)-(pos2_b))^2+(position(i,4)-(pos3_a))^2);
    k=k+1;
end
if temp1==raster_net(pos2_b,pos3_b),
    Position2(4,2)=1;
    Position2(4,3)=sqrt((position(i,5)-(pos2_b))^2+(position(i,4)-(pos3_b))^2);
    k=k+1;
end

if k>0;
    P3 = sortrows(Position2,[2 3]);
    r=0;
    count=count+1;
    k=0;
    raster_net(pos1_a,pos1_b)=0;
    switch P3(4,1)
        case 1
        if elevation(pos2_a,pos3_a)==-9999,
            if temp2-raster_net_prop2(i,9)>raster_net_prop2(i,8)+0.01,   %This if cycle is used so we do not have the depth
                                                                         of the downstream junction before reaching it.
                                                                         This
                elevation(pos2_a,pos3_a)=temp2-raster_net_prop2(i,9);    %algorithm gives always an elevation between the
                                                                         previous one (upstream) and the downstream end. We
                                                                         add
            else                                                         %0.01 m to avoid cases where [temp2-
                                                                         raster_net_prop2(i,9)]-
                                                                         raster_net_prop2(i,8)=0.0000000001 (positive)
                elevation(pos2_a,pos3_a)=1/8*(7*temp2+raster_net_prop2(i,8)); % Here is where we apply an interpolation
                                                                         when we reach the downstream elevation
            end
            temp1=raster_net(pos2_a,pos3_a);
            temp2=elevation(pos2_a,pos3_a);
            pos1_a=pos2_a;
            pos1_b=pos3_a;
        end,
        case 2
        if elevation(pos2_a,pos3_b)==-9999,
            if temp2-raster_net_prop2(i,9)>raster_net_prop2(i,8)+0.01,   %This if cycle is used so we do not have the depth
                                                                         of the downstream junction before reaching it.
```

```
                                                                This
        elevation(pos2_a,pos3_b)=temp2-raster_net_prop2(i,9);   %algorithm gives always an elevation between the
                                                                previous one (upstream) and the downstream end. We
                                                                add
    else                                                        %0.01 m to avoid cases where [temp2-
                                                                raster_net_prop2(i,9)]-
                                                                raster_net_prop2(i,8)=0.0000000001 (positive)
        elevation(pos2_a,pos3_b)=1/8*(7*temp2+raster_net_prop2(i,8)); % Here is where we apply an interpolation
                                                                when we reach the downstream elevation
    end
    temp1=raster_net(pos2_a,pos3_b);
    temp2=elevation(pos2_a,pos3_b);
    pos1_a=pos2_a;
    pos1_b=pos3_b;
end,
case 3
if elevation(pos2_b,pos3_a)==-9999,
    if temp2-raster_net_prop2(i,9)>raster_net_prop2(i,8)+0.01,  %This if cycle is used so we do not have the depth
                                                                of the downstream junction before reaching it.
                                                                This
        elevation(pos2_b,pos3_a)=temp2-raster_net_prop2(i,9);   %algorithm gives always an elevation between the
                                                                previous one (upstream) and the downstream end. We
                                                                add
    else                                                        %0.01 m to avoid cases where [temp2-
                                                                raster_net_prop2(i,9)]-
                                                                raster_net_prop2(i,8)=0.0000000001 (positive)
        elevation(pos2_b,pos3_a)=1/8*(7*temp2+raster_net_prop2(i,8)); % Here is where we apply an interpolation
                                                                when we reach the downstream elevation
    end
    temp1=raster_net(pos2_b,pos3_a);
    temp2=elevation(pos2_b,pos3_a);
    pos1_a=pos2_b;
    pos1_b=pos3_a;
end,
otherwise
if elevation(pos2_b,pos3_b)==-9999,
    if temp2-raster_net_prop2(i,9)>raster_net_prop2(i,8)+0.01,  %This if cycle is used so we do not have the depth
                                                                of the downstream junction before reaching it.
                                                                This
        elevation(pos2_b,pos3_b)=temp2-raster_net_prop2(i,9);   %algorithm gives always an elevation between the
                                                                previous one (upstream) and the downstream end. We
                                                                add
    else                                                        %0.01 m to avoid cases where [temp2-
                                                                raster_net_prop2(i,9)]-
                                                                raster_net_prop2(i,8)=0.0000000001 (positive)
        elevation(pos2_b,pos3_b)=1/8*(7*temp2+raster_net_prop2(i,8)); % Here is where we apply an interpolation
                                                                when we reach the downstream elevation
    .
```

```
                end
                temp1=raster_net(pos2_b,pos3_b);
                temp2=elevation(pos2_b,pos3_b);
                pos1_a=pos2_b;
                pos1_b=pos3_b;
            end,

        end
        pos2_a=pos1_a-1;
        pos2_b=pos1_a+1;
        pos3_a=pos1_b-1;
        pos3_b=pos1_b+1;
    end
```

%_____

%_____

```
    else                                                                    % This "Else" is used when the beginning of the
                                                                            conduit is covered (hidden) by other conduit, so
                                                                            we need to star the iterative process with an
                                                                            elevation lower than the upstream elevation.
        if raster_net(position(i,3)-1,position(i,2))==raster_net_prop2(i,1),  % The "if" and the following three "elseif" are
                                                                            used to
            pos1_a=position(i,3)-1;                                         % find in the N-S-E-W neighborhood the same
                                                                            identification of the conduit whose beginning is
                                                                            "hidden". If something is
            pos1_b=position(i,2);                                           % founded, it is recorded in "pos1_a" or "pos1_b"
                                                                            and also counted in "e" and "record". Temp2 stores
                                                                            the new elevation assumed to be the
            e=e+1;                                                          % upstream elevation minus the drop given by the
                                                                            slope.
            record=1;
            temp2=raster_net_prop2(i,7)-raster_net_prop2(i,9);
        elseif raster_net(position(i,3)+1,position(i,2))==raster_net_prop2(i,1),
            pos1_a=position(i,3)+1;
            pos1_b=position(i,2);
            e=e+1;
            record=1;
            temp2=raster_net_prop2(i,7)-raster_net_prop2(i,9);
        elseif raster_net(position(i,3),position(i,2)-1)==raster_net_prop2(i,1),
            pos1_a=position(i,3);
            pos1_b=position(i,2)-1;
            e=e+1;
            record=1;
            temp2=raster_net_prop2(i,7)-raster_net_prop2(i,9);
```

```
elseif raster_net(position(i,3),position(i,2)+1)==raster_net_prop2(i,1),
    pos1_a=position(i,3);
    pos1_b=position(i,2)+1;
    e=e+1;
    record=1;
    temp2=raster_net_prop2(i,7)-raster_net_prop2(i,9);
elseif raster_net(position(i,3)-1,position(i,2)-1)==raster_net_prop2(i,1)&&record==0,  %Same process than before, but now
                                                                                       we are trying to find elements in any of the four
                                                                                       corners' neighbors.
    pos1_a=position(i,3)-1;                                                            % However we only count using "e", not "record".
                                                                                       Because we are locating elements in the corners,
                                                                                       the elevation of
    pos1_b=position(i,2)-1;                                                            % of these cells (if found) is given by the
                                                                                       elevation upstream minus 2 times the slope.
    e=e+1;
    temp2=raster_net_prop2(i,7)-2*raster_net_prop2(i,9);
elseif raster_net(position(i,3)-1,position(i,2)+1)==raster_net_prop2(i,1)&&record==0,
    pos1_a=position(i,3)-1;
    pos1_b=position(i,2)+1;
    e=e+1;
    temp2=raster_net_prop2(i,7)-2*raster_net_prop2(i,9);
elseif raster_net(position(i,3)+1,position(i,2)-1)==raster_net_prop2(i,1)&&record==0,
    pos1_a=position(i,3)+1;
    pos1_b=position(i,2)-1;
    e=e+1;
    temp2=raster_net_prop2(i,7)-2*raster_net_prop2(i,9);
elseif raster_net(position(i,3)+1,position(i,2)+1)==raster_net_prop2(i,1)&&record==0,
    pos1_a=position(i,3)+1;
    pos1_b=position(i,2)+1;
    e=e+1;
    temp2=raster_net_prop2(i,7)-2*raster_net_prop2(i,9);
else                                                                                   % This else is used to follow the previous process
                                                                                       in case any of the 8 neighborhoods had the same
                                                                                       identification of
    for u=position(i,3)-2:4:position(i,3)+2,                                           % the conduit whose beginning is "hidden". First
                                                                                       "for" cycle covers the "i-2" and "i+2" rows
        for v=position(i,2)-2:position(i,2)+2
            if raster_net(u,v)==raster_net_prop2(i,1)&&v==position(i,2)
                pos1_a=u;
                pos1_b=v;
                e=e+1;                                                             % if the cell is found right above or below the
                                                                                       upstream junction, then the elevation is assumed
                                                                                       to be the upstream
                temp2=raster_net_prop2(i,7)-2*raster_net_prop2(i,9);               % elevation minus twice the slope.
            elseif raster_net(u,v)==raster_net_prop2(i,1)&&v~=position(i,2)
                pos1_a=u;
                pos1_b=v;
```

```
                e=e+1;
                temp2=raster_net_prop2(i,7)-3*raster_net_prop2(i,9);    % if the cell is not found right above or below
                                                                        the upstream junction, then the elevation is
                                                                        assumed to be the upstream
            end                                                         % elevation minus three times the slope.
        end
    end

    for v=position(i,2)-2:4:position(i,2)+2,                            % Second "for" cycle covers the "j-2" and "j+2"
                                                                        columns
        for u=position(i,3)-1:position(i,3)+1
            if raster_net(u,v)==raster_net_prop2(i,1)&&u==position(i,3)
                pos1_a=u;
                pos1_b=v;
                e=e+1;                                                  % if the cell is found right at the left or right
                                                                        of the upstream junction, then the elevation is
                                                                        assumed to be the upstream
                temp2=raster_net_prop2(i,7)-2*raster_net_prop2(i,9);    % elevation minus twice the slope.
            elseif raster_net(u,v)==raster_net_prop2(i,1)&&u~=position(i,3)
                pos1_a=u;
                pos1_b=v;
                e=e+1;
                temp2=raster_net_prop2(i,7)-3*raster_net_prop2(i,9);    % if the cell is not found right at the left or
                                                                        right of the upstream junction, then the elevation
                                                                        is assumed to be the upstream
            end                                                         % upstream elevation minus three times the slope.
        end
    end
end                                                                     % This is the end of the routine looking for the
                                                                        initial cell defining an element when is covered
                                                                        by other elements
%-------------------------------------------------------------------------------

if e==0                                                                 % Matrix for checking... Elements that were not
                                                                        processed...
    h=h+1;                                                              % If a variable Check2 appears when the function
                                                                        is run, then there is a mistake

    Check(h,:)=raster_net_prop2(i,:);
    Check2(h,:)=position(i,2:5);
    Check2
end

%-------------------------------------------------------------------------------

pos2_a=pos1_a-1;                                                        % pos2_a and pos2_b will store the rows above and
                                                                        below to where we are
pos2_b=pos1_a+1;                                                        % pos3_a and pos3_b will store the columns above
```

```
                                                                    and below to where we are
pos3_a=pos1_b-1;
pos3_b=pos1_b+1;
temp1=raster_net(pos1_a,pos1_b);                                    % temp1 stores the location in the raster net
                                                                    where we are to be ready to move to the next cell


if elevation(pos1_a,pos1_b)==-9999                                  % It can be possible (when a element is defined by
                                                                    2 cells) that temp2 = downstream elevation. This
                                                                    would cause a problem
    if temp2>raster_net_prop2(i,8)+0.01,                            % because before reaching the last cell defining
                                                                    the element we will already have the minimum
                                                                    (downstream) elevation. This
        elevation(pos1_a,pos1_b)=temp2;                             % "IF" is used to avoid this. It raises the
                                                                    elevation half of the slope when this happens.
                                                                    After this there will be no problem
    else                                                            % because the algorithm will always generate a
                                                                    elevation between the previous(upstream) elevation
                                                                    cell and the conduit downstream
        elevation(pos1_a,pos1_b)=temp2+raster_net_prop2(i,9)/2;     % elevation. When this correction is applied we
                                                                    also have to re-define temp2 which will have a
                                                                    value equal to the new elevation.
        temp2=elevation(pos1_a,pos1_b);
    end
end


count=1;
while r==0&&count<=raster_net_prop2(i,2),                           % This "WHILE" cycle is used to always look for
                                                                    the N-S-E-W neighbor with the same identity,
                                                                    BEFORE check diagonals
    Position1=[1:4; zeros(2,4)]';                                   % The matrix Position1 is defined. It will be used
                                                                    to detect the furthest cell from the downstream
                                                                    node
    r=1;                                                            % This cell is the one used for the next
                                                                    interpolation since it is assumed to be closer to
                                                                    the upstream.
    j=0;
    k=0;
    if temp1==raster_net(pos2_a,pos1_b),                            % The next four "if" conditions are used to find
                                                                    the next element in the N-S-E-W neighborhood with
                                                                    the same
        Position1(1,2)=1;                                           % identification as the conduit we are working
                                                                    with. Whenever we find something we also compute
                                                                    and store
        Position1(1,3)=sqrt((position(i,5)-(pos2_a))^2+(position(i,4)-pos1_b)^2); %the distance from that new location to
                                                                    the downstream junction (in matrix Position 1)
```

```
    j=j+1;
end
if temp1==raster_net(pos2_b,pos1_b),
    Position1(2,2)=1;
    Position1(2,3)=sqrt((position(i,5)-(pos2_b))^2+(position(i,4)-pos1_b)^2);
    j=j+1;
end
if  temp1==raster_net(pos1_a,pos3_a),
    Position1(3,2)=1;
    Position1(3,3)=sqrt((position(i,5)-pos1_a)^2+(position(i,4)-(pos3_a))^2);
    j=j+1;
end
if temp1==raster_net(pos1_a,pos3_b),
    Position1(4,2)=1;
    Position1(4,3)=sqrt((position(i,5)-pos1_a)^2+(position(i,4)-(pos3_b))^2);
    j=j+1;
end

if j>0;                                                    % Here we look which one of any of the cells
                                                           located is the furthest from the outlet of the
                                                           conduit.
    P2 = sortrows(Position1,[2 3]);                        % Additionally we store in "count" the number of
                                                           cells we have worked with so that when all the
                                                           cells
    clear Position1                                        % associated to a element are used we can jump to
                                                           the next element
    count=count+1;
    r=0;
    j=0;
    raster_net(pos1_a,pos1_b)=0;                           % the cell founded is deleted so it is not
                                                           available for the next iteration
    switch P2(4,1)                                         % The switch command includes the four possible
                                                           cases (N-S-E-W). In each case the new location and
                                                           elevation are defined and stored in temp1 and
                                                           temp2 respectively.
        case 1                                             Additionally, the elevation is entered in the
                                                           matrix
        if elevation(pos2_a,pos1_b)==-9999,                % "elevation" if no real elevation existed in that
                                                           position before.
            if temp2-raster_net_prop2(i,9)>raster_net_prop2(i,8)+0.01,
                elevation(pos2_a,pos1_b)=temp2-raster_net_prop2(i,9);
            else
                elevation(pos2_a,pos1_b)=1/8*(7*temp2+raster_net_prop2(i,8));
            end
            temp1=raster_net(pos2_a,pos1_b);
            temp2=elevation(pos2_a,pos1_b);
            pos1_a=pos2_a;                                 % In each case "pos1_a" and "pos1_b" store the new
```

```
                                                                position, to be used in the next iteration
        pos1_b=pos1_b;
    end,
    case 2
    if elevation(pos2_b,pos1_b)==-9999,
        if temp2-raster_net_prop2(i,9)>raster_net_prop2(i,8)+0.01,
            elevation(pos2_b,pos1_b)=temp2-raster_net_prop2(i,9);
        else
            elevation(pos2_b,pos1_b)=1/8*(7*temp2+raster_net_prop2(i,8));
        end
        temp1=raster_net(pos2_b,pos1_b);
        temp2=elevation(pos2_b,pos1_b);
        pos1_a=pos2_b;
        pos1_b=pos1_b;
    end,
    case 3
    if elevation(pos1_a,pos3_a)==-9999,
        if temp2-raster_net_prop2(i,9)>raster_net_prop2(i,8)+0.01,
            elevation(pos1_a,pos3_a)=temp2-raster_net_prop2(i,9);
        else
            elevation(pos1_a,pos3_a)=1/8*(7*temp2+raster_net_prop2(i,8));
        end
        temp1=raster_net(pos1_a,pos3_a);
        temp2=elevation(pos1_a,pos3_a);
        pos1_a=pos1_a;
        pos1_b=pos3_a;
    end,
    otherwise
    if elevation(pos1_a,pos3_b)==-9999,
        if temp2-raster_net_prop2(i,9)>raster_net_prop2(i,8)+0.01,
            elevation(pos1_a,pos3_b)=temp2-raster_net_prop2(i,9);
        else
            elevation(pos1_a,pos3_b)=1/8*(7*temp2+raster_net_prop2(i,8));
        end
        temp1=raster_net(pos1_a,pos3_b);
        temp2=elevation(pos1_a,pos3_b);
        pos1_a=pos1_a;
        pos1_b=pos3_b;
    end,

end
pos2_a=pos1_a-1;                                    % pos2_a and pos2_b will store the rows above and
                                                    below to where we are (the new location)
pos2_b=pos1_a+1;                                    % pos3_a and pos3_b will store the columns above
                                                    and below to where we are (the new location)
pos3_a=pos1_b-1;
pos3_b=pos1_b+1;
```

```
    end
    clear Position1
end                                                    % End of "WHILE" cycle that was used to give
                                                       preference to the N-S-E-W neighbors.
                                                       % Next line are used to identify cells in the
                                                       corners
%_____________________________________________________________________________________________

Position2=[1:4; zeros(2,4)]';                          % Exactly the same than before, but now we are
                                                       looking at the four corners, instead of the
if temp1==raster_net(pos2_a,pos3_a),                   % N-S-E-W directions. Beside that, the process is
                                                       totally the same. We use "Position2" instead
    Position2(1,2)=1;                                  % Position1
    Position2(1,3)=sqrt((position(i,5)-(pos2_a))^2+(position(i,4)-(pos3_a))^2);
    k=k+1;
end
if temp1==raster_net(pos2_a,pos3_b),
    Position2(2,2)=1;
    Position2(2,3)=sqrt((position(i,5)-(pos2_a))^2+(position(i,4)-(pos3_b))^2);
    k=k+1;
end
if temp1==raster_net(pos2_b,pos3_a),
    Position2(3,2)=1;
    Position2(3,3)=sqrt((position(i,5)-(pos2_b))^2+(position(i,4)-(pos3_a))^2);
    k=k+1;
end
if temp1==raster_net(pos2_b,pos3_b),
    Position2(4,2)=1;
    Position2(4,3)=sqrt((position(i,5)-(pos2_b))^2+(position(i,4)-(pos3_b))^2);
    k=k+1;
end

if k>0;
    P3 = sortrows(Position2,[2 3]);
    r=0;
    count=count+1;
    k=0;
    raster_net(pos1_a,pos1_b)=0;
    switch P3(4,1)
        case 1
        if elevation(pos2_a,pos3_a)==-9999,
            if temp2-raster_net_prop2(i,9)>raster_net_prop2(i,8)+0.01,
               elevation(pos2_a,pos3_a)=temp2-raster_net_prop2(i,9);
            else
               elevation(pos2_a,pos3_a)=1/8*(7*temp2+raster_net_prop2(i,8));
```

```
        end
        temp1=raster_net(pos2_a,pos3_a);
        temp2=elevation(pos2_a,pos3_a);
        pos1_a=pos2_a;
        pos1_b=pos3_a;
    end,
    case 2
    if elevation(pos2_a,pos3_b)==-9999,
        if temp2-raster_net_prop2(i,9)>raster_net_prop2(i,8)+0.01,
           elevation(pos2_a,pos3_b)=temp2-raster_net_prop2(i,9);
        else
           elevation(pos2_a,pos3_b)=1/8*(7*temp2+raster_net_prop2(i,8));
        end
        temp1=raster_net(pos2_a,pos3_b);
        temp2=elevation(pos2_a,pos3_b);
        pos1_a=pos2_a;
        pos1_b=pos3_b;
    end,
    case 3
    if elevation(pos2_b,pos3_a)==-9999,
        if temp2-raster_net_prop2(i,9)>raster_net_prop2(i,8)+0.01,
           elevation(pos2_b,pos3_a)=temp2-raster_net_prop2(i,9);
        else
           elevation(pos2_b,pos3_a)=1/8*(7*temp2+raster_net_prop2(i,8));
        end
        temp1=raster_net(pos2_b,pos3_a);
        temp2=elevation(pos2_b,pos3_a);
        pos1_a=pos2_b;
        pos1_b=pos3_a;
    end,
    otherwise
    if elevation(pos2_b,pos3_b)==-9999,
        if temp2-raster_net_prop2(i,9)>raster_net_prop2(i,8)+0.01,
           elevation(pos2_b,pos3_b)=temp2-raster_net_prop2(i,9);
        else
           elevation(pos2_b,pos3_b)=1/8*(7*temp2+raster_net_prop2(i,8));
        end
        temp1=raster_net(pos2_b,pos3_b);
        temp2=elevation(pos2_b,pos3_b);
        pos1_a=pos2_b;
        pos1_b=pos3_b;
    end,

end
pos2_a=pos1_a-1;
pos2_b=pos1_a+1;
pos3_a=pos1_b-1;
```

```
                pos3_b=pos1_b+1;
            end
        end
    end
end

New_DEM=DEM;
for j=1:size(DEM,1),

    for k=1:size(DEM,2),

        if elevation(j,k)~=-9999,
            New_DEM(j,k)=elevation(j,k);
        end
    end
end
 dlmwrite('J:\New_DEM_after_pipes.txt', New_DEM, ' ');
```

```
% Creation of the new DEM
% Looking for new values that have been stored in
the elevation matrix
% These new values will replace the respective
cells in the original DEM
% Matrix "New_DEM" has the corrected DEM

% Writing a text file with the matrix
```

7. APPENDIX II. Matlab code of algorithm used to compute the Morpho-climatic Instantaneous Unit Hydrograph for Urban catchments (U-McIUH)

The following code is used in the computations of the U-McIUH model described and tested in Chapter 4 "**A morpho-climatic instantaneous unit hydrograph model for urban catchments calculated from digital elevation models**". Two functions are called in the code: The function "model" is called first. This function is used to compute, in each time step, the raster of effective precipitation and the raster of travel times for all different types of cell. The function "Travel_time_final" is called from this function to compute the matrix with travel time from each cell going to the catchment's outlet. This matrix is then recovered by the function "Model" and used to generate the corresponding UH for the pulse. Finally, the pulses are convoluted with the corresponding UH an superimposed to generate the response for the entire storm event.

Required data

```
Dt          = Interval of time for convolution, delta t for precipitation (s)
Dx          = Grid cell size (m)
rain        = One column vector with rain (volumes, in mm)
fc          = Infiltration rate (mm/h)
dep_st      = Depression storage (mm)
catchment   = Matrix with ones and zero indicating the catchment
Fdr         = Flow direction matrix from ArcGIS
Hills       = Matrix with Cells representing hillslopes (ones and zeros)
Street      = Matrix with Cells representing streets (ones and zeros)
Pipes       = Matrix with Cells representing pipes (ones and zeros)
Chann       = Matrix with Cells representing channels (ones and zeros)
N_imp       = Roughness coefficient for overland flow in impervious areas
              (single value)
N_per       = Roughness coefficient for overland flow in pervious areas
              (single value)
N_s         = Roughness coefficient for streets (single value)
N_p         = Roughness coefficient for pipes (single value)
N_c         = Roughness coefficient for channels (single value)
Imper       = Matrix with imperviousness (%) for each cell (0 - 1)
Lambda      = Matrix with values of lambda for each cell
Length      = Matrix with values of flow length for each cell in meters (the
              grid resolution Dx or Dx times sqrt (2)
S_h         = Matrix with Slope for hillslope
S_s         = Matrix with Slope for streets
S_p         = Matrix with Slope for pipes
S_c         = Matrix with Slope for channels
Diam        = Matrix with Diameter of pipes
C_w         = Matrix with Channel width
Phi         = Parameter for correction of conduit lengths
```

Result

hydro is a matrix with two columns, a column indicating the time and a column indicating the flow in L/s. A hydrograph is also plotted as a result.

```
function
[hydro]=Model(Dt,Dx,rain,fc,dep_st,catchment,Fdr,Hills,Street,Pipes,Chann,N_imp,N_per,N_s,N_p,N_c,Imper,Lambda,Length,S
_h,S_s,S_p,S_c,Diam,C_w,phi)


% IMPORTANT. One can define fc = 0 and dep_st = 0 and enter the effective precipitation in the rain variable.


%__________Computation of matrices with Roughness coefficient_____________


N_hill=N_imp*Imper+N_per*(1-Imper); % computation of manning's coef. in hillslopes (matrix)
N_street=N_s*Street;                % computation of manning's coef. in streets (matrix)
N_pipe=N_p*Pipes;                   % computation of manning's coef. in pipes (matrix)
N_channel=N_c*Chann;                % computation of manning's coef. in channels (matrix)
%_____________________________________________________________________

%___Computation of total imperviousness of the catchment
Imp_tot_per=sum(catchment.*Imper)/sum(catchment);
%_____________________________________________________________________

%_____________________Computation of the instantaneous unit hydrograph_______
% There is a "for" cycle to cover all the volume in the rain vector. For each
% pulse a different unit hydrograph is computed that is dependant on the
% intensity

k=0;                % k is used to count event larger than zero
rain_count=0;       % rain_count is used to count cumulative rainfall volume

for j=1:size(rain,1)
    rain_count=rain(j,1)+rain_count;

    % This if condition is to identify the pulses that produce runoff
    if rain(j,1)>0&&rain_count>dep_st,
        k=k+1;

        rain_efect=(rain_count-dep_st);
        % The next if condition is to determine the effective precipitation,
        % which is given by either the contribution of impervious areas only or
        % by the impervious contribution plus a pervious contribution. The
        % matrix with the spatially distributed field of intensities is saved
        % in Efec_P

        if rain_efect<fc*Dt/3600,
            Efec_P=rain_efect*Imper;
            rain_pulse=rain_efect*Imp_tot_per;
        else
            if fc==0,
                Efec_P=ones(size(Imper,1),size(Imper,2))*rain_efect;
            else
```

```
        Efec_P=(rain_efect*Imper+(1-Imper).*(rain_efect-Dt*fc/3600));
    end
    rain_pulse=rain_efect*Imp_tot_per+(1-Imp_tot_per)*(rain_efect-Dt*fc/3600);
    % rain_pulse is the spatial average intensity of the pulse
end
rain_count=dep_st;

% The next four expressions are used to compute the travel time in each
% cell depending on whether is a hillslope, street, pipe or channel
% cells. The expressions are defined from the kinematic wave theory
% and compute time in seconds


D_t_hillslope=6.99*60*1*catchment.*Hills.*((N_hill.*Length)./sqrt(S_h)).^0.6.*(Efec_P*(3600/Dt)).^-
0.4.*((Lambda+1).^0.6-Lambda.^0.6);

D_t_streets=0.86/phi*60*catchment.*Street.*(N_street./sqrt(S_s)).^0.75.*Length./(Dx^2*Efec_P*(3600/Dt)).^0.25*2.
281227.*((Lambda+1).^0.75-Lambda.^0.75);

D_t_pipes=0.59/phi*60*catchment.*Pipes.*(N_pipe./sqrt(S_p)).^0.8.*Length./((Dx^2*Efec_P*(3600/Dt)).^0.2.*Diam.^(
2/15)).*((Lambda+1).^0.8-Lambda.^0.8);

D_t_channels=6.99/phi*60*catchment.*Chann.*(Length.*Chann).*((N_channel)./(sqrt(S_c))).^0.6.*(C_w./(Dx^2*Efec_P*
(3600/Dt))).^0.4.*((Lambda+1).^0.6-Lambda.^0.6);


% The next line create a vector sorted in ascending order with all the
% travel times from each cell to the outlet. This is done by calling the
% function Travel_time_final. The PDF of the vector OTravel_time corresponds to
% the IUH.

[OTravel_time]=Travel_time_final(Fdr,D_t_hillslope,D_t_streets,D_t_pipes,D_t_channels);
% OTravel_time=IUH;

% The next two lines compute the unit impulse for the corresponding rain
% pulse. Vector r is simply a vector of time (time step = Dt) that define the
% domain for the empirical density distribution of the total times.
% Matrix h (2 columns) has vector r in the first column and the
% corresponding pdf values (unit of 1/seg) in the second column

r=[0:Dt:max(OTravel_time)+Dt]';
h=[r rain_pulse*(1/Dt/size(OTravel_time,1)*histc(OTravel_time,r))];

% The next if creates the matrix "matrix" that stores in each column
% the response produced by each pulse occurring in the subsequent time.

if k==1,
```

```
            matrix=zeros(1+2*size(h,1)+size(rain,1),size(rain,1));
        end

        % Matrix store in column "j" the response for the "j" rain pulse

        matrix(j:j+size(h,1)-1,j)=h(:,2);
        clear D_t_hillslope D_t_streets D_t_pipes D_t_channels h r rain_pulse
        % clear h r rain_pulse
    end
end
if k>0,
    Q=sum(matrix,2);                          % Q = the superposition of the responses for each one of the pulses and
    time=[Dt:Dt:size(Q,1)*Dt]';               % corresponds to the sum of all the rows of matrix "matrix"
    hydro=[time,Q*sum(sum(catchment))*Dx^2];   % Total hydrograph = Q times the Area of the catchment
else                                          % Where the area of the catchment is given by sum(sum(catchment))*Dx^2
    hydro=[0 0];
end

    figure
    plot(hydro(:,1),hydro(:,2))               % Plotting the hydrograph
```

```
function [OTravel_time]=Travel_time_final(Fdr,D_t_hillslope,D_t_streets,D_t_pipes,D_t_channels)
% This function is used to compute the travel times (in seconds) from each cell within the watershed to the outlet. It
is called by the function model.
```

```
Travel_matrix=zeros(size(Fdr,1),size(Fdr,2));

a=size(Fdr,1);
b=size(Fdr,2);

for i=1:a,

    for j=1:b,
        if D_t_hillslope(i,j)<0,
            D_t_hillslope(i,j)=0;
        end
    end
end

for i=1:a,
    for j=1:b,
        if D_t_streets(i,j)<0,
            D_t_streets(i,j)=0;
        end
    end
end

for i=1:a,
    for j=1:b,
        if D_t_pipes(i,j)<0,
            D_t_pipes(i,j)=0;
        end
    end
end

aux=isnan(D_t_channels);

if sum(aux)==0,

    for i=1:a,
        for j=1:b,
            if D_t_channels(i,j)<0,
                D_t_channels(i,j)=0;
            end
        end
    end
else
    D_t_channels=zeros(size(Fdr,1),size(Fdr,2));
end

D_t_cell=D_t_hillslope+D_t_streets+D_t_pipes+D_t_channels;
```

```
% Creation of the matrix "Travel_matrix" to store the
travel times from each cell

% The next four for cycles are used to transform any
improper data (0 or -9999) into zero
% for each raster

% This is done to detect whether or not the matrix with
 travel times in channel has elements
% If the catchment does not have channels then this
 routine remove the channel component
```

```
for i=a:-1:1,

    for j=b:-1:1,


        if Fdr(i,j)>0,
            p=i;


            q=j;
            k=0;
            while Travel_matrix(p,q)==0 && D_t_cell(p,q)~=0,

                k=k+D_t_cell(p,q);


                if Fdr(p,q)==1,

                    l=p;
                    m=q+1;
                end
                if Fdr(p,q)==2,
                    l=p+1;
                    m=q+1;
                end
                if Fdr(p,q)==4,
                    l=p+1;
                    m=q;
                end
                if Fdr(p,q)==8,
                    l=p+1;
                    m=q-1;
                end
                if Fdr(p,q)==16,
                    l=p;
                    m=q-1;
                end
                if Fdr(p,q)==32,
                    l=p-1;
                    m=q-1;
                end
                if Fdr(p,q)==64,
                    l=p-1;
                    m=q;
                end
                if Fdr(p,q)==128,
                    l=p-1;
```

```
% Two for cycles to cover the entire matrix of flow
 directions. The direction (positive or negative)
% for i and j can be changed depending where the
 watershed outlet is. The algorithm is more effective as
 it goes upstream.

% i and j are the indexes of the cell whose travel time
 is being computed. p and q are temporal indexes of the
 cells connecting
% the cell i,j and the outlet.

% The while cycle is done until a cell whose travel
 time has been already computed is reached.
% The auxiliary variable k stores the summation of the
 travel time in the downstream direction

% Once k has been updated the next cell downstream is
 identified and stored in p, q
```

```
                m=q+1;
            end
            p=l;                                    % once l and m have been defined, they are assigned to
                                                    p and q to go to the next cell
            q=m;

        end
        Travel_matrix(i,j)=k+Travel_matrix(p,q);    % Finally, right before moving to the next cell i,j, we
                                                    compute the total travel time as the
    end                                             % travel time stored in k plus the travel time already
                                                    computed for the cell reached following
end                                                 % the downstream path
end
```